UNIVERSITY OF SOUTHAMPTON

Faculty of Environmental and Life Sciences
School of Ocean and Earth Science

# Habitat transitions in marine fishes-expanding the otolith toolkit

by

**Yuan Tian Chou**

https://orcid.org/0009-0007-3240-0358

*A thesis for the degree of Doctor of Philosophy*

January 2025

# University of Southampton

## Abstract

Faculty of Environmental and Life Sciences School of Ocean and Earth Science

Doctor of Philosophy

Habitat transitions in marine fishes-expanding the otolith toolkit

by

Yuan Tian Chou

Most marine teleost fishes suffer high mortality during the larval phase, therefore small differences in larval mortality can have big impacts on population and stock dynamics. Larval fish may move large distances, potentially experiencing a range of conditions which can influence mortality. Tracking the migration of fish larvae and predicting how changes in ocean conditions may influence migration routes (and potentially larval mortality) is challenging, but essential for stock management. Recent advances in tag technology have allowed monitoring in smaller species, but small body sizes and high larval mortality rates limit available data. Individual-based migration models have been developed to predict potential migration pathways but still present inherent uncertainty due to assumptions that are difficult to verify empirically. Otoliths, continually growing, paired calcium carbonate structures formed in the fish's inner ear, can potentially reveal individual migration patterns by recording ambient water chemistry experienced during growth, related to hydrography. However, linking otolith compositions to a specific spatial origin is challenging due to the unknown environmental factors and difficulties in otolith sampling techniques. This study aims to evaluate the potential of using otolith chemistry, specifically stable oxygen isotopes coupled with individual-based migration models, to reconstruct the migration history of individual small fish and to establish a connection between the theoretical movement predicted by the model and the empirical data obtained from the otolith isotope-based method. The study includes three main approaches: (1) a case study of passive drift of North East Atlantic mackerel, using simulated ocean model currents and hydrography to predict otolith isotope records for individuals following a range of pathways around the continental shelf; (2) analysis of stable isotopes of otoliths to infer aspects of thermal physiology in juvenile mackerel; (3) the application of the model-otolith isotope combination analysis method to a broader range of open-sea eel larvae for a range of

hypothetical swimming behaviours. In (1), the potential use of otolith $\delta^{18}O$ profiles, as accurate and low-cost "natural tags" for stock discrimination and broad-scale geolocation of fish, are first evaluated. In (2), estimates are obtained of the thermal performance curve of field metabolism in a wild juvenile fish, indicating that ecological factors such as food availability or competition for resources may play a more significant role in shaping an organism's overall metabolic rate than temperature alone. In (3), extension of drift analysis with different swimming vectors further explores the potential of using otolith $\delta^{18}O$ values to distinguish between successful and failed drifts, and to verify the hypothesis that NAO affects eel migration. This thesis thus provides insights into the potential of using otolith chemistry and individual-based migration models to improve our understanding of the early life history of small fish and their migration patterns, which can have important implications for the conservation, management, and recovery of fish stocks.

# Table of Contents

**Table of Contents** ..... **iii**

**Table of Tables** ..... **vii**

**Table of Figures** ..... **ix**

**Research Thesis: Declaration of Authorship** ..... **xii**

**Acknowledgements** ..... **xiii**

**Chapter 1 General Introduction** ..... **1**

1.1 Introduction ..... 1

1.2 The importance of habitat transition traceability ..... 1

1.3 Techniques for origin traceability of marine fishes ..... 2

1.4 Using otolith as natural tags ..... 5

1.5 Using $\delta^{18}O$ values to reconstruct migratory histories ..... 7

1.6 Oxygen Isotope Records of Migration from otolith ..... 9

1.6.1 Case study- tuna ..... 10

1.6.2 Case study- deep-water fish vertical migrations ..... 11

1.6.3 Case study- *Pleuronetes platessa* ..... 12

1.6.4 Case study- Japanese sardine ..... 12

1.7 Using individual-based migration models IBM to estimate migrations ..... 13

1.8 The Importance of Individual Energetics for IBM Models ..... 15

1.9 Research gaps ..... 16

1.10 Thesis aim, objectives, and structure ..... 17

1.10.1 Thesis aim and objectives ..... 17

1.10.2 Thesis structure ..... 18

**Chapter 2 Stable isotope-enabled particle drift models predict where high resolution isotope analyses can discriminate among larval trajectories in Atlantic mackerel.** ..... **21**

2.1 Introduction ..... 23

2.2 Methods ..... 27

2.2.1 Particle tracking ..... 27

2.2.2 Seawater $\delta^{18}O$ estimate ..... 29
2.2.3 Otolith $\delta^{18}O$ estimate ..... 29
2.3 Results ..... 30
2.3.1 Prediction of larval transport ..... 30
2.3.2 Larval Drift Predictions and contrasting dispersion ..... 32
2.3.3 Hydrography and inferred isotopic ratios along drift pathways ..... 33
2.3.3.1 Salinity ..... 34
2.3.3.2 Temperature ..... 34
2.3.3.3 Oxygen isotope ratio of seawater ..... 35
2.3.3.4 Oxygen isotope ratio inferred for otoliths ..... 35
2.3.4 $\delta^{18}O_{otolith}$ predictions in the spawning areas ..... 39
2.4 Discussion ..... 40
2.4.1 Simulating time-varying drift pathways of NEAM ..... 41
2.4.2 Otoliths as "natural tags." ..... 43
2.5 Conclusions ..... 45

**Chapter 3 Predicting high-resolution otolith isotope ratios along basin-scale trajectories with and without simulated swimming to inform early life history migrations: A case study with European Eel ..... 47**

3.1 Introduction ..... 48
3.2 Methods ..... 52
3.2.1 Particle tracking ..... 52
3.2.2 Seawater $\delta^{18}O$ estimate ..... 54
3.3 Results ..... 55
3.3.1 Prediction of larvae transport ..... 55
3.3.2 The hydrographic features of spawning areas ..... 60
3.3.3 Hydrography and inferred isotopic ratios along drift pathways ..... 61
3.3.4 Ocean currents during positive and negative phases of the NAO ..... 70
3.4 Discussion ..... 73
3.4.1 Predicting the probability of successful larval drift ..... 73
3.4.2 Passive drift and swimming trajectories ..... 74

3.4.3 Hydrological characteristics of spawning ground ..... 74
3.4.4 Hydrogeography and inferred isotope ratios along drift paths ..... 75
3.4.5 Comparing simulation results with catch data ..... 77
3.5 Conclusions ..... 78

**Chapter 4 First in-situ measurements of field metabolic rate in wild Atlantic mackerel ..... 80**

4.1 Introduction ..... 81
4.2 Methods ..... 83
*4.2.1* Field collection of juvenile *Scomber scombrus* ..... 84
4.2.2 Otolith preparation and isotope analysis ..... 84
4.2.3 Otolith $\delta^{18}O$ based reconstructions of experienced temperature ..... 85
4.2.4 Otolith $\delta^{18}C$ based field metabolic rate calculation ..... 85
4.2.5 Conversion to oxygen consumption rates ($mgO_2kg^{-1}hr^{-1}$) ..... 86
4.2.6 Estimation of mass-specific standard metabolic rate (SMR) ..... 86
4.2.7 Statistical analyses ..... 87
4.3 Results ..... 87
4.3.1 Sampled fish and raw isotope data ..... 88
4.3.2 Temperature reconstruction ..... 90
4.3.3 Relationship between Scaling of metabolic rate ($C_{resp}$) and otolith FMR values with Body mass ..... 90
4.3.4 Relationship between Scaling of metabolic rate ($C_{resp}$) and otolith FMR values with experienced temperature estimated based on $\delta^{18}O_{otolith}$ ..... 91
4.4 Discussion ..... 95
4.4.1 Relative metabolic level of Atlantic mackerel ..... 95
4.4.2 Body mass scaling ..... 97
4.4.3 Temperature scaling ..... 98
4.5 Conclusions ..... 99

**Chapter 5 Conclusions ..... 101**

5.1 Thesis summary ..... 101
5.2 Implications of thesis findings ..... 102

5.2.1 The application of otolith isotopes in individual-based models (IBMs): ..... 102
5.2.2 Wider implications for co-use of otolith isotope-based methods and individual-based models IBMs: ..... 103
5.2.2.1 Application in fishery management: ..... 104
5.3 Original contribution of the thesis ..... 104
5.4 Limitations of the current study ..... 105
5.5 Future work ..... 106

**List of References ..... 107**

# Table of Tables

*Table 1-1:The advantages and disadvantages of tags* ..... *4*

*Table 1-2.Summary of research to date on the use of stable isotopes on otolith in tracking marine migrations in fishes* ..... *10*

*Table 2-1. Initial Particles released position and number during the study periods.* ..... *28*

*Table 2-2.Summary of predicted salinity, temperature,* $\delta^{18}O_w$ *and* $\delta^{18}O_{otolith}$ *experienced in the four suggested spawning areas.* ..... *33*

*Table 3-1.Summary of results recorded in the present study. The reported number represents mean ± SD* ... *89*

# Table of Figures

*Figure 1-1. (A) Oxygen isotope linear regression models and (B) slopes and intercepts of the temperature fractionation equations (Willmes et al., 2019).....8*

*Figure 1-2. This study aims to build the gap between model and otolith chemistry. The flow diagram shows how the model can inform otolith chemistry when reconstructing high-resolution movements and how analysis in the field of the information can be fed back to develop a model built.....18*

*Figure 2-1. The study area and simulated spawning area during the study period, and the circulation pattern of the North Atlantic Current (NAC- red line), and shelf edge / coastal circulationurrent (yellow line).....277*

*Figure 2-2. Larval distribution simulated from April to July 1998, released from a depth of 14 m at 415 initial positions, based on survey data (black stars). Particles are released 120 times from each initial position hourly for 5 days and subsequently tracked for 100 days. The resulting Particle density (A) and age (B) are averaged on a 0.5° × 0.5° grid.....300*

*Figure 2-3. Larval dispersal simulated as mean particle density over 100 days for selected start months and locations determined from mackerel egg survey 1998: (A) March-July; (B) April-August; (C) May-September; (D) June-October; (E) July-November; (F) June-October. Particles are released at the initial positions indicated with black stars. .....32*

*Figure 2-4. The average larval days adrift within 0.5 grid cell geographic positions (days adrift) for particles released from March to July is illustrated in different time intervals:: (A) March-July; (B) April-August; (C) May September; (D) June-October; (E) July- November; (F) June-October (North Sea). Initial particle locations are indicated with black stars. .....33*

*Figure 2-5. Mean environmental properties -, sampled by particles released over March-July of 1998: (A) salinity; (B) temperature; (C) $\delta^{18}O_w$; (D) $\delta^{18}O_{otolith}$.....37*

*Figure 2-6. Ensemble means and standard deviations experienced by particles released over 1998 (see Figure 1-1): (A) salinity; (B) temperature; (C) $\delta^{18}O_w$; (D) $\delta^{18}O_{otolith}$. Monthly means and standard deviations are calculated separately for the four identified spawning areas (South, West 1, West 2, North).....38*

*Figure 2-7 The estimated bulk isotopic composition of otoliths from different geographic areas.....40*

*Figure 2-8 Ensemble means and standard deviations for inferred δ18Ootolith rings in the four spawning/drifting areas.....39*

*Figure 2-9. Combined Quarter 4 and Quarter 1 ICES survey data (as mean catch rate per hour) for age-0 mackerel during 1998/99. (Bartsch et al., 2004).....433*

*Figure 3-1 The locations where Anguilla anguilla leptocephali were collected. The size of the circles reflects the abundance at each sampling location. The red circles indicate metamorphosed larvae (data from JD McClave database, which includes Aa and Ar leptocephalus catch data from 1863 to 2007). This figure is from Miller et al. (2016). .....49*

*Figure 3-2. The study area, the simulating spawning areas, and schematic 0–200 m averaged ocean circulation; also indicated are selected meridians for sampling successful transits. .....522*

Table of Figures

*Figure 3-3. Particle density for releases in May of 1989-91 (left panels) and 2008-10 (right panels), fixed to drift at (A) 0 m, (B) 47 m, (C) 97 m, and (D) 200 m.The initial positions of these particles are indicated by black rectangles.....566*

*Figure 3-4. Particle density for releases in 1989-91 (left panels) and 2008-10 (right panels), starting (A) February, (B) March, (C) April, (D) May. The initial positions of these particles are indicated by black rectangles. .....57*

*Figure 3-5. Particle density for releases in May, fixed to drift at a depth of 200 m with swimming vectors (m $s^{-1}$) specified as (A)(D) (0.5 m $s^{-1}$, 0.5 m $s^{-1}$), (B) (E) (0.05 m $s^{-1}$, 0.05 m $s^{-1}$), (C) (F) (0.01 m $s^{-1}$, 0.01 m $s^{-1}$) for one year and two years respectively. .....58*

*Figure 3-6. Particle density for releases in May fixed to drift at a depth of 200 m with swimming vectors (m $s^{-1}$) in different directions as (A) 45º(0.05X0.05 m $s^{-1}$), (B) 30º(0.028X0.05 m $s^{-1}$) (C) 15 º(0,013*0.05 m $s^{-1}$) The initial positions of these particles are indicated by black rectangles. .....59*

*Figure 3-7. The hydrographic features of spawning areas 200m from February to May: (A) salinity (psu), (B) temperature (°C), (C) $\delta^{18}O$ w, and (D) $\delta^{18}O$ otolith. .....61*

*Figure 3-8. Particles selected for reaching 20ºW, released in May at 200m and spawning in subarea 1, in 1989 (NAO+) and 2008 (NAO-): (A), (E) particle density; (B),(F) mean age; (C),(G) mean potential temperature(ºC); (D),(H) mean salinity (psu). The initial positions of these particles are represented by black rectangles, and the subareas are depicted in grey on the map. .....62*

*Figure 3-9. Along-trajectory data for particles successfully reaching 20ºW, released in May at 200m, spawning in sub-area 1, in 1989 (NAO+) and 2008 (NAO-): (A)latitude; (B) salinity; (C)temperature (ºC); (D)$\delta^{18}O_w$; (E) $\delta^{18}O_{otolith}$. The density of particles relative to the total is represented by a color scale bar. .....632*

*Figure 3-10. Particles failing to reach 20ºW released in May at 200m and spawning in sub-area 1, in 1989 (NAO+) and 2008 (NAO-): (A),(E) particle density; (B),(F) mean age; (C),(G) mean potential temperature (ºC); (D),(H) mean salinity (psu). The initial positions of these particles are represented by black rectangles, and the subareas are depicted in grey on the map. .....663*

*Figure 3-11. Along-trajectory data for particles failing to reach 20ºW released in May at 200m and spawning in sub-area 1, in 1989 (NAO+) and 2008 (NAO-): (A)latitude; (B) salinity; (C)temperature (ºC); (D)$\delta^{18}O_w$; (E $\delta^{18}O_{otolith}$. The density of particles relative to the total is represented by a color scale bar. .....674*

*Figure 3-12. Along-trajectory data for particles in May 2008 (NAO-) at 200m with fixed swimming direction at 45, 30 and 15°: (A)latitude; (B) salinity; (C)temperature (ºC); (D)$\delta^{18}O_w$; (E) $\delta^{18}O_{otolith}$. The density of particles relative to the total is represented by a color scale bar.....669*

*Figure 3-13.Ocean current speed at different depths during the NAO+ period: (A) 0m, (B) 47m, (C) 97m, (D) 200m. Colours indicate current speeds in meters per second ($ms^{-1}$). .....670*

*Figure 3-14. Ocean current speed at different depths during the NAO- Period: (A) 0m, (B) 47m, (C) 97m, (D) 200m. Colours indicate current speeds in meters per second ($ms^{-1}$). .....7168*

*Figure 3-15. Number of model grid points where current speed exceeds 50 cm $s^{-1}$ everywhere north of 30ºN and west of 20ºW, at depths of (A) 200 m and (B) 0 m, over May 1989 to April 1991 (NAO+, blue) and May 2008 to April 2010 (NAO-, red).....7269*

*Figure 4-1. The samples of juvenile mackerel (age 0+) were collected from surveys conducted by Marine Scotland from the research vessel Scotia between 2020 and 2021. The sampling locations are indicated in*

*yellow and divided into two zones (east and west) at 50 degrees. The samples of adult mackerel (age 3) were caught by commercial trawlers in the English Channel in August 2020, and the sampling location is shown in green. ....84*

*Figure 4-2. (A) Experienced temperature (°C), (B) body mass (grams), (C) $C_{resp}$ value, and (D) field metabolic rate (FMR) ($mgO_2kg^{-1}h^{-1}$) recorded amongst all Scomber scombrus individuals between juveniles (which were sampled in the present study in North Atlantic during 2020 to 2021) and adults (which were caught off the coasts of Sussex and Devon in August 2020). Boxes represent the 25–75 percentiles, horizontal lines within represent medians, and vertical lines represent the box ± 1.5 times the interquartile range. ....90*

*Figure4-3. Individual (A) $C_{resp}$ and (B) whole-organism field oxygen consumption (oxygen consumption mmol $h^{-1}$) plotted by log body mass. On plots the black line shows the best fit, with 95% confidence intervals shaded in grey, with points coloured by life stage. ....91*

*Figure4-4. The relationship of $C_{resp}$ values with temperature of full data set. The field metabolic rate (FMR) and inverse temperature following the Arrhenius modelof (A)full data set (C) Adult(E) Juvenile. k is Boltzmann's constant ($8.62 \times 10^{-5}$ $eVK^{-1}$), T is the absolute temperature in K, and M is body mass in grams.93*

*Figure 4-5. The relationship of $C_{resp}$ values with temperature of Eestern and Western area. The field metabolic rate (FMR) and inverse temperature following the Arrhenius model of k is Boltzmann's constant ($8.62 \times 10^{-5}$ $eVK^{-1}$), T is the absolute temperature in K, and M is body mass in grams. ....94*

*Figure 4-6. The relationship of $C_{resp}$ values with temperature of juveniles from Eestern of fall and winter. The field metabolic rate (FMR) and inverse temperature following the Arrhenius model of k is Boltzmann's constant ($8.62 \times 10^{-5}$ $eVK^{-1}$), T is the absolute temperature in K, and M is body mass in grams. ....95*

*Figure 4-7. Relative oxygen consumption based on our comparison of experimental results with FishBase. The oxygen consumption of our study on mackerel are shown in red, while those of other species in the Scombridae family are shown in green. The oxygen consumption of other species are shown in yellow.....96*

*Figure 4-8. Relative oxygen consumption data ....97*

# Research Thesis: Declaration of Authorship

Print name:

Title of thesis: Habitat transitions in marine fishes-expanding the otolith toolkit

I declare that this thesis and the work presented in it are my own and has been generated by me as the result of my own original research.

I confirm that:

1. This work was done wholly or mainly while in candidature for a research degree at this University.
2. Where any part of this thesis has previously been submitted for a degree or any other qualification at this University or any other institution, this has been clearly stated.
3. Where I have consulted the published work of others, this is always clearly attributed.
4. Where I have quoted from the work of others, the source is always given. With the exception of such quotations, this thesis is entirely my own work.
5. I have acknowledged all main sources of help.
6. Where the thesis is based on work done by myself jointly with others, I have made clear exactly what was done by others and what I have contributed myself.
7. None of this work has been published before submission

Signature: .....Date:.....

# Acknowledgements

In the process of completing this doctoral dissertation, I wish to extend my sincere gratitude to all those who have supported and encouraged me. First and foremost, I would like to thank my mentors, Dr. Clive, Dr. Bob, and Dr. Ewan, for their unwavering guidance and encouragement throughout my academic journey, whether it be in academic research, thesis writing, or doctoral studies.

I am also grateful to my lab mates, Sarah, Joe, and Julia, for accompanying me through the ups and downs of doctoral life. Your support and friendship have been invaluable to me. Special thanks to my dear friend, Macro, for accompanying and supporting me during the final year of thesis writing.

I want to express my heartfelt appreciation to my husband, Max, for his continuous support and encouragement from afar in the UK. Your love and understanding have been my unwavering motivation.

A special thank you to Megan and Bastian for their assistance and guidance in isotopic analysis. Your expertise has been instrumental in driving my research forward. I also want to thank Vince for providing timely computer software support during remote work.

I am grateful to Dr. Elliott for the valuable advice provided during the thesis writing process. Your professional guidance has made my thesis more comprehensive. I also want to thank my colleague, Riyar, for the encouragement and support during the thesis period, your companionship has made me feel warm and courageous.

Finally, I want to express my gratitude to Dr. Jinyi Zhang for the encouragement and support on the academic journey. Your guidance has enabled me to move forward with determination.

Last but not least, I want to extend a special thank you to Dr. Kotaro and Dr. Paul Kemp for their careful reading and valuable advice on my thesis. Your support means a lot to me.

In this journey, there have been many people who have helped and supported me. Without you, I would not have been able to complete this thesis. I deeply appreciate your dedication and support, and it will always be remembered in my heart.

# Chapter 1 General Introduction

## 1.1 Introduction

The migration of marine fish over large distances is a well-known phenomenon, but the specific patterns vary depending on species, climate, and lifecycle (Secor,2015). The changing habitat requirements of fish through ontogeny and physical/biological characteristics of oceanic habitats are major factors affecting migration patterns (Fisher & Hunter, 2018; Hixon et al., 2008). Larval dispersal migration is a critical event in the life history of many marine fishes, influencing recruitment success and retention or dispersion of larvae (Kimirei et al., 2013).

Understanding the distribution shifts experienced by larval fishes is, therefore, particularly important in enhancing the conservation, management, and recovery of fish stocks. However, tracking migration of fish larvae is challenging due to high mortality rates and small size, technological limitations, and low recatch rates (Stutchbury et al., 2009). Although numerous individual-based migration models coupled with fish bioenergetics have been developed to estimate migrations of larval fish (Okunishi et al., 2012; Phillips et al., 2015; Boyd et al., 2020; Mawer et al., 2023), they still include assumptions such as the location and timing of spawning, which may vary due to environmental changes leading to uncertainty..

Otolith chemistry records ambient water chemistry and has been used extensively to infer stock structure and connectivity patterns (Campana, 1999; Sturrock et al., 2012). However, linking otolith compositions to a specific spatial origin has been difficult. This study will assess the potential for using otolith chemistry, specifically stable isotopes, combined with individual-based migration models, to reconstruct the migration history of small fish at the individual level.

## 1.2 The importance of habitat transition traceability

The migration patterns of marine fishes can be seen as a circular process, referred to as the migration triangle (Harden Jones, 1968) . This concept combines the idea of hydrographic containment with fish eggs and larvae migrating from the spawning grounds to nursery grounds and then joining the adult population at feeding grounds before returning to the spawning grounds to reproduce (Cushing, 1975, 1981). The dispersal migration of larvae is a crucial ecological process that determines the scale of distribution and abundance of species (Di Franco et al., 2015). Understanding the distribution of larval fishes is essential for efficient fisheries management and species conservation, particularly in the context of global climate change.

Habitat transition traceability can provide insights into how fish populations respond to environmental changes. The information can then be used to inform the design of conservation and management strategies, such as the establishment of marine protected areas or the implementation of fishing regulations that protect key habitats (Hining et al., 2000; Sakamoto et al., 2019)

## 1.3 Techniques for origin traceability of marine fishes

Marine fishes are challenging to observe directly. Traditional methods of determining fish movement are mainly achieved by observing the distribution and the abundance of fish of different size classes to estimate their movement paths, e.g., Dorf & Powell ( 1997). However, changes in the distribution, abundance, and size structure may not reflect the actual movement of individual fish (Elsdon & Gillanders, 2003). Thus, these traditional methods may fail to reconstruct migratory patterns accurately. External tags and point mark-recapture techniques have been developed to track movements (Wang et al., 2019). However, tagging studies are limited by low recapture rates, with values as low as 1.9% (Hansen &Jacobsen, 2003), Insufficient data may affect migration estimates. The appropriate spatial distribution of sampling and recapture efforts needed to obtain a specified level of precision are challenging issues. The cost of vessels and labour also restrict the recapture sample size and duration of sampling. Even though encouraging tag returns from commercial fishing vessels is a cost-effective reporting method, the distribution of recaptures can be biased by unequal fishing efforts, irregular reporting rates, and fishery-closed areas. Capture returns may reflect the commercial fleet's activity more than the true extent of fish migration (Bolle et al., 2005), making many tagging experiments costly and with low reward or biased results. Furthermore, the time scale of recaptures can be from months to years, and no information is collected on the fish during the interim period from release until recapture, meaning that the methods do not allow for detailed reconstructions of movement patterns.

The recent development of animal-borne electronics improves the information collected during the interim period. Advanced methods of electronic tags, including data storage tags (DST, also named archival tags), radio and acoustic transmitters, and pop-up satellite archival tags (PSAT), have been applied for fish telemetry, providing a complete, accurate picture of migration patterns. DST are tags with sensors that store the recorded environmental, physiological, and positional data as often as every 1-15 minutes over extended periods (Thorstad et al., 2013). However, the tagged fishes still need to be retrieved for downloading data. The recapture rates mainly depend on fishery activity.

Archival electric tags solve one problem: i.e., tagged fish need not be recaptured by the fishery, allowing the movements of tagged fish to be recorded accurately and without biases that can confound the interpretation of migration. Acoustic telemetry is commonly used in marine environments, and radio telemetry is preferred in shallow, freshwater environments. Typical systems include a transmitter (tag) with a unique sound signal and a receiver for detecting the signals when the tag comes within a close range over extended periods(Arnold & Dewar, 2001). Both forms of telemetry can provide data on the environmental conditions the tagged animals experienced, such as depth and temperature, which download by a real-time satellite link or by the receivers. Modern tags may be as small as 5 mm in diameter and have been successfully applied to various juvenile and adult marine animals (Arnold & Dewar, 2001). However, this technology cannot be used on all life stages of fish; the constraints of transducer size and battery volume remain when an extensive range or extended transmission life is required, coupled with small sizes and fragility of early juvenile fishes.

Telemetry experiments typically generate large volumes of data, making the storage, handling, manipulation, and standardized analysis of data challenging (Hartog et al., 2009). As a result, the analysis of telemetry data is often descriptive, and the data are seldom used to test hypotheses directly. Despite generating unbiased and informative data on commercially important fish species, telemetry studies are rarely considered in stock identification, stock assessments, or fishery management in general (Thorsteinsson, 2002; Willis et al., 2009) Finally, transmitters and receivers are relatively expensive, and the financial constraints of many studies often lead to small sample sizes. The transmitters made by one company cannot be detected by receivers made by another company, which may lead to even fewer opportunities to collect data on the movements of a tagged fish (DeCelles & Zemeckis, 2014).

Pop-up satellite archival tags (PSAT) work through the satellite network to upload and communicate data. When the tag monitors constant depth for a predefined period or deeper than limited depth or reaches its programmed release time, it will pop-up and start transmitting a summary of the archived data to polar-orbiting ARGOS satellites. The satellites then transfer the data to base stations on earth. As a consequence, it collects information on the environment of the fish, such as light, pressure, temperature, and fish position at the pop-up time, and stored light, temperature, and depth data can be used to calculate fish movements between be tagged and the pop-up location (Thorstad et al., 2013). The use of PSAT has proved valuable for identification and reproducing the migration histories of large fish such as bluefin tuna in the Atlantic based on recorded light levels and temperatures (Block et al., 2005) However, PSATs are relatively large. They must be attached externally, and should not impede the swimming performance of the fish, which limits the size and species of fish that can be tagged. Larval fish are

mostly less than 10 mm in length. However, the smallest tag is more than 100mm, so larvae are still too small for using external tags, but even if tags were small enough, no matter the insertion of tags into the body or external attachment of tags might affect growth, health, and survival, (Ross & McCormick, 1981), and higher risk of entanglement, erosion of scales or muscles and fungal infection. It also may affect the behaviour and swimming performance of the fish by increasing drag and restricting movements. Moreover, the high mortality during the larvae stage would limit the available sample sizes (Garrido et al., 2015). As a result, the problem of using artificial tagging for tracking larvae fish is still awaiting resolution.

Table 1-1:The advantages and disadvantages of tags

| | Recovered | Advantage | Disadvantages |
|---|---|---|---|
| Traditional External tags | Need | •Applicable to large numbers of fish<br>• Can give a broad geographical and seasonal return distribution<br>•Can not apply to tiny fish<br>• Long tag-retention time | •Information is limited to the identification of the origin of fish<br>• Precision of the information on recoveries may be effect by recoveries<br>come from fisheries |
| DST | Need | •Have sensors to collect and store environmental data such as temperature and depth. Some types could even be monitored and stored physiological data such as heart rate and internal temperature. | •The accuracy of position based on light intensity can be problematical because the bias might come from the cloud cover, differences in the opacity of water, and the depth at which the fish may swim. |
| Acoustic tags & Radio telemetry | Do not need | •Can be attached to juvenile and adult marine animals<br>•Provide surrounding water characteristics that the tagged animals experience | •Cannot be used on all life stages of fish<br>•The tag size and battery volume remain to be restricted by the requirement |

| | | | |
|---|---|---|---|
| | | •Download by a real-time satellite link or by the receivers<br>•Can communicate with and log details of tags that come within close range over extended periods. | for extensive range or extended transmission life<br>•Large volumes of data can make the storage, handling, and manipulation of data very difficult<br>•Few standardized analytical methods have been adopted<br>•Transmitters and receivers are expensive and cannot be detected by receivers made by another company, which often leads to small sample sizes |
| PSAT | Do not need | •Provide data of surrounding water characteristics that the tagged animals experience<br>•Download by a real-time satellite link after release or access archival data when the tag is retrieved. by the receivers<br>•Can communicate with and log details of tags that come within close range over extended periods. | •Tags are expensive, so often be precluded by cost<br>•Attachment might affect growth, health, and survival<br>•Size constraints, with observations mainly restricted to the adult |

## 1.4 Using otoliths as natural tags

Because of the problems related to the artificial tagging of some fish, the use of natural tags to determine fish movement has received greater attention (Elsdon & Gillanders, 2003), including tissue isotopic analysis (Steffan et al., 2013), the use of parasites as biological indicators (Klapper et al., 2016), genetic techniques, and morphological characteristics. However, many of these approaches are limited by the need for reference sample(s) and the inability to identify individual movements. A promising method for individual fish traceability is the use of otolith chemistry

(Campana, 1999). Otoliths are calcium carbonate structures in the inner ear of teleost fishes and they are widely used in fisheries science and management for several reasons. One important use of otoliths is to determine the age and growth of fish. Otoliths form daily growth increments, which can be counted to estimate the age of the fish and provide information on the fish's growth rate and size over time. Another advantage of otoliths is that they are metabolically inert, which means that they continuously incorporate elements or compounds into their growing surface without resorption (Campana, 1999; Elsdon & Gillanders, 2003). This allows researchers to analyse the chemical composition of otoliths and obtain information on the fish's habitat use, migration patterns, and feeding behaviour throughout its entire life.

Otoliths are relatively pure calcium carbonate structures, but they also contain a wide range of trace elements that can provide valuable information about the fish's environment, behaviour, and life history. Some of these trace elements, such as Li, Mg, Mn, Cu, Zn, Sr, and Ba, are potentially useful for tracking habitat use in fish and discriminating among different populations or stocks (Sturrock et al., 2012). Trace element concentrations in otoliths can also be used to determine the natal origin of fish (Fowler et al., 2017; Geffen et al., 2011; Grammer et al., 2017; Smith et al., 2016; Taillebois et al., 2017; Tripp et al., 2020), population structure and dynamics stocks (Turan, 2006; Wang et al., 2018). Additionally, these trace elements can be used to detect migratory timing and habitat utilization patterns of anadromous species, such as salmon and eels (Secor et al., 1995).

Inferring stock identity via otolith chemistry has limitations due to various factors such as diet, ontogeny, and genetics that may affect the interpretation of otolith chemical composition. The contribution of water and diet to otolith chemistry can vary (Jansen et al., 2015; Sturrock et al., 2012; Walther & Thorrold, 2006), and the bioaccumulation of elements through the food chain can also impact otolith composition. This means that diet effects could lead to different otolith chemical compositions even if fish occupy the same habitat. Therefore, the diet will have a confusing effect on reconstructing migratory histories. Changes in otolith chemistry throughout a fish's life due to age-related physiological changes, growth rate, and life stage can further complicate the interpretation of otolith chemistry (Sturrock et al., 2012; Miller & Hurst, 2020). Genetic influences on otolith elemental incorporation also need to be considered. Therefore, otolith trace element chemistry can often only be used to test the most likely match for individual or population of fishes between different populations, rather than as a tool to reconstruct migratory histories. Moreover, technical limitations exist in the marine environment due to the homogeneous distribution of commonly used elements (e.g., Mg, Ca, Sr) in otolith chemical analysis, and differences at a small scale cannot be detected (Sturrock, 2012).

In principle, the age-based analysis of the trace elements in fish otoliths could reflect the chemical composition of the ambient water from the time before hatching to death, providing a detailed record of the environment with timescale to which the fish was exposed. However, in practice, the assay and interpretation of this chemical record remain challenging, primarily due to physiological filters between the water and the otolith as outlined above, and partially because of technical difficulties.

## 1.5 Using $\delta^{18}O$ values to reconstruct migratory histories

The isotopic composition of oxygen in otoliths (hereon referred to as $\delta^{18}O_{otolith}$ values) can be predicted based on the ambient temperature and oxygen isotope composition of the surrounding water. (Kim & O'Neil, 2005). Many recent studies have focused on using the stable isotope ratio of oxygen in otolith aragonite to reconstruct migratory history to overcome the limitations of trace element analyses in reconstructing spatial origin. Unlike trace elements, where spatial-temporal variations in seawater compositions are complex and uncertain, spatial variations in water $\delta^{18}O$ values and temperature generate predictable differences in the $\delta^{18}O_{otolith}$ values in fishes inhabiting different water bodies; hence, $\delta^{18}O$ is a useful temperature proxy when discussing fish migration (Darnaude et al., 2014).

Isotopes are atoms with the same number of protons, but which differ in the number of neutrons. The oxygen isotope $^{16}O$ is dominant and has 8 protons and eight neutrons. However,$^{18}O$ is an isotope with 8 protons and ten neutrons. The slight difference in isotopic masses generates differences in the strength of bonds and the kinetics of reactions or phase changes. Changes in relative abundances of isotopes (termed isotopic fractionation) occur when a chemical, biological, or physical process changes the isotope ratios of the source material. At high latitudes, the discharge of isotopically light river water and glacial meltwater to the sea results in lower sea surface water $\delta^{18}O$ values. For example, the seawater $\delta^{18}O$ value is more than −2‰ lower in many northern polar latitudes. However, tropical areas or highly evaporative regions are rich in $^{18}O$ values where $^{16}O$ evaporates preferentially, such as the subtropical gyres and in semi-enclosed basins (Hobson & Wassenaar, 2018.). Isotope fractionation in nature exhibits variations in both magnitude and direction. The estimation of migration or movement involves comparing the isotopic composition of otoliths with that of the surrounding seawater, considering factors such as seawater temperature.

The isotopic ratios of oxygen from water are incorporated into fish body water at near isotopic equilibrium. However during precipitation of otolith aragonite, oxygen isotopes are fractionated

in an equilibrium process, the extent of fractionation depending on temperature (greater fractionation  at lower temperatures). The thermal sensitivity of isotopic fractionation between water and otolith follows a linear relationship of the form:

$\delta^{18}O_{otolith} - \delta^{18}O_{water} = B - A\ T_{water}$

Here A is the slope coefficient, B is the regression intercept, and $T_{water}$ is the water temperature in °C. $\delta^{18}O_{otolith}$ values show in an inverse relationship with  water temperature, with an increase of approximately 0.25‰ in the $\delta^{18}O_{otolith}$ value per 1°C decrease in water temperature. The slope and intercept of the selected $\delta^{18}O$ fractionation equations may be correlated (r = −0.99). Even though species appeared to cluster to taxonomy and ecology, intercepts differ among taxa( Figure 1-1). The reasons for the differences in the $\delta^{18}O$ fractionation equations between different studies and species require ongoing research (Willmes et al., 2019). Morisette et al. (2022) argue for a common slope across species, but provide evidence that taxon effects may influence the intercepts.

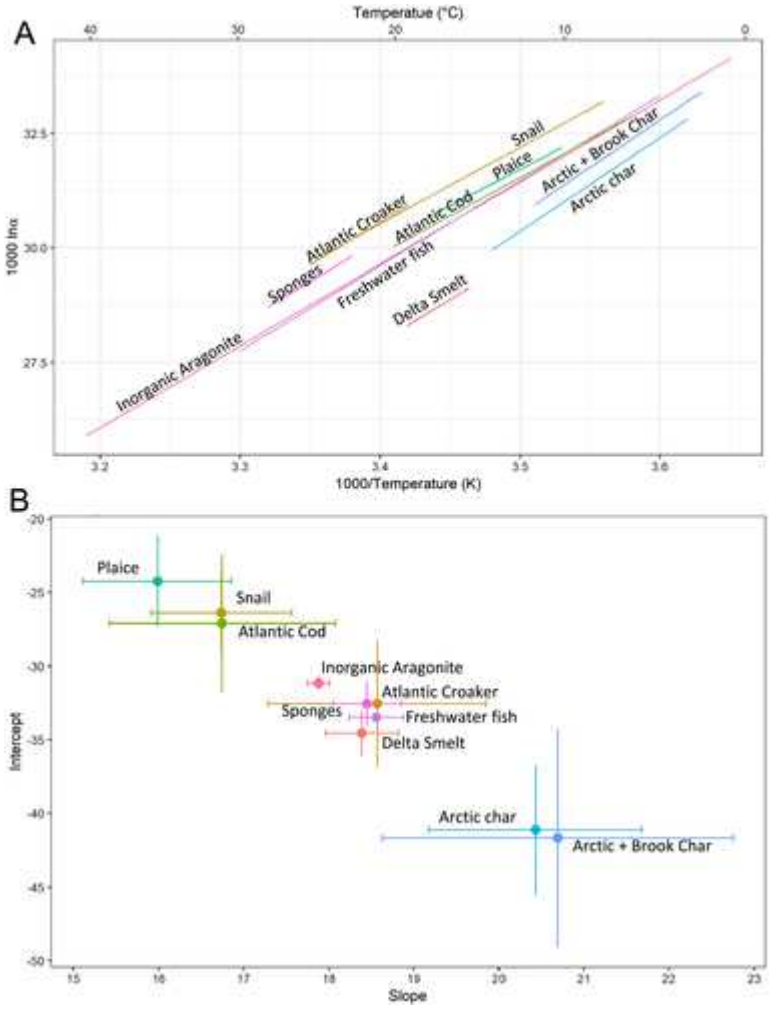


Figure 1-1. (A) Oxygen isotope linear regression models and (B) slopes and intercepts of the temperature fractionation equations (Willmes et al., 2019).

## 1.6 Oxygen isotope records of migration from otoliths

A summary of studies using a stable-isotope approach to track migration in marine fishes is presented in Table 1-2. Oxygen isotopes are useful in providing information on migration in open marine environments, including the location and timing of movement across temperature gradients or between waterbodies with different isotopic compositions.

Table 1-2.Summary of research to date on the use of stable isotopes on otolith in tracking marine migrations in fishes

| Stable isotopes | Reference | Species | Locations |
|---|---|---|---|
| **$\delta^{13}C$, $\delta^{18}O$** | Longmore et al., (2014) | *Coryphaenoides rupestris* | North-east Atlantic Ocean |
| **$\delta^{13}C$, $\delta^{18}O$** | Begg & Weidman, (2001) | *Melanogrammus aeglefinus* | North-west Atlantic |
| **$\delta^{13}C$, $\delta^{18}O$** | Clarke, Munch, Thorrold, & Conover, (2010) | *Menidia media* | North-eastern coast of the United States |
| **$\delta^{13}C$, $\delta^{18}O$** | Trika & Muhling (2010) | *Utjanus griseus* | southern Florida regions |
| **$\delta^{13}C$, $\delta^{18}O$** | Shiao et al., (2009) | *Thunnus maccoyii* | Central Indian Ocean |
| **$\delta^{13}C$, $\delta^{18}O$** | Newman, Allsop, et al., (2010) | *Polydactylus macrochir* | northern Australia |
| **$\delta^{13}C$, $\delta^{18}O$** | Newman, Wright, et al., (2010) | *Scomberomorus semifasciatus* | northern Australia |
| **$\delta^{13}C$, $\delta^{18}O$** | Rooker, Secor, DeMetrio, et al., (2008) | *Thunnus thynnus* | North Atlantic Ocean, Mediterranean Sea |
| | Schloesser et al., (2010) | *Thunnus thynnus* | Canadian waters |
| **$\delta^{13}C$, $\delta^{18}O$** | Shephard et al. (2007) | *Hoplostethus atlanticus* | Porcupine Bank |
| **$\delta^{18}O$** | Sakamoto et al., (2019) | *Japanese sardine* | Kuroshio-Oyashio region |
| **$\delta^{18}O$** | Darnaude & Hunter, (2018) | *Pleuronetes platessa* | North Sea |
| **$\delta^{18}O$** | Hane et al.(2020) | *Thunnus Orientalis* | Pacific Ocean |
| **$\delta^{18}O$** | Higuchi et al., (2019) | *Scomber japonicus* | Kuroshio-Oyashio region |
| **$\delta^{18}O$** | Shiao et al.(2016) | *Alepocephalus umbriceps, Talismania okinawensis, Rouleina watasei, Xenodermichthys nodulosus* | Taiwan waters |
| **$\delta^{18}O$** | Shiao et al.(2010) | *Thunnus orientalis* | Pacific Ocean |

### 1.6.1 Case study- tuna

Atlantic bluefin tuna (*Thunnus thynnus*) are highly migratory, commercially valuable, and under intense fishing pressure. Two separate stocks of this species are managed based on their different spawning areas: the Mediterranean Sea and the Gulf of Mexico. Although it was previously assumed that there was no mixing between these stocks, evidence from genetics (Albaina et al.,

2013) and continued declines in their populations have called this assumption into question. Therefore, it is important to gain a better understanding of the connectivity between the two stocks.

The Eastern region is characterised by waters more enriched in surface water $\delta^{18}O$ due to the high evaporation rates, low riverine input, and restricted circulation compared to the Western region (USA Atlantic Ocean). Otolith $\delta^{18}O$ values can serve as a natural marker for tunas, with differences in $\delta^{18}O$ values between Eastern and Western nurseries used to reliably predict their nursery origin (Rooker et al., 2008; Trueman et al., 2012). The difference between Eastern and Western Atlantic nurseries was found to be greater than inter-annual variability within each nursery, indicating that these biological markers were relatively stable over the investigated period (Fraile et al., 2015). The trans-Atlantic movement of adolescents from east to west was also observed by isotope-based methods (Fraile et al., 2015; Schloesser et al., 2010; Thorrold et al., 2001) and through tagging work (Block et al., 2005), indicating stock mixing. Isotope-based methods for estimating stock origin and trans-oceanic migrations in Atlantic bluefin tuna have been incorporated as stock assessment tools by the International Commission for the Conservation of Atlantic Tuna, highlighting the contribution of isotope-based methods to marine resource management and conservation (Hobson & Wassenaar, 2018). The $\delta^{18}O$ profiles in otolith have also been used to reflect different locations of the first winter signal between tuna with natal origin from the Pacific Ocean and the Japan Sea in a study by Shiao et al.(2010).

### 1.6.2 Case study- deep-water fish vertical migrations

Otolith $\delta^{18}O$ profiles can be used to reconstruct vertical migrations of deep-water fish during their lifetime as many of these fish undergo a pelagic or mesopelagic phase as larvae or juveniles whose locations are difficult to determine through trawl surveys. Several studies have used $\delta^{18}O$ values to reconstruct shifts in the residence depth of deep-water fish. The age-based profiles for stable isotopes of oxygen in otoliths of three commercially important species on the Irish continental slope, including orange *(Hoplostethus atlanticus),* roundnose grenadier (*Coryphaenoides rupestris*) and roundnose grenadier (*Micromesistius poutassou*), were sampled to understand the habitat and metabolic activity (Longmore et al., 2014; Shephard et al., 2007; Trueman et al., 2012). The oxygen isotope and estimated of depth at age show varying allopatric residence depths in *C. rupestris* and *H. atlanticus*, whereas *M. poutassou* shows no evidence of migration to deeper waters. Similarly, isotope-based methods were used in studies by Chang et al., 2015 and Shiao et al., 2017 to analyse four slickhead species, revealing common patterns of shallow pelagic larvae, followed by ontogenetic depth migrations of juvenile life. These studies

demonstrate that the isotope-based method can provide information on both horizontal and vertical migration by reflecting temperature variation.

### 1.6.3 Case study- *Pleuronetes platessa*

In a study of plaice (*Pleuronetes platessa)* conducted by Darnaude et al. *(*2014), researchers used otolith $\delta^{18}O$ values and archival data storage tags to investigate movement ecology of wild plaice. While $\delta^{18}O_{otolith}$ values have been shown to be a reliable tool for stock discrimination and broad-scale geolocation of fish, this study highlighted errors in using otolith $\delta^{18}O$ values to estimate environmental temperature, which may be due to difficulties in reconstructing salinity-related effects on water $\delta^{18}O$ values. The study suggests that salinity variance is often overlooked in studies using otolith $\delta^{18}O$ values, and that the relative changes in seawater temperature or salinity can produce distinct otolith $\delta^{18}O$ values that are unrelated to the temperature $\delta^{18}O$ relationship. While otolith $\delta^{18}O$ values are a useful tool for studying fish populations, it is important to consider the potential impact of salinity variations on these values when estimating environmental temperature.

Otolith isotope analyses are limited by the volume of aragonite required for isotopic analyses. Modern isotope ratio mass spectrometers such as the Thermo Finnegan MAT252 system coupled to a Kiel device acid digestion system can reliably determine $\delta^{18}O$ values from 10-20µg of otolith powder, but this still may represent weeks or months of otolith growth depending on the size and growth rate of the otolith. The development of micro milling and microvolume isotope analysis has enabled researchers to obtain high-resolution otolith $\delta^{18}O$ profiles with accurate sampling at 1/1,000 mm scales and analysis of sub-microgram carbonate samples (>0.2µg)(Nishida et al., 2020).

### 1.6.4 Case study- Japanese sardine

Sakamoto et al. (2019) used microvolume isotope analysis to reconstruct the migration history of an individual Japanese sardine(*Sardinops melanostictus*) with high resolution from the core and edge of the otolith and combine a high-resolution otolith stable oxygen ratio profile and numerical simulation to reproduce fish migration history. They successfully reconstructed migration history with high resolution around the core (20 to 30 d) and edge (10 to 15 d) by using microvolume isotope analysis (measured by continuous-flow IRMS (CF-IRMS)).

The study showed that this method could be a valuable alternative to tagging and electronic loggers for revealing migration routes in early life stages. However, the study also highlighted the challenge of estimating temperature history and migration routes from otolith $\delta^{18}O$ profiles alone

without salinity data and precise estimates of water $\delta^{18}O$ values. Therefore, to achieve accurate geolocation using biomineral $\delta^{18}O$ values, precise estimates of water $\delta^{18}O$ and/or salinity data are required. The uncertainty surrounding these factors currently limits the precision of geolocation using otolith $\delta^{18}O$ values alone. Nonetheless, the development of micro milling and microvolume isotope analysis represents a significant advancement in the study of fish migration patterns and provides valuable insight into the early life stages of fish.

It is important to note that otolith $\delta^{18}O$ values can provide valuable information about the latitudinal movements of fish as changes in water temperature and isotopic compositions can be reflected in the otolith. However, it is challenging to estimate longitudinal positions based on otolith $\delta^{18}O$ values, as temperature and salinity vary less and less predictably by longitude.

To estimate potential movements across temperature and/or salinity gradients, it is necessary to have information on water temperature and isotopic compositions. With this information, differences in otolith $\delta^{18}O$ values between distinct water masses can be estimated, allowing for the tracking of potential movements. Therefore, while the development of micro milling and microvolume isotope analysis has allowed for high-resolution otolith $\delta^{18}O$ profiles, there are still limitations to the method, and additional data on water temperature and isotopic compositions are required for accurate geolocation. The uncertainty of high-resolution scale environment information and the difficulties of sampling can make it challenging to use otolith $\delta^{18}O$ values to reconstruct movements across smaller thermal and/or salinity gradients. As a result, the method is mainly used to reconstruct movements across larger thermal and/or salinity gradients.

## 1.7 Using individual-based migration models (IBM) to estimate migrations

Numerical simulation models are constructed using a set of mathematical equations, relying on computers to obtain approximate solutions to underlying physical problems. These models include various types, such as climate models, atmosphere-ocean physics models, and biogeochemical models, each designed to simulate different aspects of the Earth's systems. For example, the Intergovernmental Panel on Climate Change (IPCC) Earth System Model efforts, particularly the models in Phase 6 of the Coupled Model Intercomparison Project (CMIP6), emphasize common forcing and diagnostics through 21 dedicated model intercomparison projects (MIPs) (Eyring et al., 2016). Central to these efforts are "framing pathways," which provide consistent drivers like emissions and land surface states, enabling the development of climate futures and supporting impact and vulnerability studies (Frieler et al., 2024; Warszawski et al., 2014). These pathways integrate across IPCC's physical science, impact, and socioeconomic

communities, forming the backbone for scenarios explored in CMIP6, including those in the ScenarioMIP component (Riahi et al., 2017; O'Neill et al., 2016). In recent years, simulation modelling also integrated with biology to form Biophysical models. Biophysical models have become increasingly important tools in fisheries management, as they can predict the connectivity within stocks and early life stage dispersal. These models use mathematical techniques to represent and simulate physical and biological oceanographic processes, allowing for the examination of complex relationships between environmental factors and fish migration.

One of the main benefits of biophysical models is that they can predict likely developments that have not been observed or proved directly by incorporating high-resolution temporal and spatial oceanographic data, combined with existing survey datasets (Röckmann et al., 2011). This allows for more accurate predictions of fish populations and can inform management decisions. Another benefit of biophysical models is that they can be used to analyse ecological and environmental interactions in detail. To put these models into practice, early-life-stage transport patterns obtained from hydrodynamic models can be coupled with ongoing field-sampling programs. This approach allows researchers to predict the movement of fish populations more accurately and can be used to develop more effective management strategies (Hinrichsen et al.,2011).

Individual-Based Models (IBMs) within biophysical models are popular tools for simulating the movements and spatial distribution of hatchlings and juveniles in ecological systems. Unlike traditional models, IBMs capture the complexity of individuals throughout their life cycle, incorporating factors like life history, age classes, real-time adaptation, and environment modification based on individual behavior. Many models use the assumption that juveniles drift passively with the ocean current. It means that the swimming activity of fish during the larvae stage is considered very limited. Even for older individuals, current induced drift is seen as a major effect of the movement (Gaspar et al., 2012). In these models, trajectories of thousands of particles, each representing a single individual, are simulated using readily available Lagrangian particle-tracking software fed with surface currents produced by ocean circulation models. These trajectories are then used to characterize the spatial distribution of the studied population and its evolution with time (Gaspar & Lalire, 2017; Scott et al., 2014). Recently, numerous examples of individual-based migration models have been developed to estimate migrations of the fish's life history (Christensen et al., 2008; Okunishi et al., 2012; Sigurthsson et al., 2009).

Models are an inexpensive, practical alternative to extensive sample collection. However, it is important to note that IBMs are not without limitations. One significant limitation is that they assume that individuals in the population are identical and that they are not affected by genetic, physiological, or behavioral differences. This is a critical assumption, as individual differences in

behavior, physiology, or genetics can affect migration behavior, and failing to account for these differences can lead to biased estimates of population dynamics (Miller et al., 2017).

Additionally, the accuracy of individual-based models relies on the accuracy of input data, such as spawning area, migration depths, migration period, obtaining accurate and reliable data can be challenging in marine environments, which may have errors and uncertainties. Therefore, it is essential to validate the model results with empirical data to ensure their accuracy and reliability. However, validating model results with empirical data can also be challenging in marine environments due to logistical constraints and difficulties in sampling. Thus, a comprehensive and collaborative approach that integrates multiple data sources, such as tagging studies, otolith chemistry, and oceanographic surveys, is often necessary to validate the model results effectively.

## 1.8 The Importance of individual energetics for IBM Models

Animal movement is driven by the individual's available energy, creating a strong link between physiology and movement patterns. The study of energetics can provide a basis for predicting movement patterns and responses to environmental changes (Malishev & Kramer-Schadt, 2021), making it a valuable metric for describing movement ecology and can be used as a performance-based predictor of fish habitat suitability (Del Raye & Weng, 2015). Process-based approaches, like individual-based models (IBMs), can simplify the study of movement ecology by focusing on common mechanisms that connect behavior to fitness consequences across scales. DEB-IBMs are a type of IBM that uses Dynamic Energy Budget theory to capture energy uptake and use by individuals (Kooijman & Kooijman, 2010), connecting ecology and physiology from first principles. By incorporating energetics frameworks, it is possible to model movement patterns of individuals with universal, internal mechanisms (e.g., Gallagher et al.,2021) for marine mammal population dynamics. Metabolic rate, which influences habitat suitability and growth rate, also informs bioenergetic models. Fish metabolism is closely tied to temperature, making it a critical predictor of energy and oxygen requirements and growth potential. However, laboratory-based respirometry experiments may not fully represent natural conditions (Jutfelt et al., 2018), and field metabolic rates in marine ecosystems can be challenging to measure.

Recent studies have demonstrated the potential for retrospective estimation of field metabolic rate (FMR) in teleost fishes using the stable isotopic composition of carbon in otolith aragonite (Chung et al., 2019; Martino et al., 2020; Trueman et al., 2019). Otolith biomineral contains carbon from two sources: dissolved inorganic carbon (DIC) in the ambient water and respired dietary carbon. The isotopic difference between these two sources allows for the approximation of the proportion of metabolic carbon in the otolith ($C_{resp}$) through a two-component mixing

model. This new method enables the determination of individual-level variations in FMR expressed by fish in their natural environment in response to external conditions experienced (Trueman et al., 2019).

## 1.9 Research gaps

This review emphasizes the importance of tracking habitat transitions in larval fish and the limitations of artificial tagging for small fish. Isotope-based methods are superior to trace elements in reconstructing individual migration paths. Recent developments in high-precision micro-milling systems and microvolume isotope analysis (such as SIMS $\delta^{18}O$ otolith analysis and continuous flow isotope ratio mass spectrometry system (CFIRMS) show great promise for revealing early life stages of mobile pelagic fish larvae such as Japanese sardine, chub mackerel, and bluefin tuna. However, high-precision micro-milling and isotope analysis systems are expensive, and time-consuming, and isotope analysis systems cannot differentiate small differences in values; therefore, this method can currently only be applied when fish migrate across large thermal and/or salinity gradients. Hence, predicting when high-resolution otolith isotope analyses might produce accurate results can save resources and expand the scope of this research method.

While models can be cost-effective and efficient in providing predictions, they may not always capture local-scale details of the system or process being modeled. Additionally, models are based on certain assumptions, and these assumptions may introduce uncertainties that can be difficult to verify empirically. Therefore, it is important to evaluate the reliability and accuracy of models carefully, especially when they are used to inform decisions with significant consequences. It is also essential to continuously improve and update models as new data and information become available to minimize uncertainties and improve their predictive capabilities.

Fish metabolism is an essential parameter for modelling the behavior and dynamics of fish populations in aquatic ecosystems. However, accurately measuring fish metabolic rates in natural conditions can be challenging, as laboratory-based respirometry experiments may not fully represent the range of environmental conditions that fish experience in the wild. Additionally, obtaining field metabolic rates for individual fish in marine ecosystems can be difficult and time-consuming. Isotopic approaches to recovering experiences metabolic rates in wild fishes are promising, and the required isotopic data is provided alongside solution-based analyses of $\delta^{18}O_{otolith}$ values, offering coupled insight into movement paths, experienced temperatures and the resulting energetic expenditure.

## 1.10 Thesis aims, objectives, and structure

### 1.10.1 Thesis aims and objectives

Isotope-based methods, like high-precision micro-milling systems and microvolume isotope analysis, show promise for understanding early life stages of pelagic fish larvae. However, their cost and dependence on environmental gradients require careful consideration. Cost-effective models should be cautiously assessed for reliability, while isotopic approaches for measuring fish metabolic rates offer valuable insights into movement paths and energetic expenditure, improving our understanding of fish population dynamics. Until now, only a scant number of studies have merged these two methodologies, overlooking the promising opportunity to extract a rich array of mutually reinforcing information. This thesis aims to bridge the gap between theoretical modelling and empirical data by using the otolith isotope-based method to improve our understanding of the early life history characteristics of fish and their responses to environmental changes (Figure 1-2).

The first objective involves using particle drift modelling to determine whether high-resolution otolith analyses of North East Atlantic mackerel larvae can discriminate among different larvae drift scenarios. This could inform management strategies for mackerel populations and help us better understand the behaviour of larval fish.

The second objective involves extending drift analysis with different swimming vectors to explore the potential of using otolith $\delta^{18}O$ to distinguish between successful and failed drifts, and to verify the hypothesis that North Atlantic Oscillation (NAO) affects eel migration. This could help us better understand the migration patterns of eels and how they may be affected by changing ocean conditions.

The third objective aims to estimate the thermal performance curve of field metabolism in a wild juvenile fish and investigate how temperature affects fish metabolism. This could help predict how fish populations will respond to climate change and provide insights into the thermal sensitivity of fish.

The thesis aims to represent the initial effort in employing an ocean model to predict the potential of high-resolution otolith analyses and applying it to improve the experimental design response, addressing the limited integration of otolith chemistry and migration models in existing studies. This research stands as the sole means to verify the efficacy of the model and proposes recommendations for model design and field sample collection. By combining field-collected biological samples (otoliths) with virtual model simulation methods, an attempt is made to

overcome current limitations in otolith applications for studying the movement of larval fish. The study also tests assumptions of individual biological models and the realism of simulations. These breakthroughs in application seek to understand how the environment influences the migratory behavior of larval fish—a crucial aspect for resource management.

Despite difficulties in sampling, otoliths serve as valuable records of growth, environmental characteristics, and acquisition of preservable traits. Coupled with high-resolution model simulations of environmental factors, they provide invaluable data. Moreover, otoliths, capable of recording the growth of larval fish, shed light on energetics, offering a basis for predicting movement patterns and responses to environmental changes. This makes otoliths a valuable metric in describing movement ecology and a performance-based predictor of fish habitat suitability. Therefore, this study also attempts to develop a newly developed proxy to measure in-situ field metabolic rate (FMR) in wild juvenile fishes. Future changes in temperature or food availability could potentially alter their aerobic scope. The otolith FMR serves as a valuable monitoring tool for assessing eco-physiological vulnerability in wild populations. Furthermore, the study explores the potential of otolith isotope records to verify hypotheses in an eel migration model. Various hypotheses related to the impact of environmental variability on eel migration behavior are investigated, particularly the influence of the NAO index on migration routes and its consequent effects on migration success rates. This investigation contributes to a deeper understanding of the intricate relationship between environmental factors and eel migration dynamics.

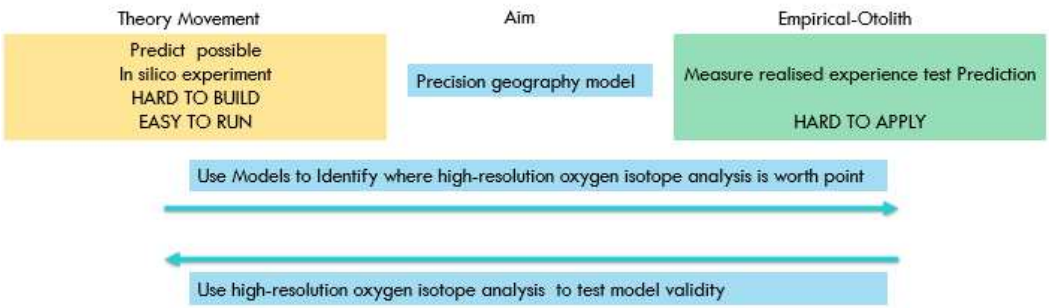


Figure 1-2. This study aims to build the gap between model and otolith chemistry. The flow diagram shows how the model can inform otolith chemistry when reconstructing high-resolution movements and how analysis in the field of the information can be fed back to develop a model built.

### 1.10.2 Thesis structure

Chapter 1- Definitions: Otolith toolkit

Chapter 1 provides a review of the importance and difficulties of tracking the early life history migrations of fish larvae. Additionally, it presents definitions of key concepts related to the otolith toolkit, which will be utilized throughout the thesis.

Chapter 2-Predicting high-resolution otolith isotope ratios along passive drift trajectories to shed light on early life history migrations: A case study with Atlantic mackerel. Chapter 2 will focus on testing the potential of using the otolith oxygen isotope-based method to reconstruct larval drift scenarios. Specifically, I apply the drift model to predict high-resolution otolith isotope ratios along passive drift trajectories for a case study with Atlantic mackerel. This involves drawing on particle drift modelling techniques to predict the oxygen isotope time file. This chapter provides insights into the usefulness of otolith analyses in understanding larval fish behaviour and may inform management strategies for mackerel populations.

Chapter 3- Predicting high-resolution otolith isotope ratios along basin-scale trajectories with and without simulated swimming to inform early life history migrations: A case study with European Eel. In Chapter 3, I focus on predicting high-resolution otolith isotope ratios along trajectories with and without simulated swimming to inform early life history migrations. This chapter features a case study with the European Eel, where I will draw upon particle drift modelling techniques and predict the oxygen isotopes time file. By doing so, I aim to understand the potential of using otoliths to verify the hypothesis that NAO affects eel migration. This research could provide valuable insights into the migration patterns of eels and how they may be impacted by changing ocean conditions.

Chapter 4-Investigates the thermal sensitivity of field metabolic rate in wild Atlantic mackerel, which is a fundamental assumption in the IBM model. I conduct the first in-situ measurements of field metabolic rate in this species and explore the scaling of $C_{resp}$ values with body mass and temperature of Northeast Atlantic mackerel. This chapter provides valuable insights into how temperature affects fish metabolism and may help predict how fish populations will respond to climate change.Chapter 5-Conclusion

Chapter 5-Synthesizes information across the thesis and discusses the potential and limitations of the isotope-based method and IBM in understanding fish movement. This chapter provides a personal perspective into the potential of using otolith chemistry and individual-based migration models to improve our understanding of the early life history of small fish and their migration patterns, which can have important implications for the conservation, management, and recovery of fish stocks.

# Chapter 2 Stable isotope-enabled particle drift models predict where high resolution isotope analyses can discriminate among larval trajectories in Atlantic mackerel.

**Abstract**

Marine fish commonly transition across distinct habitats throughout their lifetimes, particularly during the larval stages, when they are especially difficult to track. Such transitions are necessary as environmental demands and predation pressures change dramatically with increases in body size. Fish larvae suffer high natural mortality rates, and varying environmental experiences during early life stages can have a large impacts on population demographics. Understanding the nature of habitat use, habitat connectivity, and ontogenetic timing of habitat transitions is therefore key to establishing effective management practices covering whole life histories for commercially, recreationally, and ecologically significant species. Tracing individual larval movements is challenging as larvae are too small for most conventional tagging approaches, and because of the high natural mortality. Otolith chemistry is an attractive alternative for reconstructing fish movements where movements occur across suitable chemical gradients. The stable isotope composition of oxygen in otolith aragonite is a valuable tracer, being predictably related to widely measured and/or modelled ocean variables (temperature and salinity). Emerging high resolution analytical methods enable the subsampling of larval otoliths and the generation of time-resolved isotopic records that potentially reveal larval movements. However, such analyses are logistically challenging and costly, preventing their routine use. A priori determination of when such approaches are likely to generate useful information would enable tailored and cost-effective design for high resolution otolith isotope projects. Here we develop isotope-enabled particle drift models a to predict whether high-resolution otolith analyses of northeast Atlantic mackerel (*Scomber scombrus*) larvae have the potential to discriminate among potential spawning origins or different larvae drift scenarios trajectories. Larval drift simulations were conducted from March to July 1998. The simulations revealed distinct drift patterns associated with four spawning areas. The drift pathways and timescales varied significantly between regions, with larvae in the southern spawning areas remaining near their spawning areas, while those in the western regions exhibited more complex and extensive northward movements. The simulations also predicted the ambient salinity and temperature experienced by drifting larvae, which in turn influenced the oxygen isotope ratios ($\delta^{18}O$) predicted to be recorded in otoliths. Predicted $\delta^{18}O$

values in otoliths varied spatially and temporally, and mean $\delta^{18}O_{otolith}$ values differed significantly between some spawning areas, with higher values observed in the western areas compared to the North Sea. The study highlighted the potential of $\delta^{18}O_{otolith}$ as a natural tag for identifying the geographic origin of mackerel larvae. We identify key regions of the otolith (corresponding to periods of drift) most likely to discriminate among spawning origins, and therefore potentially focussing targeted high resolution analyses . By comparing $\delta^{18}O_{otolith}$ values in the otolith core and marginal areas, it is possible to infer the spawning origin and drift pathways of the fish. Results suggest that a combination of low-resolution and high-resolution otolith sampling could effectively discriminate between different spawning areas and improve our understanding of larval drift patterns. The potential and limitations of using $\delta^{18}O_{otolith}$ to identify early life history characteristics are also discussed. The results suggest that the method is directly transferrable to species with pelagic larval stages and may help to focus resources on species and regions where larval drift questions are reasonably tractable using stable isotope tracers.

**Key words:** $\delta^{18}O$, otolith, larvae distribution, particle drift

## 2.1 Introduction

Understanding the nature of habitat use, habitat connectivity, and ontogenetic timing of habitat transitions is key to establishing management practices covering whole life histories for commercially, recreationally, and ecologically significant species (Chiang et al., 2020; Hining et al., 2000; Nishida et al., 2020; Sakamoto et al., 2019). While artificial tags are a common tool for tracking fish and their environments, they are typically too large to use on larvae. Otoliths, which are calcium carbonate structures in the inner ears of fish, contain a record of the daily growth increments and an archive of the oxygen isotope ratio (expressed as $\delta^{18}O$ values), which varies according to the $\delta^{18}O$ value of ambient water and experienced ambient water temperature (Kim and O'Neil 2005). Isotope-based methods, notably $\delta^{18}O$ analysis of fish otoliths, are extensively used to trace the habitat transition of many fish species. This technique can trace experienced water temperature without the need for artificial tag attachment (Higuchi et al. 2019; Lin et al. 2012; Sakamoto et al. 2019). Changes in the isotopic composition of an otolith can provide information about movement across temperature gradients or between different water masses characterised by distinct temperatures and/or $\delta^{18}O$ values This method has been used to track both horizontal and vertical fish migration (Longmore et al., 2010; Vieira et al., 2019, Sakomoto et al 2019). Recent developments in high-precision micro-milling systems and microvolume isotope analysis (such as secondary ion mass spectrometry (SIMS) $\delta^{18}O$ otolith analysis and continuous flow isotope ratio mass spectrometry system (CFIRMS) has enabled accurate $\delta^{18}O$ analysis ($<\pm0.1‰$) of $CaCO_3$ at amounts as low as 0.2 µg. These methods have been applied to yield the high resolution analyses of $\delta^{18}O$ values of early life stages of Japanese sardine, chub mackerel, bluefin tuna and Pacific cod(Hane et al., 2022; Helser et al., 2018; Muto et al., 2022; Sakamoto et al., 2019; Sakomoto, 2024).

Although most commercially important marine fish species undergo pelagic egg and larval life stages, relatively few studies have applied isotope-based methods to pelagic larvae in marine environments. The limitations of such methods to the larval stages include: 1) the challenge of collecting recently hatched larvae from open marine ecosystems; 2) the limited amount of calcified material deposited at the natal origin and early larvae stages; 3) analytical difficulties in detecting differences in oxygen isotope ratios where environmental gradients are potentially less pronounced. These constraints, coupled with the high costs and time-consuming nature of high-precision micro-milling systems and microvolume isotope analysis, hinder the broader application of this method. However, the micro-sampling approach surpasses traditional tagging constraints and proves beneficial in revealing population structure and early life transport particulaly in successfully recruited individuals. This information is crucial for understanding the environmental conditions necessary for fish survival, providing insights into how environmental variabilities drive

fluctuations in fish populations. The high practical costs and time-demanding nature of micro-volume isotope analyses means that it would be highly beneficial to predict *a priori* when high-resolution otolith isotope analyses might yield informative results, allowing for a more effective and widespread application of isotope-based methods.

Individual-Based Models (IBMs) offer a comprehensive approach to capturing the intricacies of individual organisms throughout their life cycle. These models incorporate various factors such as life history, age classes, real-time adaptation, and environmental modification based on individual behaviour. IBMs have gained popularity as effective tools for simulating the movements and spatial distribution of early life stages of marine species, specifically hatchlings and juveniles, when swimming ability is considered to be very limited. During this period, the current-induced drift is a major driver of fish movement (Gaspar et al., 2012). Particle drift models thus form a core input for simple IBMs in which trajectories of thousands of particles, each representing a single individual, are simulated using readily available Lagrangian particle-tracking software fed with surface currents produced by ocean circulation models. These trajectories are then used to characterize the spatial distribution of the studied population and their evolution with time(Gaspar & Lalire, 2017; Scott et al., 2014).

Recently, numerous individual-based migration models have been developed and used to simulate ontogenetic migrations for various fish species (Christensen et al., 2008; Okunishi et al., 2012; Sigurthsson et al., 2009). By using IBMs, researchers can incorporate various environmental and biological factors that influence migration, such as ocean currents, water temperature, salinity gradients, and fish behaviour in response to habitat cues. IBMs provide a detailed, dynamic view of fish migrations by simulating individual behaviours and interactions with the environment. This approach not only enhances our understanding of fish life histories but also aids in the conservation and management of species by predicting how changes in the environment might impact essential migratory behaviours. For example, Okunishi et al. (2012) applied an IBM approach to model the migrations of Atlantic herring and Japanese sardines, integrating biological responses to environmental conditions, particularly temperature. Their model demonstrated how the migration of Japanese sardine larvae and juveniles is influenced by sea temperature and ocean currents. Models offer an inexpensive, practical alternative to extensive sample collection but generally lack local-scale detail and are based on critical assumptions—such as the location of spawning grounds and the timing of individual migrations.; hence, without in situ validation, the results are complicated to verify empirically, presenting inherent uncertainty.

Nonetheless, particle drift models generate plausible larval drift trajectories associated with fish spawning behaviour. When combined with hydrographic models predicting water temperature and salinity at high temporal resolution, particle drift model output can be used to predict the isotopic composition of otolith aragonite growth during each timestep of a drift simulation (Sakomoto et al 2019, Sakomoto 20204). This synthetic approach allows for exploration of the sensitivity of isotopic composition in otoliths, prior to committing to costly laboratory analysis. By coupling modelled drift and isotope-based methods, this approach not only provides insights into the characteristics of early larval life but also improves our understanding of the technique's limitations.

Atlantic mackerel *Scomber scombrus* is an ideal model species to test the combined use of modelled drift and isotope-based methods for the following reasons: (1) Mackerel are pelagic (Jansen et al., 2012), predominantly found in the upper 50 m (Bartsch, 2005); (2) mackerel larvae drift passively; (3) early growth rates are high and vary between individuals (D'amours et al., 1990); (4) precise otolith microstructure in mackerel ideally suits the development of a precise milling technique.

The Northeast Atlantic mackerel (NEAM) spawning season starts in late January along the Spanish and Portuguese coasts, reaching a peak in April, followed by Western stocks from March to June and North Sea stocks in June. However, in the late 1960s-70s, NEAM's spawning collapsed, shifting northward. Recent observations suggest mackerel expansion around Iceland during warm North Atlantic periods, potentially linked to rising NEA summer temperatures. Yet, due to gaps in understanding the relationship between mackerel juveniles drifting and their environment, knowledge is lacking on climate change impacts on mackerel habitat patterns (Berge et al., 2015; Trenkel et al., 2014). The focus here on mackerel ideally provides insights into the spawning and nursery grounds and can inform the management and conservation of their populations. Additionally, knowledge of the early life history of mackerel can help to improve the accuracy of stock assessments.

Variation in temperature and salinity levels in the different marine environments where mackerel spawn can have a significant impact on their isotopic signatures recorded in their otoliths. The North Atlantic Current (NAC)(Figure2-1) brings warm, high salinity surface waters into the Northeast Atlantic. These waters subsequently circulate around the subpolar gyre, subject to cooling and freshening (Stendardo et al., 2020). Meanwhile, cold fresh polar surface waters enter the region via the East Greenland Current through the Denmark Strait , with a smaller addition of isotopically light glacial meltwater from Greenland glaciers (Azetsu-Scott and Tan, 1997). Local river inputs around the Iberian Peninsula, France, and the UK have a minor contribution to the

region (Benetti et al., 2017). The Northeast Atlantic is characterized by intermediate salinity due to the mixing of source waters with a range of salinity and associated $\delta^{18}O$ values. In contrast, North Sea water is a mixture of relatively saline Atlantic inflow, brackish Baltic outflow, and locally important river inputs rivers (Mikalsen and Sejrup, 2000). This mixing of different water sources results in varying salinity levels and $\delta^{18}O$ values in the North Sea region.

Here, we utilized individual-based drift models to predict the environmental conditions experienced by north east Atlantic mackerel (NEAM) during early life stages and their resulting $\delta^{18}O_{otolith}$ values under different drift scenarios. By analysing predicted values, we investigated whether larval drift tracks could lead to systematically different $\delta^{18}O_{otolith}$ values to determine the potential for isotope-based tracking in guiding sample selection for high-resolution isotope analyses.

To assess the accuracy of isotope-based tracking, we used large ensembles of virtual particle trajectories and examined the spatial-temporal variability of ambient temperature and salinity during drift history. The isotopic composition of water bodies experienced by drifing particles was estimated based on modelled salinity and published relationships between salinity and water $\delta^{18}O$ values. Finally water temperature (from models) and reconstructed water $\delta^{18}O$ values were used to predict otolith $\delta^{18}O$ values at each timestep of the model. By coupling modeled drift with isotope-based methods, our approach not only provides insights into the characteristics of early larval life such as life history trait, migration, population structure, stock fluctuation and its connectivity with population structure but also enhances our understanding of the limitations of these techniques. This synthetic approach to estimate cost-effictiveness contributes to methodological advances, and it is crucial to anticipate when high-resolution otolith isotope analyses might be expected to yield precise results. The rest of the chapter is outlined as follows. In Section 2, I outline methods for virtual particle tracking (Sect. 2.1) and for estimating seawater and otolith $\delta^{18}O$ (Sects. 2.2, 2.3). In Section 3, I present predicted larvae drift in terms of distribution (Sect. 3.1) and timing (Sect. 3.2), followed by consideration of the associated ambient environment (Sect. 3.3), inferred otolith isotopic ratios (Sect. 3.4). In the discussion, I consider the implications of simulated otolith data for field sampling (Sect. 4.1), and the utility of otolith $\delta^{18}O$ values as "natural tags" of a target species. In conclusion (Sect. 5), I summarize key findings and reflect on the prospects for wider application of otolith analysis for surveying and assessing fish populations, from a life cycle perspective.

## 2.2 Methods

I first outline the particle tracking calculation (Sect. 2.1) (Figure 2-1), providing the Lagrangian data used to predict local oxygen isotope fractions in seawater (Sect. 2.2) and otoliths (Sect. 2.3).

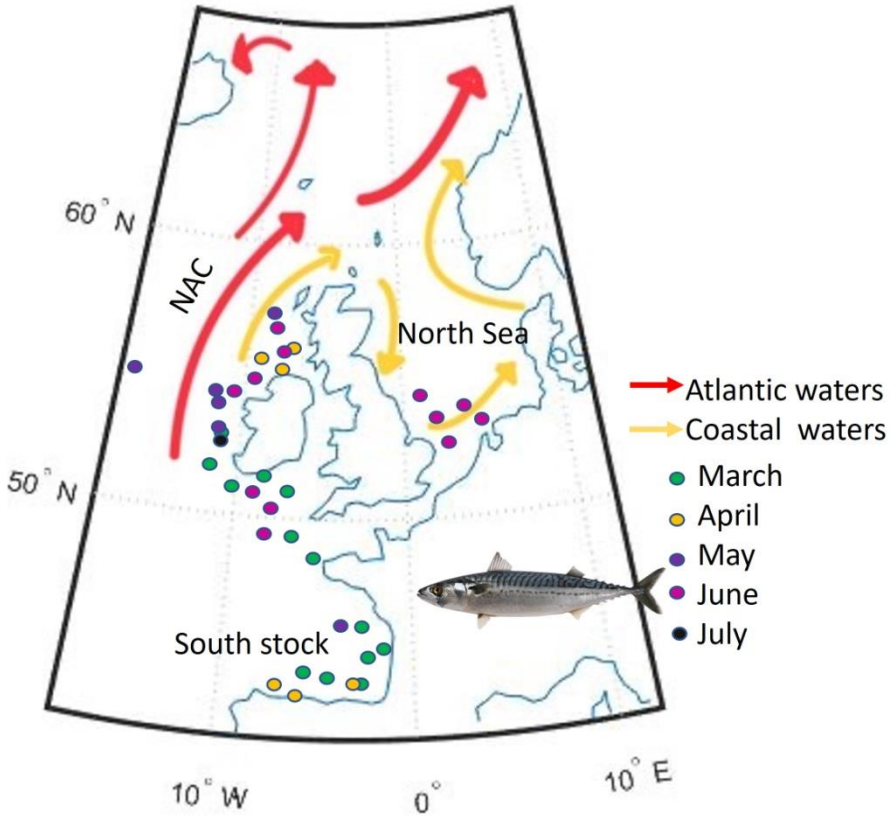


Figure 2-1. The study area and simulated spawning area during the study period, and the circulation pattern of the North Atlantic Current (NAC- red line), and shelf edge / coastal circulation current (yellow line).

### 2.2.1 Particle tracking

Northeast Atlantic mackerel (NEAM) eggs and larvae are here regarded as virtual 'particles' that passively drift with ocean currents, with no active movement, or movement in response to external stimuli. To efficiently calculate the trajectories for a large ensemble of such particles, we use the ARIANE mass-preserving algorithm (Blanke & Raynaud, 1997), developed at the Laboratoire de Physique des Océans (LPO, Brest, France) for use with output from the NEMO (Nucleus for European Modelling of the Ocean, Madec, 2008) family of Ocean General Circulation Models. Output used here is averaged 5-daily from a hindcast spanning 1988 that was undertaken with the eddy resolving ORCA12 configuration setup of the DRAKKAR project (e.g.,Blaker et al.,

2015; Duchez et al., 2016; Marzocchi et al., 2015) The ORCA12 configuration has a horizontal resolution of 1/12° and 75 vertical levels, with finer grid spacing near the surface.

Particles are released monthly from March, starting during the spawning season, based on mackerel egg survey data from 1998. The releases continue until July, subsequently, the particles were tracked for 100 days, as mackerel beyond this duration were considered to possess swimming capabilities that could potentially impact the accuracy of passive drift models from the release. Since mackerel spawn near the water surface, particles were released from a depth of 14 meters at 415 initial positions obtained from the actual survey conducted in 1998. To enhance simulation accuracy, particles were released 120 times per hour for five days. Along with position and time, the ambient temperature and salinity were recorded. The particle ensemble is statistically analysed on a 0.5° × 0.5° grid by calculating the average age, temperature, and salinity, of particles passing through each 0.5° grid cell, considering the entire 100-day duration of each experiment. To evaluate particle dispersal, particle density is calculated as the number of particle occurrences per 0.5° grid cell divided by the total number of particle occurrences throughout the experiment.

The NEAM spawning season starts from the southern spawning, along the coast of Spanish and Portuguese waters in late January. Spawning peaks in April and is followed by western stock spawning from March to June (Berge et al., 2015; Cunningham et al., 2007), and northern stocks in the North Sea in June (Cunningham et al., 2007; Jansen et al., 2012). Particles were released at locations based on the surveys of 1988 ICES triennial mackerel egg survey data (Table 2-1). Particles were released hourly for 5 days from all release sites recorded between March and July over 1998. Considering that larval and early post-larval stages extend to 50-100 days, while residing predominantly in the upper 50 m (Bartsch, 2005), we simulated drift for 100 days from an initial depth of 14 m.

Table 2-1. Initial Particles released position and number during the study periods.

| *year* | *month* | *number of initial position* | *start position (latitude)* | | | *start position (longitude)* | | | *Total release* |
|---|---|---|---|---|---|---|---|---|---|
| *1998* | 3 | 120 | 43.45 | ~ | 53.25 | -12.72 | ~ | -1.75 | 14400 |
| | 4 | 95 | 42.75 | ~ | 56.25 | -10.24 | ~ | -1.75 | 11400 |
| | 5 | 55 | 43.37 | ~ | 56.75 | -14.25 | ~ | -1.50 | 6600 |
| | 6 | 133 | 43.65 | ~ | 60.00 | -12.29 | ~ | 8.00 | 15960 |
| | 7 | 7 | 52.25 | ~ | 55.74 | -14.26 | ~ | -9.28 | 840 |

### 2.2.2 Seawater $\delta^{18}O$ estimate

The temperatures and salinities of ambient water in the NEMO hindcast corresponding to each predicted cell occupied by a drifting particle were extracted and used to predict corresponding oxygen isotope ratios of the ambient water ($\delta^{18}O_w$). These $\delta^{18}O_w$ predictions were inferred from salinity (*S*), using two different regional regressions between $\delta^{18}O_w$ and salinity. In the Northeast Atlantic, the linear regressions relating salinity to $\delta^{18}O_w$were calculated as follows:

Northeast Atlantic: $\delta^{18}O_w = 0.47S - 16.06$ (1)

North Sea: $\delta^{18}O_w = 0.274S - 9.3$ (2)

The Northeast Atlantic regression follows the measurements from surface waters (Benetti et al., 2017), and the North Sea regression follows earlier studies (Darnaude et al., 2014; Harwood et al., 2008a).

### 2.2.3 Otolith $\delta^{18}O$ estimate

The isotopic composition of oxygen in the otolith, $\delta^{18}O_{otolith}$, was predicted from an isotopic equilibrium expression recently proposed for Japanese Mackerel (Nakamura et al., 2020), given ambient $\delta^{18}O_w$ and temperature,

$$\delta^{18}O_{otolith} - \delta^{18}O_{seawater} = -0.25\ T + 4.46 \quad (3)$$

The time series of $\delta^{18}O_{otolith}$ is thus constructed from temperature and salinity along particle trajectories representative of drifting mackerel larvae.

The bulk isotopic composition of the otoliths was recalculated based on the daily growth width, following the method of Cotano et al. (2003), to estimate the proportion of elements within the otolith and their contribution to the overall composition.

## 2.3 Results

Commencing with the drift experiments, I first examine the distribution of passively drifting particles (i.e. mackerel larvae), while the local mean age of particles indicates drift timescales. I then focus on the along-trajectory temperature and salinity that are key to predicting the isotopic ratios that would be recorded in the otoliths. Using this information, I then infer $\delta^{18}O_{otolith}$ values.

### 2.3.1 Prediction of larval transport

The simulation results were presented in terms of mean particle density and age, as depicted in The dispersal of particles was found to be concentrated along the shelf-edge, ranging from the Bay of Biscay in the south to the Hebridean shelf in the north. The 'youngest' particles were found to follow track the core of the European Slope Current. Particle density was found to be relatively high over the northeast Porcupine Bank, extending along the adjacent shelf, while more sporadic occurrences followed the shelf margin of the Bay of Biscay and along the Iberian peninsula. Figure 2-2 .

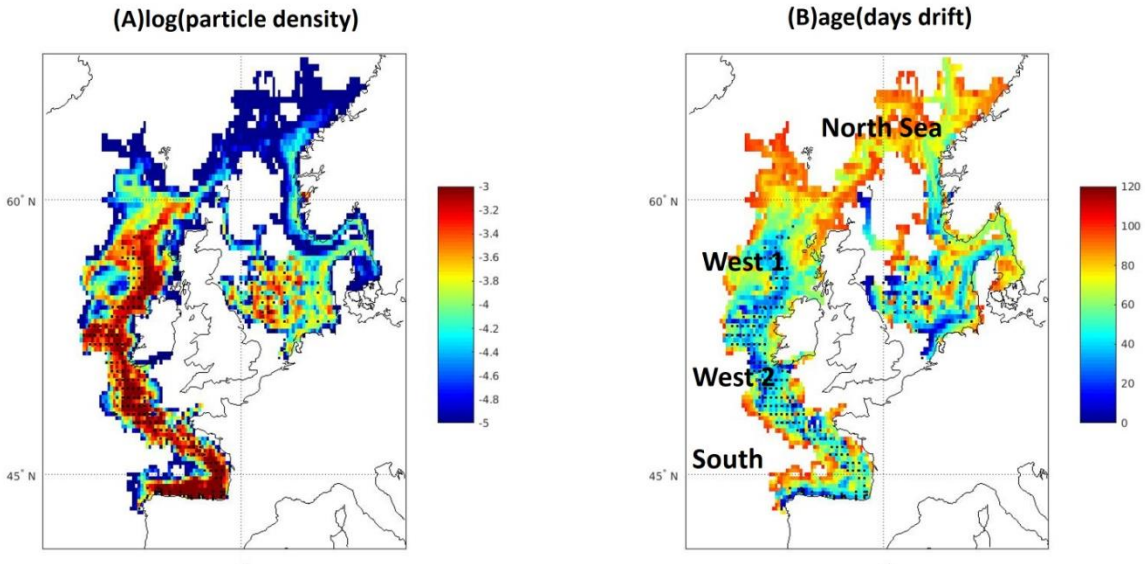


Figure 2-2. Larval distribution simulated from April to July 1998, released from a depth of 14 m at 415 initial positions, based on survey data (black stars). Particles are released 120 times from each initial position hourly for 5 days and subsequently tracked for 100 days. The resulting particle density (A) and age (B) are averaged on a 0.5° × 0.5° grid.

The spawning area is partitioned into four origin areas to capture variations in spawning pulses, each of which tends to produce different drift trajectories: South (42-48°N), West 1 (48-54°N), West 2 (54-66°N), and North Sea (2°-8°E, 54-59°N). This four way categorization deviates from the previous classification of three distinct stock spawning regions (refer to the discussion). I also

examine the distributions of larvae released in different months of 1998(Figure 2-3), with initial distributions specified along the shelf break of the northeast Atlantic between March and July (Figure 2-3.B-E) and in the North Sea in June (Figure 2-3.F).

In March (Figure 2-3.A), particles are initially located along the shelf edge of the southeast Bay of Biscay and to the west of Ireland. Over the 100-day simulation, most larvae stay near these spawning areas' coastal and shelf edge locations. In April, with no samples collected between the Bay of Biscay and the Hebridean shelf, the larval distribution remained in two separate patterns by the end of stimulation, while some particles initially located near the north Porcupine Bank reached the northern North Sea after 100 days (Figure 2-4.B). Similar drift towards the North Sea is observed for particles released in May and June (Figure 2-3.C-D), with June releases approaching the Norwegian coast after 100 days. Spawning activity ceases in the Bay of Biscay after June, while the high density of spawning around the Porcupine Bank in June (Figure 2-3D) decreases substantially in July, with limited drift along the Hebridean shelf break from July to November (Figure 2-3.E). Spawning in the North Sea is evident during June, leading to high particle density in the southern North Sea from June to October, with some dispersion along the Norwegian coast and into the northern North Sea (Figure 2-3.F).

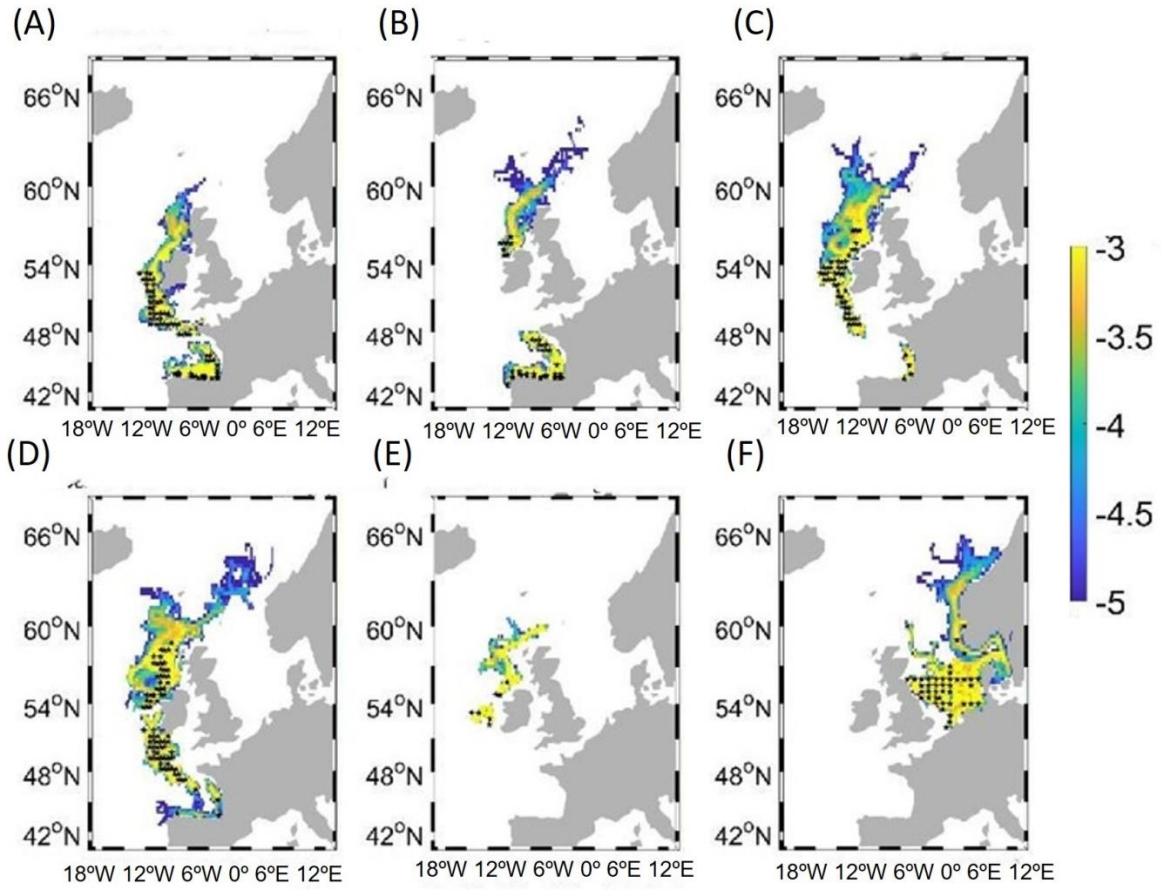

Figure 2-3. Larval dispersal simulated as mean particle density over 100 days for selected start months and locations determined from mackerel egg survey 1998: (A) March-July; (B) April-August; (C) May-September; (D) June-October; (E) July-November; (F) June-October. Particles are released at the initial positions indicated with black stars.

### 2.3.2 Larval drift predictions and contrasting dispersions

The average larval drift days within 0.5 grid cell geographic positions for particles released in 1998 are shown in Figure 2-3(B), revealing four distinct drift patterns. To further analyse these patterns, maps displaying particle days adrift were generated, shown in Figure 2-4. Particles released in the southern zone (42-48°N) do not drift far from the implied spawning area, with most remaining within the Bay of Biscay after 100 days. In contrast, particles released in the zone 48-54°N have a more complex drift pathway, though they too remain close to the release locations after 100 days. For particles released north of 54°N, a more extensive northward movement is evident, with particles dispersed throughout the northern area as far north as 66°N, and a small fraction reaching the northern North Sea. The drift pathways for particles released in the North Sea are diverse, with a significant fraction of these particles drifting towards the Baltic outflow, subsequently joining the Norwegian Coastal Current and mixing downstream with particles released north of 54°N in the northeast Atlantic.

.

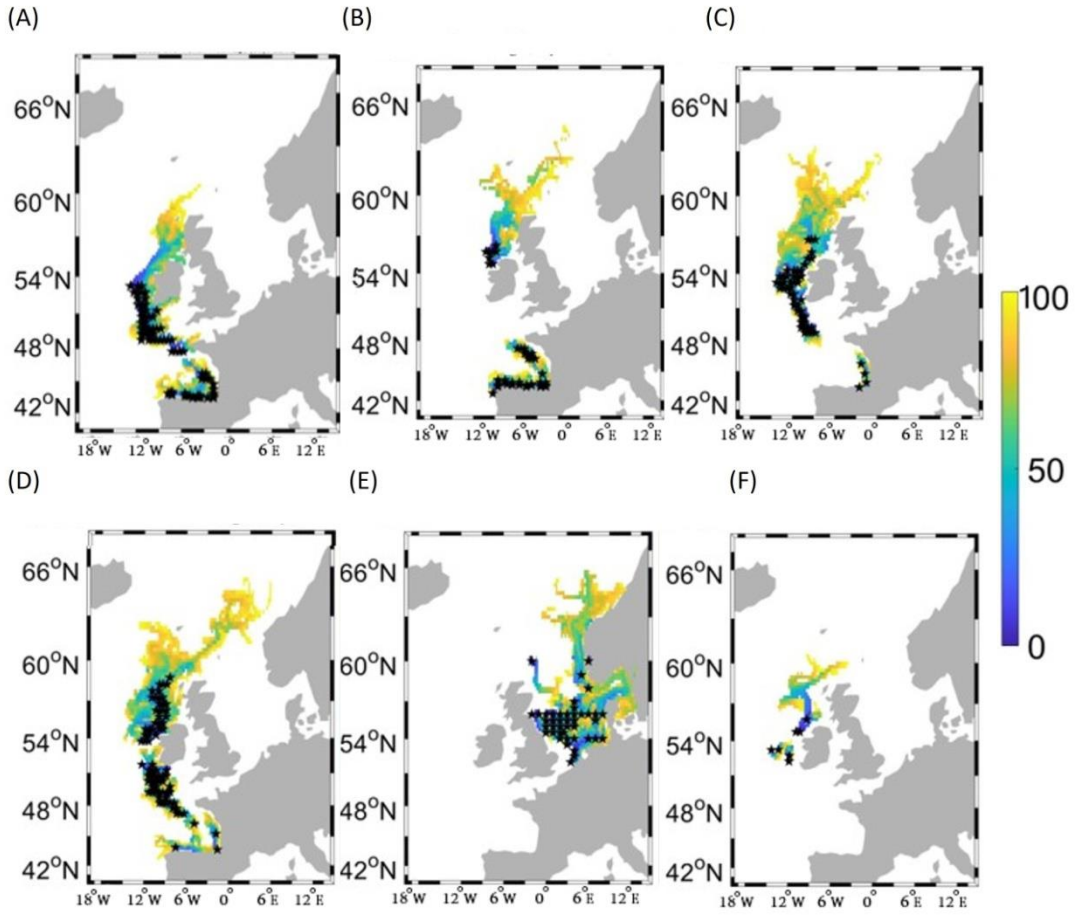


Figure 2-4. The average larval days adrift within 0.5 grid cell geographic positions (days adrift) for particles released from March to July is illustrated in different time intervals:: (A) March-July; (B) April-August; (C) May September; (D) June-October; (E) July-November; (F) June-October (North Sea). Initial particle locations are indicated with black stars.

### 2.3.3 Hydrography and inferred isotopic ratios along drift pathways

The ambient salinity and temperature experienced along simulated particle trajectories used to infer estimates for δ18Ow and $\delta^{18}O_{otolith,}$ were logged. For particles released between March-July 1998, gridded particle-mean properties are shown in Figure 2-5,Table 2-2. In Figure 2-6 I show time series of monthly ensemble-mean properties for the four selected spawning/drifting areas.

Table 2-2.Summary of predicted salinity, temperature, $\delta^{18}O_{w,}$ and $\delta^{18}O_{otolith}$ experienced in the four suggested spawning areas.

| Area | Salinity (‰) | Temperature | $\delta^{18}O_w$ | $\delta^{18}O_{otolith}$ |
|---|---|---|---|---|

| | | | | |
|---|---|---|---|---|
| South | 35.55 ± 0.17 | 12.74 ± 0.50 | 0.65 ± 0.08 | 1.93 ± 0.11 |
| West2 | 35.51 ± 1.42 | 11.76 ± 0.14 | 0.63 ± 0.07 | 2.15 ± 0.34 |
| West1 | 35.47 ± 0.12 | 10.97 ± 0.81 | 0.61 ± 0.06 | 2.33 ± 0.22 |
| North | 34.20 ± 1.37 | 10.19 ± 2.60 | 0.52 ± 0.38 | 1.99 ± 0.84 |

#### 2.3.3.1 Salinity

The mean salinity experienced by particles was 35.26‰ (Figure 2-5.A), with a maximum of 35.89 psu in the Bay of Biscay and a minimum of 16.23‰ associated with Baltic outflow to the North Sea. In the West1 and West2 areas, the salinities averaging 35.47‰ and 35.51 ‰ respectively, are slightly higher than the North Sea, averaging 34.2‰. Salinity minima are also evident adjacent to coasts, notably in the vicinities of major riverine outflows along the coasts of the Netherlands, Germany, and Denmark (downstream of the Rhine) and the Eastern Bay of Biscay (downstream of the Garonne). Local salinity gradients are most significant around the northern North Sea, where salinity can vary by around 9 ‰ by moving from relatively high salinity of the central North Sea to the fresh Norwegian Coastal Current.

Looking to the month-by-month ensemble-mean salinities (Figure 2-6.A), there is a slight decrease over the 100 days following the earliest particle tracking from March to May, when particles are initially located only in the Western and South release areas. During the second release period (June to September), particles released in the North Sea are subject to strong freshening, accompanied by an increased variability. An initial freshening trend is also evident for particles released from the South area in June, followed by a salinity increase in the final month, again subject to a significant variation. Small-scale salinity trends are obtained for particles released from West 1 and West 2, with minimal variance. For July releases from West 1 and West 2, drifting until October, salinity remained relatively constant.

#### 2.3.3.2 Temperature

Particles in our simulations were experienced a mean temperature of 11.9°C (Figure 2-5.B), with a maximum of 20.3°C in the Bay of Biscay in September and a minimum of 2.76°C in the northern North Sea in June. Substantial temperature gradients are evident across the Western shelf break, from warm offshore waters to cool onshore waters, including the Bay of Biscay. In the North Sea, temperature decreases northward from a mean of 12.1°C in the southern coastal zone to 9.8°C in

the northeast North Sea. Due to significant temperature gradients across the shelf break, particles in the Western areas, drifting off the coast of Ireland and the Hebrides, experience temperatures ~7°C lower than those particles drifting further offshore. Particles drifting in the North Sea might likewise experience two very different temperature regimes, the cold nearshore Norwegian Coastal Current (NCC) and the warm offshore Norwegian Atlantic Current (NAC). The North Sea is a region where temperature variance is the highest of our four identified spawning area.

The average temperatures in the South, West 1, and West 2 areas show slight cooling trends from March to May (Figure 2-6.B). A significantly increasing trend was observed from June to September, consistent with the warming season. The North Sea showed the largest warming trend at a rate of up to 2°C month$^{-1}$. Over June-July, mean temperature increased at almost 2°C month$^{-1}$ in the West 2 area, slowing to 1.16°C month$^{-1}$ by August, close to the warming rate for particles in the South area. Slower warming of 0.63°C month$^{-1}$ prevails in the poleward West 1 area. Over July-October, warming persisted for West 1, with slight cooling for particles drifting from West 2.

#### 2.3.3.3 Oxygen isotope ratio of seawater

The average oxygen isotope ratio of seawater ($\delta^{18}O_w$) experienced by particles was 0.55‰ (Table 2-2). As $\delta^{18}O_w$ values are linearly related to salinity (see Equations (1) and (2)) the spatial patterns in Figure 2-5(A),(C) and the time series in Figure 2-6.(A),( C) are identical. Values of $\delta^{18}O_w$ reach a maximum of 0.81 ‰ in the high-salinity southern latitudes and a minimum of -4.85 ‰ in the Baltic outflow. Across the western areas, values of $\delta^{18}O_w$ were similar averaging 0.65 ‰, distinctly higher than those in the North Sea, averaging 0.52 ‰. In coastal zones $\delta^{18}O_w$ minima are evident, notably in the Eastern North Sea and the Bay of Biscay. Salinity-related $\delta^{18}O_w$ variance is greatest in the North Sea spawning area, with a range of 5.45 ‰, from local maxima in the relatively saline central North Sea to minima associated with fresh coastal waters of the Baltic outflow.

Looking at the time series (Figure 2-6.(C)), $\delta^{18}O_w$ values declines slightly along particle trajectories in the western and southern areas over March-May. A larger decrease is evident from June-September in the North Sea, at a rate of up to -1.8‰ month$^{-1}$, with stronger variance. As for salinity, a negative $\delta^{18}O_w$ trend in the south area over June-July reverses by August. Likewise, with salinity, $\delta^{18}O_w$ declines gradually for West 1 and West 2 areas, with a small variance, while remaining relatively steady over July-October in West 1 and West 2.

#### 2.3.3.4 Oxygen isotope ratio inferred for otoliths

The average oxygen isotope ratio inferred for otoliths associated with the drifting particles is 2.0 ‰ (Figure 2-5.D). As $\delta^{18}O_{otolith}$ values are inversely proportional to temperature (Equation 3),

spatial patterns and temporal trends are a reversal of those for temperature. Salinity has less influence on the value of $\delta^{18}O_{otolith}$ values across most of our study area, except for coastal zones and in the North Sea. Maximum and minimum $\delta^{18}O_{otolith}$ values of 3.22 ‰ and -4.85 ‰, respectively, are found in the North Sea. To the west, mean values of $\delta^{18}O_{otolith}$ gradually increase from the South area (1.93‰) to the northern West 1 area (2.33‰), averaging 1.86 ‰ across South and Western areas, notably higher than an average of 1.99 ‰ across the North Sea. $\delta^{18}O_{otolith}$ reaches its lowest values in coastal zones, the eastern North Sea, and the Bay of Biscay. Directly related to temperature variance, $\delta^{18}O_{otolith}$ variance is largest across the North Sea spawning area.

Again, considering the time series of $\delta^{18}O_{otolith}$ for the four selected areas (Figure 2-6.D), a slight increase over March-May is evident in larvae from the West 1 and West 2 areas, while remaining steady in the South area, with limited variance. Over June-September, $\delta^{18}O_{otolith}$ values decline more significantly: by up to 0.55 ‰ $month^{-1}$ in the North Sea, with correspondingly higher variance; by 0.29 ‰ $month^{-1}$ in West 2; by 0.16 ‰ $month^{-1}$ in West 1; by only 0.06 ‰ $month^{-1}$ in the South area. $\delta^{18}O_{otolith}$ continues to decline in West 1 over July-October, while slightly increasing in West 2.

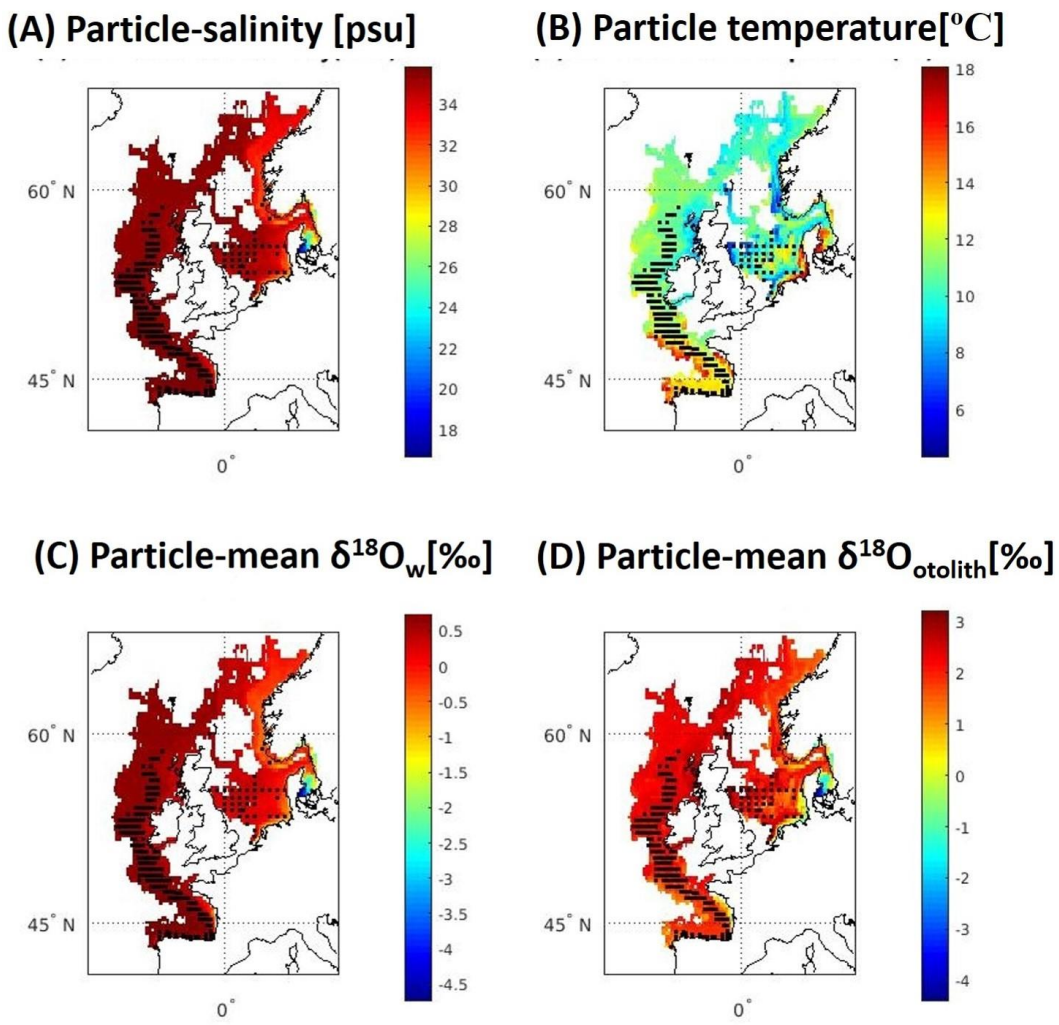


Figure 2-5. Mean environmental properties -, sampled by particles released over March-July of 1998: (A) salinity; (B) temperature; (C) $\delta^{18}O_w$; (D) $\delta^{18}O_{otolith}$.

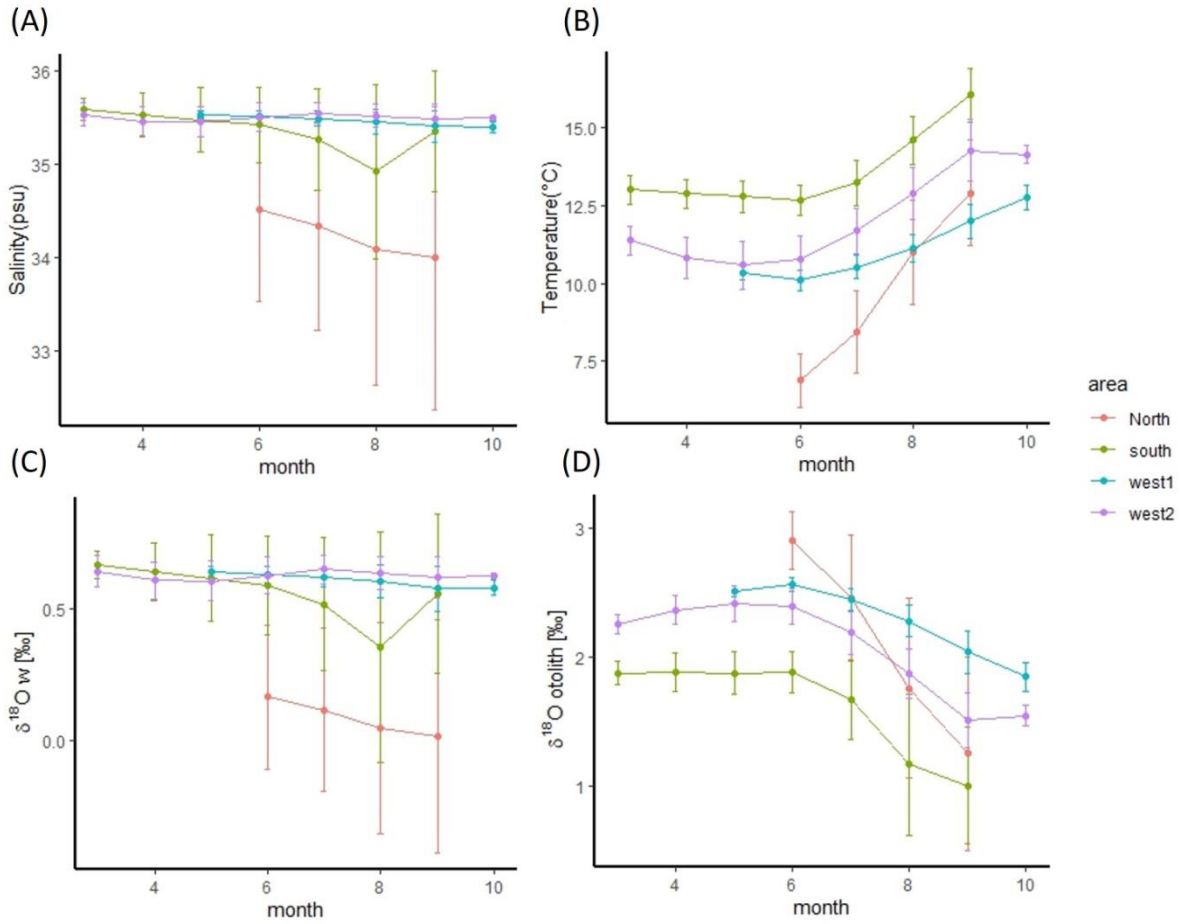


Figure 2-6. Ensemble means and standard deviations experienced by particles released over 1998 (see Figure 1-1): (A) salinity; (B) temperature; (C) $\delta^{18}O_w$; (D) $\delta^{18}O_{otolith}$. Monthly means and standard deviations are calculated separately for the four identified spawning areas (South, West 1, West 2, North).

Differences in estimated isotopic compositions of whole otoliths among different geographic areas (Figure 2-7) were tested using ANOVA (p value=0.004184 <0.05), revealing significant differences among the four regions. In the North area, the $\delta^{18}$ $O_{otolith}$ values hover around 1.88‰, showing slight variation as indicated by the error bars. This suggests some degree of environmental variability affecting the isotopic composition within this region. Conversely, the South area has $\delta^{18}$ $O_{otolith}$ values approximately at 1.83‰, with minimal variation among the samples. The small error bars suggest a more uniform environment or less variability in factors influencing the isotopic composition in this area. The West1 area exhibits the highest $\delta^{18}$ $O_{otolith}$ values, around 2.28‰, with very slight variation as shown by the small error bars. This indicates a relatively stable environmental condition influencing the isotopic composition. In contrast, the West2 area has $\delta^{18}$ $O_{otolith}$ values around 2.14‰, with slight variation among samples, which may be due to the significant range of movement experienced by the larvae in this region, causing some environmental variability.

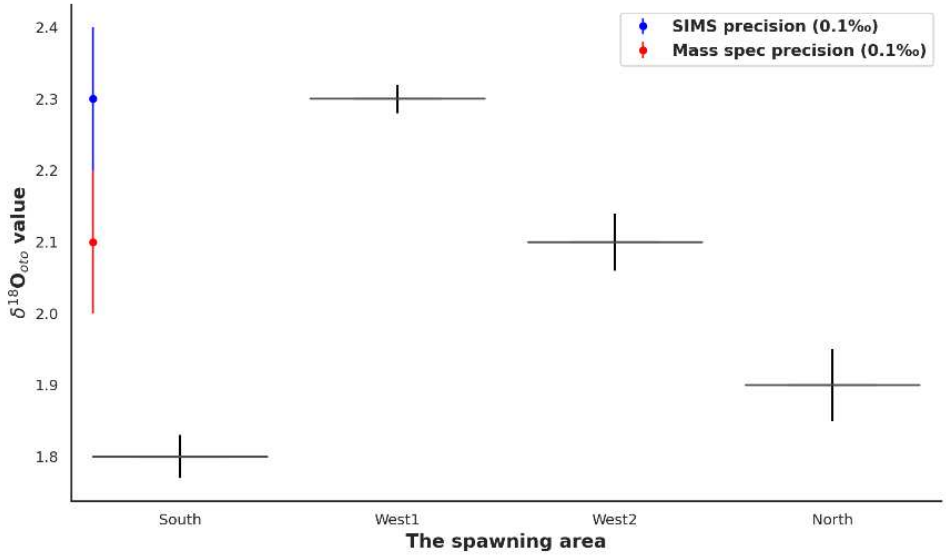


Figure 2-7 The estimated bulk isotopic composition of otoliths from different geographic areas.

### 2.3.4 $\delta^{18}O_{otolith}$ predictions in the spawning areas

Spawning areas had different temperature and salinity characteristics, resulting in different simulated $\delta^{18}O_{otolith}$ values, summarised in Figure 2-88. The average $\delta^{18}O_{otolith}$ value differed statistically between each spawning area (ANOVA test <0.05), increasing poleward. Mean $\delta^{18}O_{otolith}$ values are higher in the three western areas than in the North Sea, which is clearly influenced by isotopically light Baltic outflow.

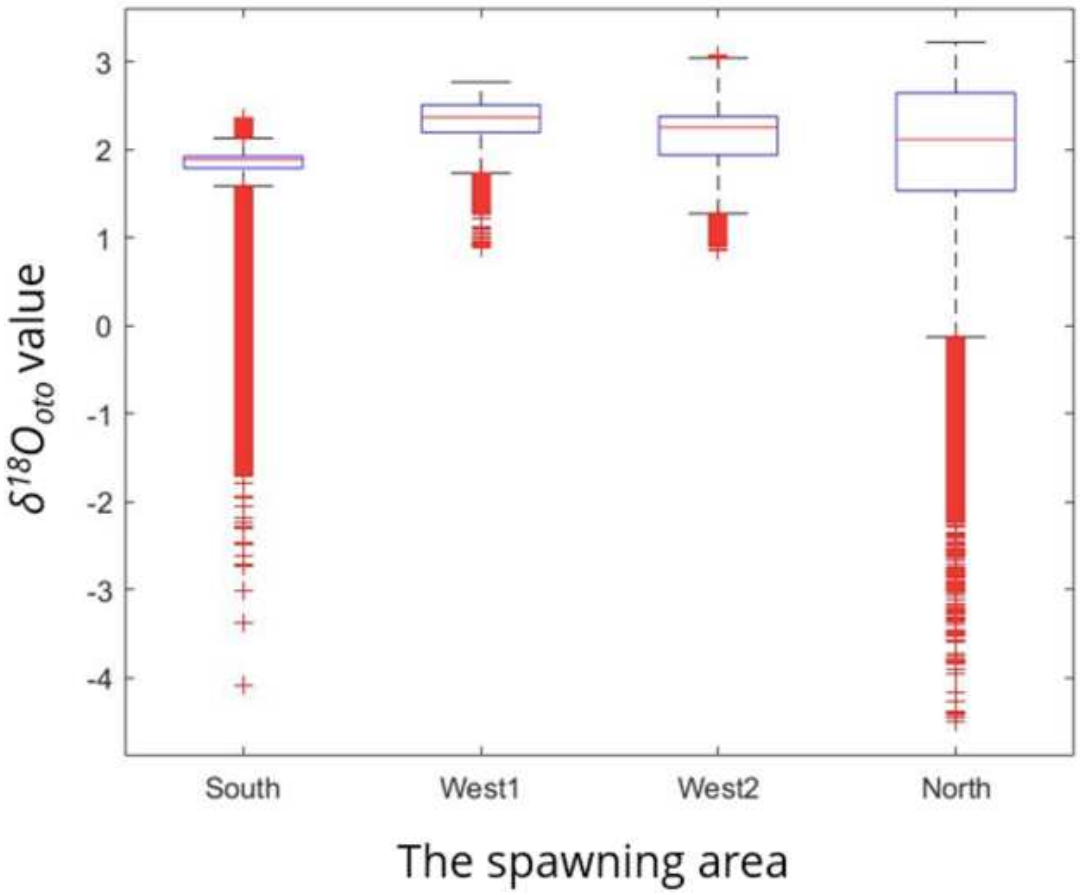


Figure 2-8. Ensemble means and standard deviations for inferred $\delta^{18}O_{otolith}$ rings in the four spawning/drifting areas.

## 2.4 Discussion

I predicted the drift of Northeast Atlantic mackerel (NEAM) larvae from trajectories of virtual particles embedded in near-surface ocean currents of an ocean model, Initially seeded in a range of spawning locations between March and July, we distinguish between drift in four distinct areas as South (42-48°N), West 1 (48-54°N), West 2 (54-66°N), and the North Sea (2°-8°E, 54-59°N). These areas were identified based the concentration of larvae and local dispersal characteristics observed in the simulations. The ability to predict the fate of larvae spawned over extended geographical ranges is vitally important for effective area-based management of such stocks, notably when these span multiple jurisdictional boundaries.

Given the observed temperature and salinity gradients along model particle trajectories, we further quantified the potential of otolith $\delta^{18}O$ values to distinguish between larvae drifting in the four areas and thus to characterize experienced drift from different spawning areas. The results allow prediction of likely sources of variance in otolith $\delta^{18}O$ records and suggest improvements in

isotopic analysis. This method is directly transferrable to species with similar pelagic larvae stages and may help to focus limited resources on species and regions where questions regarding larval drift are reasonably tractable using stable isotope tracers.

### 2.4.1 Simulating time-varying drift pathways of NEAM

Particle drift simulations indicate a continuous larval presence from northwest of Ireland, through the Porcupine Bight and along the shelf-edge of the Celtic Sea to the Bay of Biscay. The four distinct areas were identified based on the pathways and timescales of particle drift as well as the concentration of larvae and local dispersal characteristics observed in the simulations. Specifically, particles released in the southern zone (42-48°N) do not drift far from the implied spawning area, with most remaining within the Bay of Biscay after 100 days. For particles released north of 54°N, a more extensive northward movement is evident, with particles dispersed throughout the northern area as far north as 66°N, and a small fraction reaching the northern North Sea. The drift pathways for particles released in the North Sea are diverse, with a significant fraction of these particles drifting towards the Baltic outflow, subsequently joining the Norwegian Coastal Current and mixing downstream with particles released north of 54°N in the northeast Atlantic.

The particle drift simulations showed that larvae in the South area largely remain in the main spawning areas, in the longitude range 5-7°W (Figure 2), due to limited net transport associated with alternating easterly and westerly winds in the upwelling season (Bartsch, 2005; Haynes & Barton, 1990). Simulated larval drift from the southern sector of the western stocks (48-51°N) also drifted only a limited distance from the spawning area. Larvae concentrated over the Porcupine Bank, associated with an anti-cyclonic gyre local to this bathymetry. Poleward of 51°N, western stocks are subject to more extensive northward movement, consistent with previous findings (Bartsch and Coombs, 1997; Bartsch, 2005).

Comparing simulation results to the closest available sampling data from the combined Quarter 4 and Quarter 1 ICES survey for age-0 mackerel during 1998/99 (Figure 2-7) indicated a high overlap between the simulated model distributions and the high catch rates of juveniles in the northern Porcupine area. The highest juvenile catch rates were observed in the northern Porcupine Bight, northern North Sea, and around the Bay of Biscay as far as the Portuguese coast. However, it was observed that the actual juvenile nursery areas tended to be further inshore than predicted by the model.

There were differences between the model results and surveys in three areas in particular. Firstly, the North Sea results showed low correspondence with the survey, as the high density of modelled larvae predicted to penetrate as far north and east as the northern North Sea did not

correspond with the locus of high juvenile catch rates in the northwest and northeast areas of the North Sea. Secondly, in the Celtic Sea, surveys found larval and juvenile mackerel close to the Cornish coast, while simulated particles typically concentrated in the middle of the Celtic Sea. Finally, model particles were concentrated along the north coast of Spain and France while compared with field observations found of juveniles present only off the French coast (Bartsch, 2005).

The drift model used in this study was limited to simulating passive transport of larvae and juveniles over a 100-day period. Due to the weak swimming abilities of larval stages, and their reliance on oceanic factors such as currents, tides, and waves for movement, their distribution is primarily governed by these physical forces. Larvae survive by feeding on small planktonic organisms in the water, making environmental changes a crucial factor affecting their survival rates (Houde, 2008). However, as the larvae develop into juvenile fish during this extended timeframe, it becomes increasingly less plausible that they remain passive, and it is likely that active swimming will increasingly contribute to distribution patterns (Bartsch, 2005). Our particle drift simulations from March to July may provide reliable distributions only until the end of the passive transport phase in June, by which time most post-larvae have reached a size of over 80 mm (Bartsch et al., 2004). The first bottom trawl survey started in October and recovered juveniles around 170 mm in length, indicating that active swimming behaviors likely become more important for determining the distribution patterns of juvenile fish as they grow and develop. Active swimming ability is also a crucial factor for the survival of late-stage larvae. This discrepancy could be one of the reasons for discrepancies between the simulated and actual sampling results.

Temperature is also likely to play a significant role in the growth and development of these fish. Warmer temperatures can accelerate growth rates and potentially lead to an earlier onset of active swimming behaviors. If the discrepancy in distribution patterns observed between the model and field observations is due to juvenile fish actively migrating (swimming) to nursery areas after the end of the passive transport phase, then understanding the influence of temperature on their swimming behavior and using otolith oxygen isotope signals to determine the onset of active swimming may be important, especially in nearshore areas where salinity fluctuations can be significant.

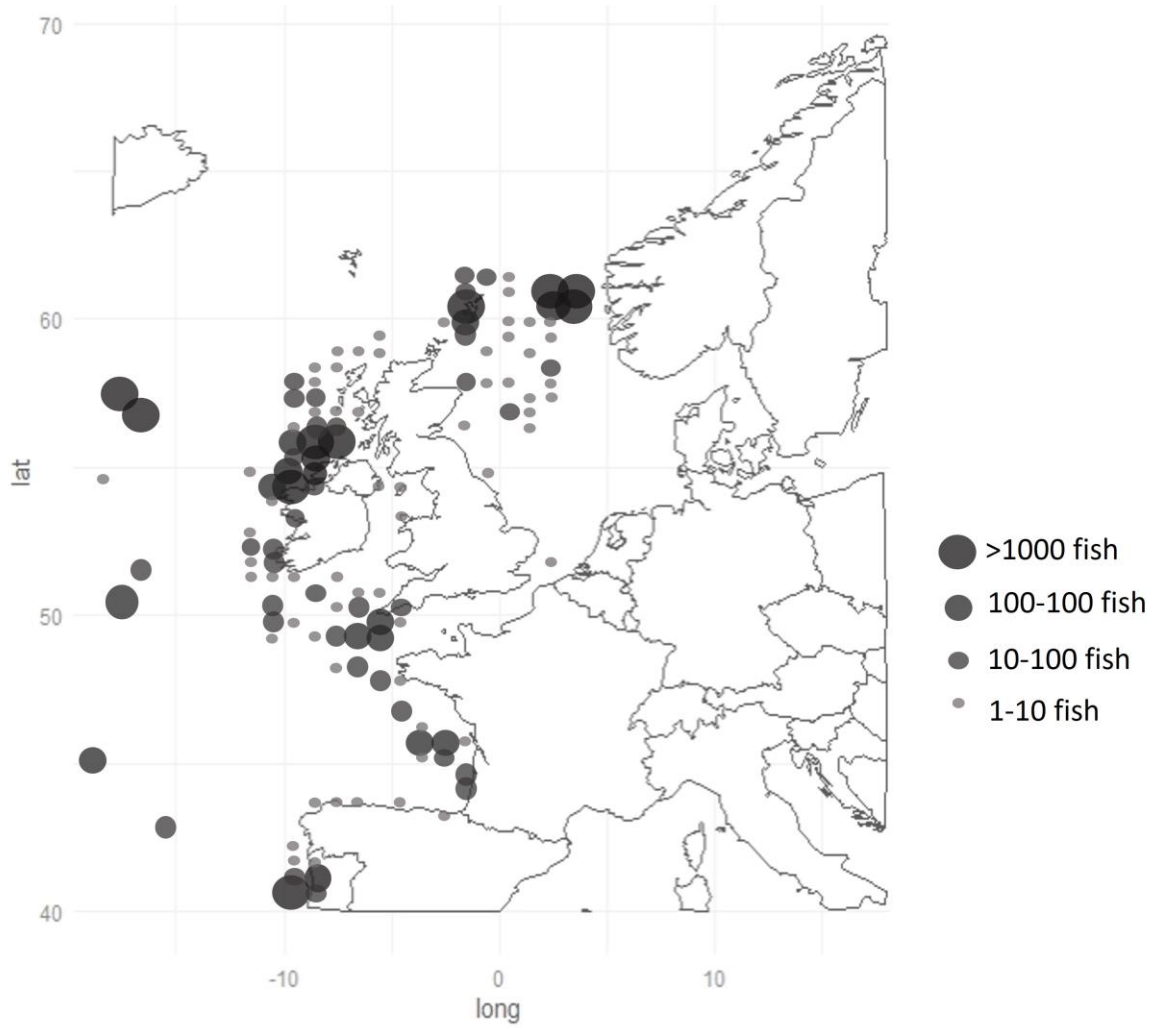


Figure 2-7. Combined Quarter 4 and Quarter 1 ICES survey data (as mean catch rate per hour) for age-0 mackerel during 1998/99. (Bartsch et al., 2004)

### 2.4.2 Otoliths as "natural tags."

I used a simple individual-based migration model to identify possible migration routes starting from the spawning ground and ending after 100 days of passive drift. Simulations predict that $\delta^{18}O_{otolith}$ values will increase gradually from south to north and show marked differences between spawning regions,, demonstrating the potential utility of otolith $\delta^{18}O$ values as a natural tag of stock origin.

The common assumption is that variation in otolith $\delta^{18}O$ values generally reflect the corresponding latitudinal movements when temperature and salinity are effectively uniform along zonal directions. However, we found that fine scale salinity variations could not be overlooked, even in fully marine environments , as previously identified (Darnaude et al. 2014, Darnaude and Hunter, 2018).

The greatest salinity range in high latitudes of the North Atlantic is found in the summer months due to land or sea ice melting, increasing freshwater runoff to the ocean. Cold, fresh coastal waters provide a clear signal in simulated otolith $\delta^{18}O_{otolith}$ values when larvae drift from offshore to inshore habitats. These salinity gradients thus provide the possibility to track larvae in longitude as well as latitude (Trueman et al., 2012). Simulated $\delta^{18}O_{otolith}$ variance was higher in the Bay of Biscay ('South' area) and in the North Sea, where $\delta^{18}O_{otolith}$ analysis might best reflect differences in the salinity experienced by the larvae during their transport between offshore and inshore environments.

In other areas, temperature effects dominate variation in simulated $\delta^{18}O_{otolith}$ values, which increase with latitude . Comparing the four identified spawning/drifting areas, we found that predicted $\delta^{18}O_{otolith}$ values were higher and showed less variance in the Northeast Atlantic area, as high salinity surface waters from North Atlantic Current (NAC) produce high $\delta^{18}O_w$ values and cool temperatures result in increased $^{18}O$ incorporation in otolith aragonite. In contrast, in the North Sea, water is a mixture of relative saline Atlantic inflow, brackish Baltic outflow, and locally important river runoff resulting in lower $\delta^{18}O_w$ values and the highest variance among the four identified spawning/drifting areas. Across all four regions, seasonal temperature changes dominate $\delta^{18}O_{otolith}$ variability. Over March-June, $\delta^{18}O_{otolith}$ values remain relatively steady. Over summer, $\delta^{18}O_{otolith}$ decreases with rising temperature, as poleward drift is more than offset by seasonal warming. $\delta^{18}O_{otolith}$ changes are thus dominated by seasonal temperature changes rather than the movement from waters warmer to cooler latitudes. Only in some regions are $\delta^{18}O_{otolith}$ changes more clearly related to changing salinity, and hence $\delta^{18}O_w$, as larvae drift across salinity gradients from spawning ground to the collection site. The ambient $\delta^{18}O_w$ signal recorded in $\delta^{18}O_{otolith}$ may nevertheless be vital to understanding the transport of small pelagic fishes in early developmental stages from their spawning grounds(offshore) to juvenile nursery areas (inshore).

Daily age is also useful to identify the origin. Our results suggest that a comparison between the $\delta^{18}O_{otolith}$ values in the otolith core and edge areas could allow discrimination among spawning areas from single point analyses of core or marginal otolith isotope data (e.g. Figure 2-8) However, the observed variability is substantial due to the relatively short monitoring period, leading to a significant overlap in simulated $\delta^{18}O_{oto}$lith values between regions.

There is greater potential to discriminate among spawning areas and their associted drift pathways based on a combination of absolute $^{18}O_w$ values and the temporal changes in $^{18}O_{otolith}$ values during drift (Figure 2-6). Because $\delta^{18}O_{otolith}$ values are relatively constant in March-June, there appears to be little value in high-resolution micro mill sampling. For the summer period (e.g., June-August), significant differences in the rate of change of $\delta^{18}O_{otolith}$ values among drift

pathways were found, implying potential for discrimination. If samples with age<0 and readable daily growth rings are obtained, it is at least theoretically possible to retroactively count the daily increments to determine the date of growth, and therefore birth date which would allow best practice in high resolution otolith analysis. The results from our simulation modelling therefore suggests a optimal strategy to use otolith $\delta^{18}O$ analyses to infer larval drift pathways in Atlantic mackerel sampled as adults in the UK shelf seas as follows:

(1) If the fish were born in the spring, a low-resolution sampling of core regions may identify a contribution of spawning origin grounds from either southern or North Sea / Baltic regions as only these regions yield δ18Ootolith values below 1‰ (e.g. Figure 2-7).

(2) For fish born in the summer, for more detailed discrimination high resolution milling should be targeted to produce at least monthly resolution samples during a growth period from 30 to 90 days. This is equivalent to an otolith increment distance of 30-50µm. However, if otolith samples are above age 1 or the date of catch is unknown, we can only determine the daily age, not the date. In this case, estimating the otoliths' depositional timing is not possible, making this scenario inapplicable.

The advantage of low-resolution milling is that the $\delta^{18}O_{otolith}$ history can be obtained easily. With this method, the milling and analysis of one individual can be completed in approximately 1 week, whereas precise high-resolution milling requires a very long experimental time of approximately 2 months to complete the entire process for one individual(Muto et al., 2022).This time cost could be reduced by selecting the milling resolution by prediction from the model. Nevertheless, the long experimental time required for precise high-resolution milling is unavoidable

In this study, we show that the $\delta^{18}O_{otolith}$ values have the potential to generate unique in situ validation measures to distinguish the spawning area by sampling the otolith cores and marginal area. As ion probes and other spatial sampling techniques improve, the otolith would be suited to studying migrations in larval and juvenile fishes and become a viable option for tracking movements of fully marine fishes (Hobson & Wassenaar 2018; Trueman et al., 2012).

## 2.5 Conclusions

Here, I use individual-based drift models to simulate salinity and temperature experienced by individual migration pathways of the larval and juvenile pelagic Northeast Atlantic mackerel, with high time and space resolution. Predictions of otolith $\delta^{18}O$ profiles indicate differences between four areas of spawning/drifting. My results reveal the potential utility of otolith $\delta^{18}O$ profiles.

I confirm that otolith $\delta^{18}O$ values could be used as highly accurate, low-cost "natural tags" for stock discrimination and broad-scale geolocation of fish, thereby complementing the results from tagging experiments and other population descriptors. Indeed, the proposed approach could be applied to many other species and locations and provide valuable data for conservation and sustainable fisheries management. Even though I found significant spatial variations in stable-isotope compositions the underlying isotopic variation is not static. Rather, it will vary dynamically with a changing environment, so yearly changes must be considered when transposed to other periods. One caveat is that the current drift calculations do not include active movement such as swimming and vertical migration, as the early life stage of mackerel is assumed to drift passively.

This approach is valuable not only for revealing population structure and early life transport but also for its distinctive and robust capability to examine the environmental history of successfully recruited individuals. This information is critical for comprehending the environmental conditions essential for fish survival, offering insights into how environmental variabilities contribute to fluctuations in fish populations. The fluctuation in fishery resources is believed to hinge on the proportion of individuals that survive the high mortality rate during the early developmental stages (larval period) and integrate into the resources produced in a given year. As the swimming capabilities of larvae during this stage are extremely weak, or even entirely absent, their distribution and movement are predominantly governed and transported by oceanic physical factors such as currents, tides, and waves. They depend on feeding on small planktonic organisms and plants in the water, making environmental changes a pivotal factor influencing their survival rates. Moreover, the timing, distribution, and quantity of larvae can be utilized to deduce the spawning grounds and spawning period of the parent population. The quantity of larvae can also be employed to estimate the resource level of the parent fish and predict potential future additions. This allows for the comparison of the relative quantities of economically important fish populations in the same or different regions, as well as the exploration of long-term trends in specific populations. However, all of these aspects require a foundation in the study of larval species composition, aggregation structure, and the spatiotemporal distribution dynamics.

# Chapter 3 Predicting high-resolution otolith isotope ratios along basin-scale trajectories with and without simulated swimming to inform early life history migrations: A case study with European Eel


## Abstract

Despite significant efforts, our knowledge of the spawning grounds, larval migration behaviour, and pathways of endangered European eels remain limited. However, understanding the behaviour and pathways of eel larvae is essential for effective management and conservation strategies, especially since long migrations may make eels more vulnerable to the effects of climate change. This study aimed to investigate the potential use of otolith isotopes to verify European eel spawning locations and test hypotheses about the impact of ocean dynamics, specifically swimming behaviour and North Atlantic Oscillation (NAO) index, on eel larvae migration. The study used virtual particle trajectories to predict the drift of eels from four subareas of spawning locations at different depths, with the highest success rate observed in May at a depth of 200 meters. The study also found that during NAO+ periods, eels required a longer time for migration and had a lower migration success rate. Otolith $\delta^{18}O$ values were used to distinguish successful and failed drifts and verify the hypothesis that NAO affects eel migration. Moreover, the study found that otolith oxygen isotope ratios can distinguish the characteristics of spawning locations during NAO+ periods. This study demonstrates the possibility of using a combined model and otolith analysis for validating each other's findings and highlights the potential of using stable isotopes to address questions about the recruitment success of migratory species.



**Keywords:** $\delta^{18}O$, otolith, European eel distribution, passive drift, simulated swimming

## 3.1 Introduction

The European eel is a catadromous species migrating from the fresh and brackish waters of Iceland and northern Scandinavia in the north, and the Mediterranean and North Africa in the south, back to the spawning area in the Sargasso Sea. After hatching, eel larvae (leptocephali) drift across the North Atlantic to the European coasts, where they metamorphose into glass eels after three years (Schmidt, 1923). The European eel population has been in decline since the 1980s across its entire distribution range. In response, various legislative measures and conservation directives have been implemented to protect the species, which has been listed as critically endangered on the International Union for Conservation of Nature (IUCN) Red List of Threatened Species (Jacoby et al., 2014). The decline is attributed to several factors, with hypotheses suggesting that issues may arise during either the continental or oceanic phases of the eel's life cycle. Specifically, marine factors such as shifts in the Gulf Stream are believed to adversely affect the survival of leptocephali larvae during their transoceanic migration (Meulenbroek et al., 2020). During this relatively long passive phase, eel larvae are exposed to environmental conditions that can strongly influence their survival success during migration and recruitment. Despite extensive larval surveys in the Sargasso Sea over a century, eggs and spawning adults that could provide direct evidence of exact spawning locations within Sargasso Sea spawning areas have never been collected. In this context, the spawning ecology of the European eel is not yet fully understood and is subject to various (Bonhommeau et al., 2010; Tesch, 1989). Some of these assumptions include the following:

1) The Sargasso Sea is the primary spawning area for European eels: While there is strong evidence to suggest that the Sargasso Sea is the primary spawning area for European eels, and observations from leptocephalus catch data spanning from 1863 to 2007 indicate higher larval fish density in that region compared to the findings of Miller et al. (2016)(Figure 3-1), this conclusion has not been definitively proven. Some researchers have suggested that this species may have additional spawning areas in other parts of the North Atlantic (Chang et al., 2020). It is hypothesized that the spawning areas of the European eel (*Anguilla anguilla)* and the American eel (*A. rostrata*) are situated along the Mid-Atlantic Ridge, between longitudes 50° W and 40° W. This region lies outside the Sargasso Sea, which has traditionally been considered the spawning ground for both species since the early twentieth century. A number of investigations that found recently hatched European eel larvae (< 12 mm) in a 2000 km wide region from 70° W eastward to 50° W (Westerberg et al.2017; Miller et al.2019). Despite these findings, conclusive evidence that precisely identifies the specific locations and timing of spawning sites has yet to be obtained, leaving key aspects of the spawning process still largely unknown.

2) The determination of the spawning location and timing is supported by additional larval collection methods, as documented by Miller et al. (2016) and Chang et al. (2020), and the use of satellite trackers, as demonstrated by Wright et al. (2022), which provided data confirming that mature eels reach the region of the Sargasso Sea. Spawning occurs at specific times within the Sargasso Sea; while it is known that European eels spawn there during the spring and summer months, the exact timing and specifics are not well understood.

3) Larvae may have distinct migration routes and behaviours; some researchers have suggested that swimming with preferential orientations are likely during larvae migration (Miller and Tsukamoto 2017; Miller et al. 2019). For example, eels found on the British coast may have a longer leptocephalus drift phase than eels found from Spain and African coast and may therefore experience different environmental conditions during their migration.

4) Environmental conditions during the leptocephalus drift phase can influence recruitment success. During their relatively long passive phase of leptocephalus drift across the North Atlantic, eel larvae are exposed to various environmental conditions that influence their survival success and recruitment to European coasts. For example, some researchers argue that ocean warming in the eel spawning area since the early 1980s has modified marine production and eventually affected the survival rate of European eels at early life stages (Bonhommeau et al., 2008) and that the North Atlantic Oscillation (NAO) influences the timing and duration of leptocephalus migration and recruitment success of European eels (Bonhommeau et al. 2008).

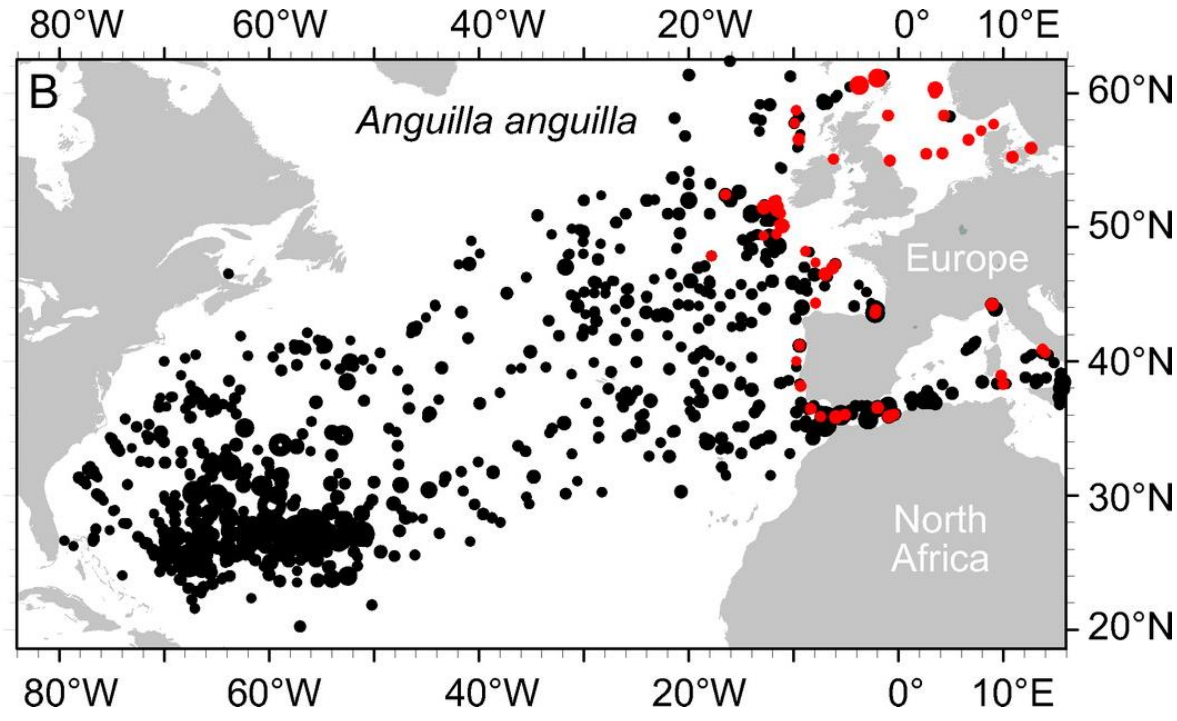


Figure 3-1 The locations where *Anguilla anguilla* leptocephali have been collected. The size of the circles reflects the abundance at each sampling location. The red circles indicate metamorphosed

larvae (data from JD McClave database, which includes *A. anguilla* and *A. rostrata* leptocephalus catch data from 1863 to 2007). This figure is from Miller et al. (2016).

Lagrangian simulations with large ensembles of drifting particles have significant potential to quantify early life stage dispersal (Baltazar-Soares et al., 2014). The Atlantic lagrangian model has validated migration durations for eel leptocephalae exceeding two years (Kettle and Haines, 2006), and historical estimates based on ocean current speeds or larval sizes suggest around three years (Schmidt, 1922; Tesch, 2003). Despite this, the assumption of a 2-3 year migration period remains contentious. Otolith studies on glass eels estimate shorter crossing and recruitment durations to estuaries, ranging from 7 to 15 months (Arai et al., 2000; Wang and Tzeng, 2000; Bonhommeau et al., 2008; Miller, 2015). However, the recruitment age derived from otolith measurements may be biased. This is due to potential periods without otolith ring deposition between glass eel hatching and their migration to estuaries ( Cieri and McCleave, 2000). Water temperatures below 15°C decreased otolith material deposition in anguillid glass eels and below 10°C otolith deposition can halt (Fukuda et al., 2009), and an opaque zone often found in the outer part of otoliths in glass eels can obscure increments (Antunes & Tesch, 1997). Recent developments in high-precision micro-milling systems and microvolume isotope analysis (such as SIMS $\delta^{18}O$ otolith analysis and continuous flow isotope ratio mass spectrometry system (CFIRMS)) enable accurate $\delta^{18}O$ analysis (<±0.1‰) of $CaCO_3$ at amounts as low as 0.2 µg. These methods have been applied to the core region of otoliths in *Anguilla japonica* glass eels, suggesting that stable isotope micro-analysis is a powerful method to extrapolate the unknown spawning ecology of fishes (Shirai et al., 2018). However, in a broader application for geolocation in larval stages, such methods are limited due to analytical difficulties in detecting differences in oxygen isotope ratios where environmental gradients are potentially less pronounced. Both systems are expensive and time-consuming, so it is imperative to predict when high-resolution otolith isotope analyses might be expected to produce precise results. Coupling the early-life-stage transport patterns obtained from hydrodynamic models and in-situ isotope-based methods allows us to examine the potential and limitations of using the isotope-based method and modelling to identify the early life history characteristics and how to benefit from these two methods to assess the prospects for isotopic analysis of sampled larvae.

The European eel larvae drift with the Gulf Stream, part of the North Atlantic subtropical gyre. Formed in the Eastern part of the Gulf of Mexico, the Gulf Stream flows through the Straits of Florida and continues along the east coast to Cape Hatteras, which flows away from the continent (Gangopadhyay et al., 1992). Approximately at 50°W, the Gulf Stream is split into several branches. The largest one, known as the North Atlantic Current (NAC), reaches the west coast of Europe and later turns north. The second branch turns south-eastwards to form the Azores

Current to finally return and circulate into the subtropical gyre (Tomczak & Godfrey, 2003). The North Atlantic Oscillation (NAO) is a climatic phenomenon characterized by changes in atmospheric pressure between the subtropical high-pressure system near the Azores and the subpolar low-pressure system near Iceland. This phenomenon is recognized for its impact on the climate in the North Atlantic region. Knights (2003) and Friedland et al. (2007) delved into the investigation of potential correlations between variations in the recruitment of A. *anguilla* (European eel) and the North Atlantic Oscillation (NAO) within the Atlantic region. However, the mechanisms and effects causing these influences remain elusive due to the inability to track the trajectories of juvenile eels and the complex interplay of environmental factors.

Here, we sample properties along individual particle trajectories in a series of experiments to predict $\delta^{18}O_{otolith}$ values in eel larvae subject to contrasting drift scenarios. Salinity along particle trajectories is used to estimate the oxygen isotope ratios of the surrounding water. Regression models are further used with temperature along trajectories to generate a synthetic record of the isotopic composition of drifting otoliths. This synthetic approach is then used to explore the sensitivity of isotopic composition in otoliths before committing to costly laboratory analysis.

In these experiments, 'successful' drift is defined as crossing a selected meridian. Predicted $\delta^{18}O_{otolith}$ values are then used to test whether different successful and unsuccessful drifting larvae, subject to positive and negative NAO phases, are likely to yield systematically different $\delta^{18}O$ values. If so, we further examine where and when any separations are likely to be maximized in the drift history. Such an approach could thus guide sample selection and analysis for time and resource-intensive high-resolution isotope analyses. In summary, the potential and accuracy of isotope-based tracking are evaluated with large ensembles of virtual particle trajectories and the associated spatial-temporal variability of ambient temperature and salinity during drift history.

The rest of the chapter is outlined as follows. In section 2, I outline methods for virtual particle tracking (Sect. 2.1) and estimating seawater and otolith $\delta^{18}O$ values (Sects. 2.2, 2.3). In section 3 I present predicted larvae drift in terms of distribution (Sect. 3.1) and timing (Sect. 3.2), followed by consideration of the associated ambient environment (Sect. 3.3) and inferred otolith isotopic ratios (Sect. 3.4). In the Discussion section, I discuss the impact of depth and time on the probability of successful eel recruitment (Sect. 4.1), explore potential swimming speed ranges and migration times through active swimming behaviours (Sect. 4.2), compare temperature and salinity characteristics of spawning grounds during different NAO periods, as well as the potential impact of these oceanic environmental changes on migration paths and times, and the utility of otolith $\delta^{18}O$ values as "natural tags" to confirm various hypotheses related to European eel migration. Finally, in conclusion, I summarize key findings and reflect on the prospects for broader

application of otolith analysis for surveying and assessing fish transport from a life cycle perspective subject to environmental conditions that are variable in time and space.

## 3.2 Methods

I first outline the particle tracking calculation (Sect. 2.1)), providing the Lagrangian data used to predict local oxygen isotope fractions in seawater (Sect. 2.2) and otoliths (Sect. 2.3).

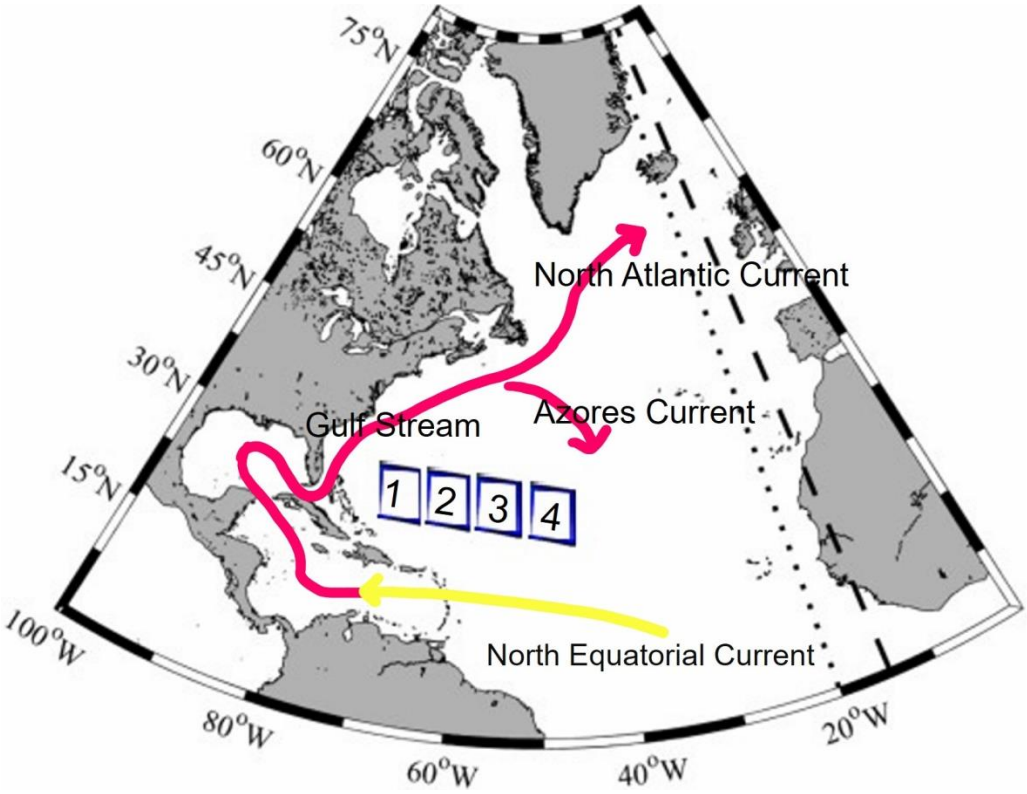


Figure 3-2. The study area includes simulated spawning regions and a schematic of the 0–200 m averaged ocean circulation. The European eel larvae drift with the Gulf Stream, which splits at 50°W into the North Atlantic and Azores Currents. Dotted meridian lines mark positions in the simulation where eel larvae are deemed to have successfully migrated. The dashed lines indicate the points where the simulations end.

### 3.2.1 Particle tracking

The initial conditions of the simulation required some biological realism, but the purpose was not to make a detailed, realistic model of leptocephalus behaviours. Instead, I regarded leptocephali as virtual 'particles' that passively drift with ocean currents, with optionally an additional swimming vector. To efficiently calculate the trajectories for a large ensemble of such particles, i

use the ARIANE mass-preserving algorithm (Blanke & Raynaud, 1997), developed at the Laboratoire de Physique des Océans (LPO, Brest, France) for use with output from the NEMO (Nucleus for European Modelling of the Ocean, Madec, 2008) family of Ocean General Circulation Models. Output is averaged 5-daily from a hindcast spanning 1989 and 2008 undertaken with the eddy-resolving ORCA12 configuration setup of the DRAKKAR project (Blaker et al., 2015; Duchez et al., 2016; Marzocchi et al., 2015) The ORCA12 configuration has a horizontal resolution of 1/12° and 75 vertical levels, with finer grid spacing near the surface.

Particles are released within the geographical area (25–29°N and 70–50°W) during the spawning season from February to June. The determination of the spawning location and timing is supported by additional larval collection methods, as documented by Miller et al. (2016), and the use of satellite trackers, as demonstrated by Wright et al., 2022, which provided data confirming that mature eels reach the region of the Sargasso Sea. Despite the satellite tracking data confirming the arrival of mature eels in the vicinity of Sargasso Sea, specific evidence regarding the exact spawning location remains lacking. Therefore, in this experiment, four sub-areas (Figure 3-2) were defined to narrow the spawning area. 100 particles were released hourly for five consecutive days from all release sites during model February and July of 1989 and 2008. The release sites were distributed across a 1-degree grid. The larvae eel particles were tracked at various fixed depths, with simulations conducted at four specific depth levels: 0 m, 47 m, 97 m, and 200 m. These depths were chosen based on the highest distribution density intervals observed in larval eel sampling (Munk et al., 2010). Regarding the model simplification of excluding vertical swimming, this decision was likely made to reduce the complexity of the model and to focus on horizontal advection and diffusion processes. As a result, diel vertical migration was not included in the model. The subsequent positions are recorded at five days intervals forwards in time for 720 days. Constant swimming is defined with a vector specifying eastward and northward components, direction, and speed.

Along with position and time, the ambient temperature and salinity encountered by the particles are recorded. The particle ensemble is statistically analysed on a 1° × 1° grid by calculating the average age, temperature, and salinity of particles passing through each 1° grid cell, considering the entire 720-day duration of each experiment. To evaluate particle dispersal, ‘particle density’ is calculated as the number of particle occurrences per 1° grid cell divided by the total number of particle occurrences throughout the experiment.

The following set of experiments was undertaken:

Release location is varied from spawning sub-areas N=1-4, for May at a depth of 200m, no swimming;

Subsequently selecting spawning sub-area N=1-4, the release time is varied from February to May at depth 200 m, no swimming.

May releases for sub-area N=1-4 are specified at four fixed depths (X = 0, 47, 97, and 200 m) , no swimming;;

May releases at depth 200 m are specified with the non-zero swimming vector (m $s^{-1}$) varied as follows: (0.5 m $s^{-1}$, 0.5 m $s^{-1}$); (0.05 m $s^{-1}$, 0.05 m $s^{-1}$); (0.01 m $s^{-1}$, 0.01) m $s^{-1}$; direction 45º(0.05 m $s^{-1}$, 0.05 m $s^{-1}$), 30º(0.028 m $s^{-1}$, 0.05 m $s^{-1}$), and 15º(0.013 m $s^{-1}$, 0.05 m $s^{-1}$).

May releases at 200 m, sub-area N=1, without swimming, are contrasted in years of positive NAO (1989-91) and negative NAO (2008-10).

Drift patterns are examined for all experiments. Selected experiments are then chosen for a more complete analysis of inferred isotopic histories.

### 3.2.2 Seawater $\delta^{18}O$ estimate

The temperature and salinity of ambient water in the NEMO hindcast corresponding to each predicted cell occupied by a drifting particle were extracted and used to predict corresponding oxygen isotope ratios of the ambient seawater ($\delta^{18}O_w$). These $\delta^{18}O_w$ predictions were inferred from salinity (*S*), using two different regional regressions between $\delta^{18}O_w$ and salinity. In the Northeast Atlantic and Gulf Stream, the linear regressions relating $\delta^{18}O_w$ to salinity follow as,

North Equatorial Current: $\delta^{18}O_w = 0.47S - 16.06$ (1)

Gulf Stream: $\delta^{18}O_w = 0.28S - 9.03$ (2)

The regressions are based on measurements in earlier studies (Benetti et al., 2017)

### 3.2.3 Otolith $\delta^{18}O$ estimate

The otolith isotopic ratio, $\delta^{18}O_{otolith}$, is calculated by using a regression recently proposed for Japanese eel (Shirai et al., 2018) given ambient $\delta^{18}O_w$ and temperature:

$$\delta^{18}O_{otolith} - \delta^{18}O_w = -0.153\ T + 1.418 \quad (3)$$

The time series of $\delta^{18}O_{otolith}$ is thus constructed from temperature and salinity along particle trajectories representative of drifting eel larvae. While the equation used may not be entirely reliable due to the ion microprobe's limited accuracy in measuring absolute values, and there is a potential discrepancy of up to 4°C, corresponding to 1‰, I still employ this formula primarily to study the trends in migration route variations.

## 3.3 Results

Starting with the drift experiments, we examine the successful distribution rate of passively drifting particles (no swimming) fixed at four depths and started in different months and positions. I then focus on the along-trajectory temperature and salinity key to the isotopic ratios recorded in the otoliths. Using this information, I finally infer the resulting otolith records.

### 3.3.1 Prediction of larvae transport

I organise results following the logic of the various experiments outlined in the sect. 4.1; showing maps of log (particle density) for a selected year combination (1989-1991 and 2008-2010). I related the starting position and time to investigate the importance of these factors for larval migration success. There was a strong effect of depth and year on the success of reaching the selected meridian of 20°W (Figure 3-3). The arrival success was lowest for the depth level 0m and 46.6m; this was because a large proportion of the particles recirculated southward into the equatorial counter current and crossed 20°W between 19°N and the equator. The percentage of particles that succeeded in crossing 20°W for depth fixed at 200m was highest among four depths in 1989 to 1991(NAO+) and 2008 to 2010(NAO-). The success rate in NAO- period (0.0012 %) was significantly higher than in the NAO+ period (0.00069 %).

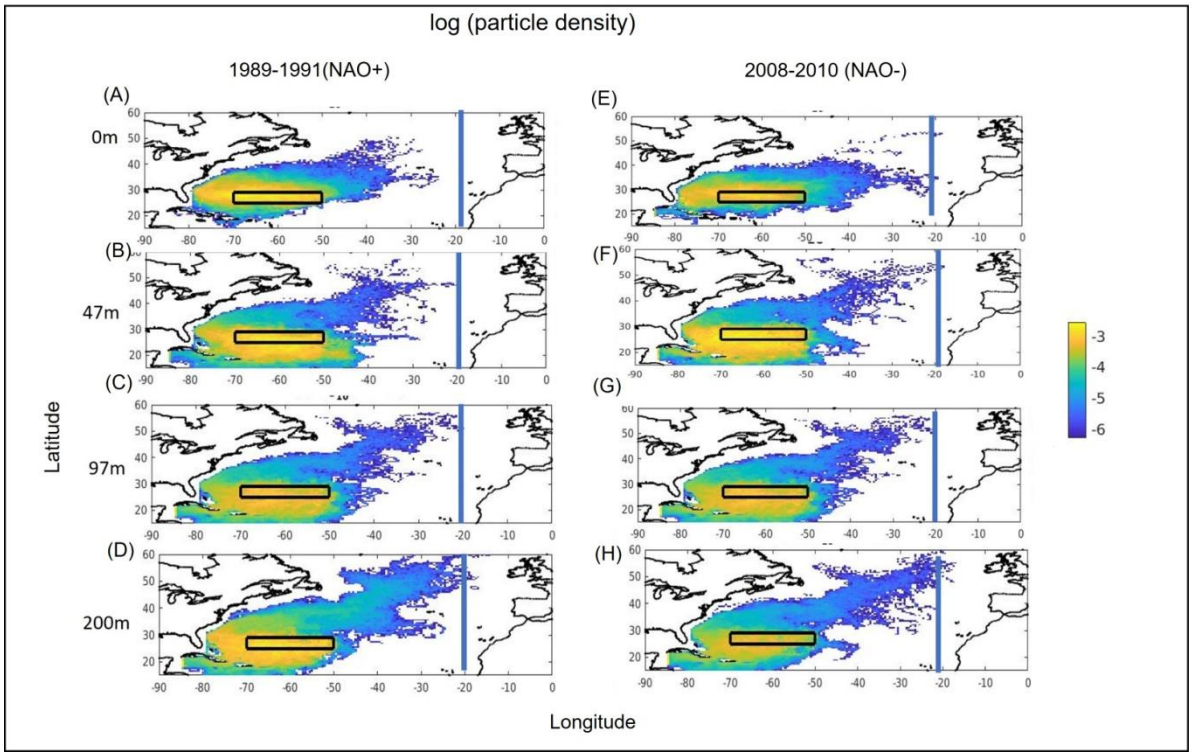


Figure 3-3. Particle density for releases in May of 1989-91 (left panels) and 2008-10 (right panels), fixed to drift at (A) 0 m, (B) 47 m, (C) 97 m, and (D) 200 m. The initial positions of these particles are indicated by black rectangles.

Particles succeeded in crossing 20°W in different months fixed at 200m, in numbers largely independent of release month for the simulation from 1989 to 1991, but with a pronounced higher arrival number from 2008 to 2010 (NAO-), especially for releases during April to May. The arrival success was highest when the release and fixed depth level was 200m (Figure 3-4). The starting position had a high influence on the probability of arrival at 20°W during the simulation for 1989-91 (NAO+) For particles released from the Western part of the spawning area ('Spawning1') the success percentage (0.002%) was slightly lower than 0.0027% during the simulation for 2008-10 (NAO-) Only 5 particles started from Easternmost 'Spawning 3' during NAO- successfully crossed 20°W.

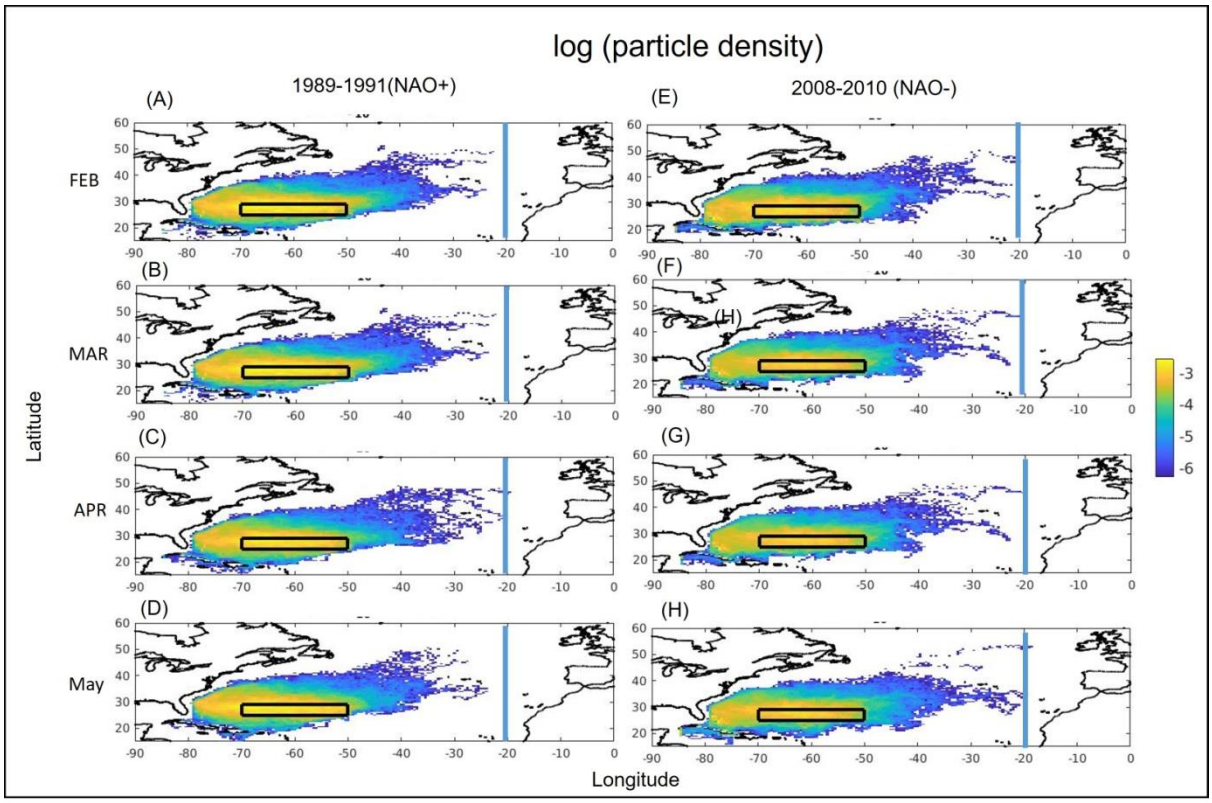


Figure 3-4. Particle density for releases in 1989-91 (left panels) and 2008-10 (right panels), starting (A) February, (B) March, (C) April, (D) May. The initial positions of these particles are indicated by black rectangles.

I then incorporated the swimming behaviour of eels into our simulations and tested the effect of three swimming speeds of 0.5, 0.05, and 0.01 m $s^{-1}$ for one and two years; the simulation started

in 2008

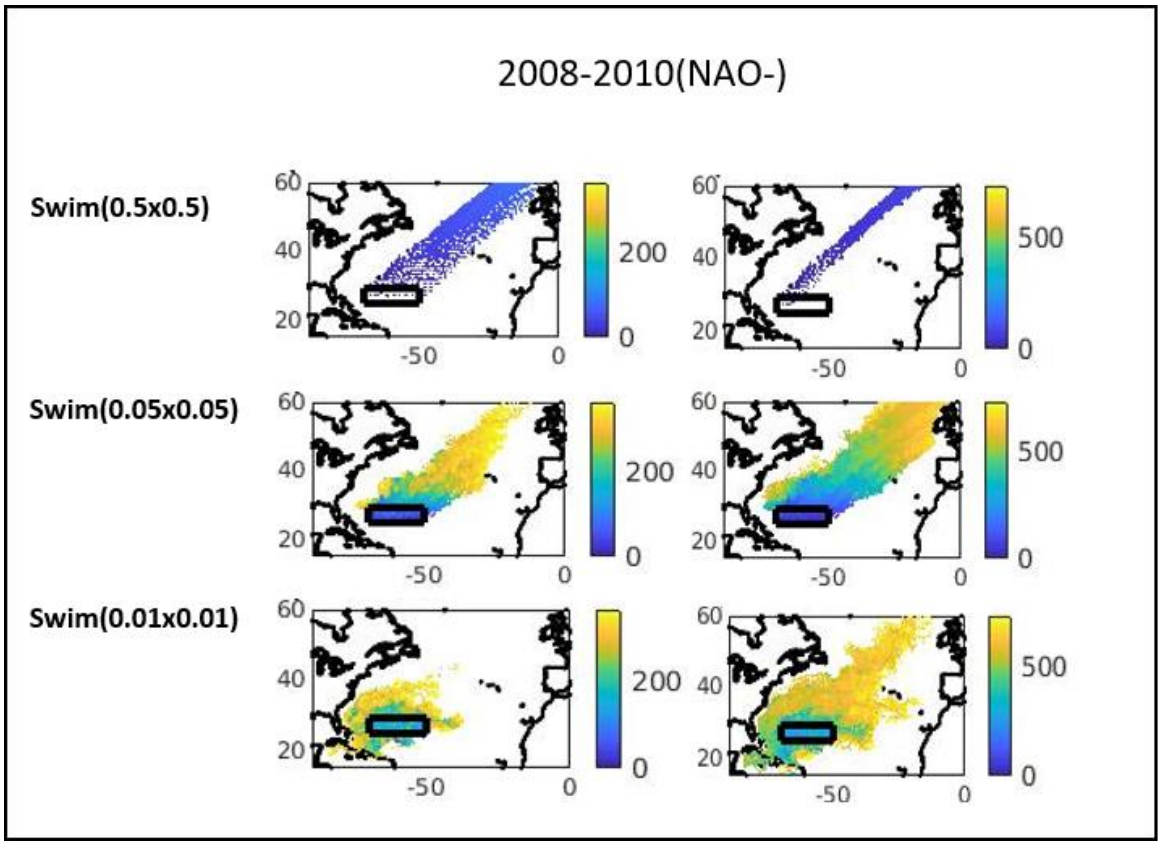


Figure 3-5). I found that at a speed of 0.5 m $s^{-1}$, almost all eels could reach their destination within 30 days, but this speed does not match the real ecological environment and observed eel movement speeds. At a speed of 0.05 m $s^{-1}$, I found that the proportion of eels successfully reaching 20°W after was increased to 54.74% after two years. I then tested a swimming speed of 0.01 m $s^{-1}$, close to the passive floating speed. I found that no eels successfully reached our target area of 20°W after one year, but after two years, some of the eels successfully migrated. Therefore, I subsequently set the swimming speed between 0.05 and 0.01 m $s^{-1}$ and tested the differences in directional swimming paths at different angles, anticlockwise from eastward.

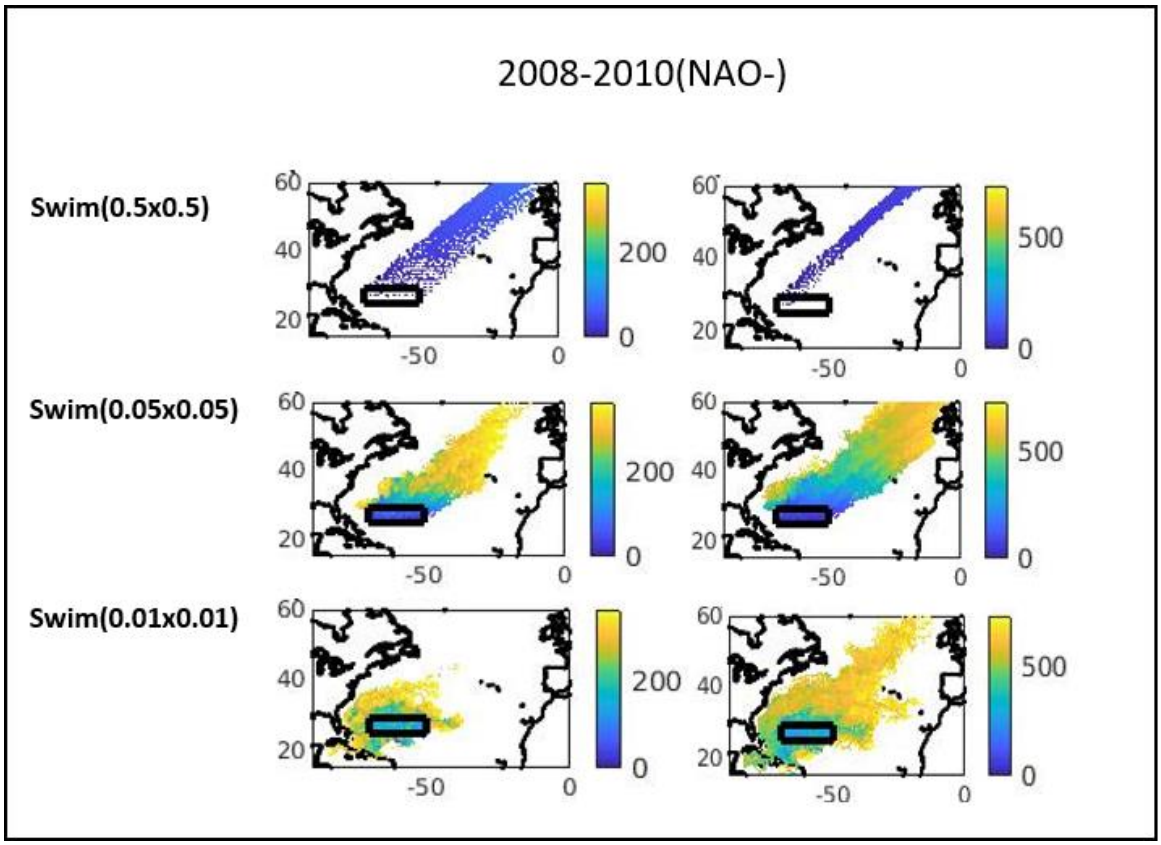


Figure 3-5. Particle density for releases in May, fixed to drift at a depth of 200 m with swimming vectors (m $s^{-1}$) specified as (A)(D) (0.5 m $s^{-1}$, 0.5 m $s^{-1}$), (B) (E) (0.05 m $s^{-1}$, 0.05 m $s^{-1}$), (C) (F) (0.01 m $s^{-1}$, 0.01 m $s^{-1}$) for one year and two years respectively.

Next, I conducted simulations on the directional swimming behaviour of eels during their migration. To align with the actual sampling distribution of eels and the primary regions of fresh eel habitation, I tested the hypothesis of fixed swimming angles at 45 degrees (representing the direction to UK and Northern Europe habitation), 30 degrees (representing Spain habitation), and 15 degrees (representing South Africa habitation) over a period of two years. As shown in Figure 3-6, eels migrating at a 45° angle have a higher probability of reaching the northern coast of Europe from the UK. Additionally, at 30°, 2.45 % of eels succeed in the Portugal and Spain region, while at 15°, 7.48 % of eels reach the southern coast of Europe.

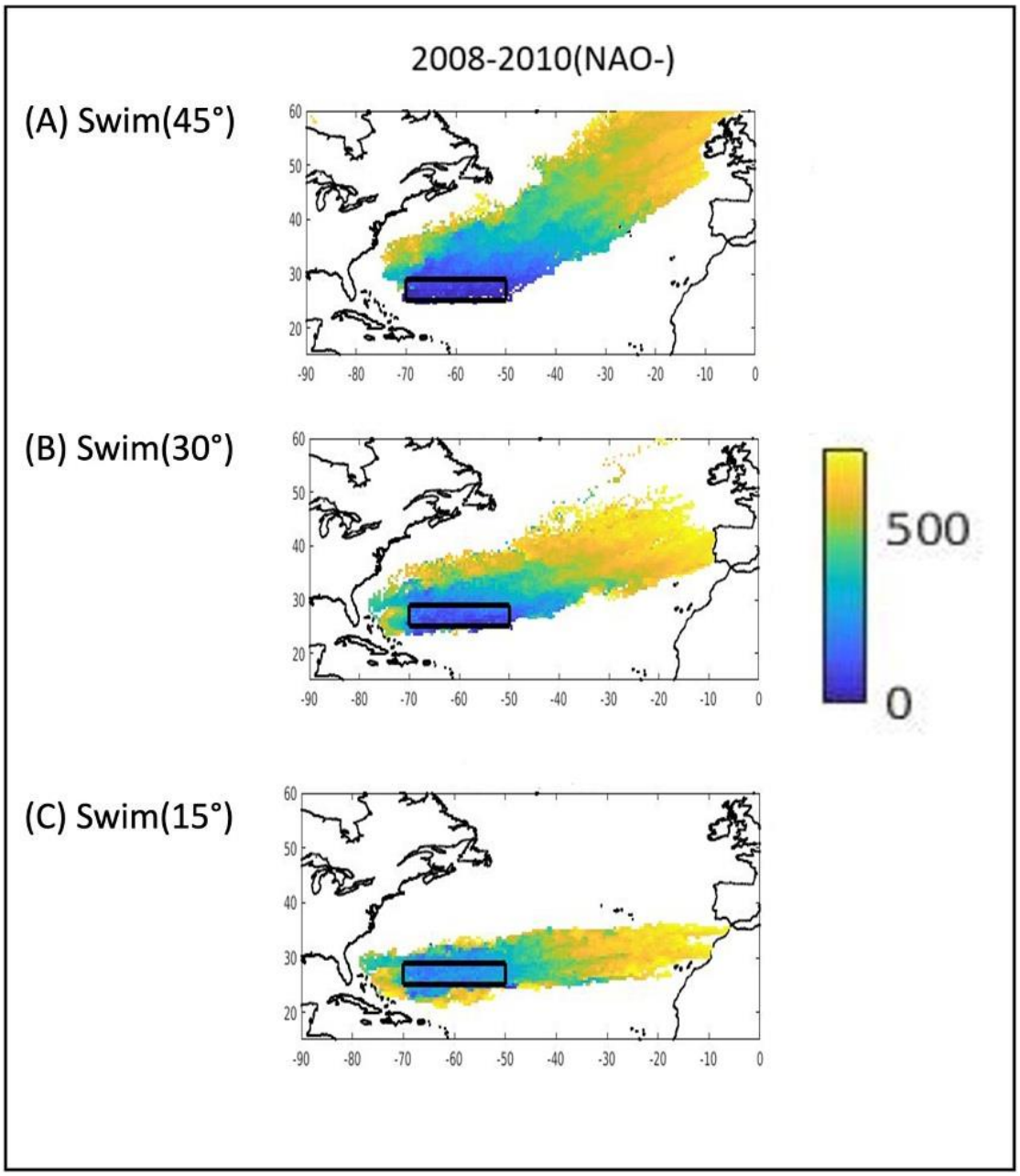


Figure 3-6. Particle density for releases in May fixed to drift at a depth of 200 m with swimming vectors (m $s^{-1}$) in different directions as (A) 45º(0.05X0.05 m $s^{-1}$), (B) 30º(0.028X0.05 m $s^{-1}$) (C) 15 º(0,013*0.05 m $s^{-1}$) The initial positions of these particles are indicated by black rectangles.

### 3.3.2 The hydrographic features of spawning areas

As I aimed to understand the differences in the spawning area of eels at a depth of 200 meters during different North Atlantic Oscillation (NAO) years, I compared the temperature, salinity, and $\delta^{18}O$ values at this depth. Overall, the average salinity of the spawning ground in the period of NAO+ is 36.65 psu, which is higher than that of NAO- (36.39 psu) (Figure 3-7). There is no significant difference in temperature between the two periods ($p<0.05$). The average value is 19.14°C, and there is no difference in most months ($p<0.05$), but in April of NAO+, the

temperature is 0.4°C higher than the other periods, and the salinity is also 0.4 psu higher than the average, resulting in $\delta^{18}O$ values appear lower compared to other years and months. However, the differences between spawning sub-areas were not significant.

.

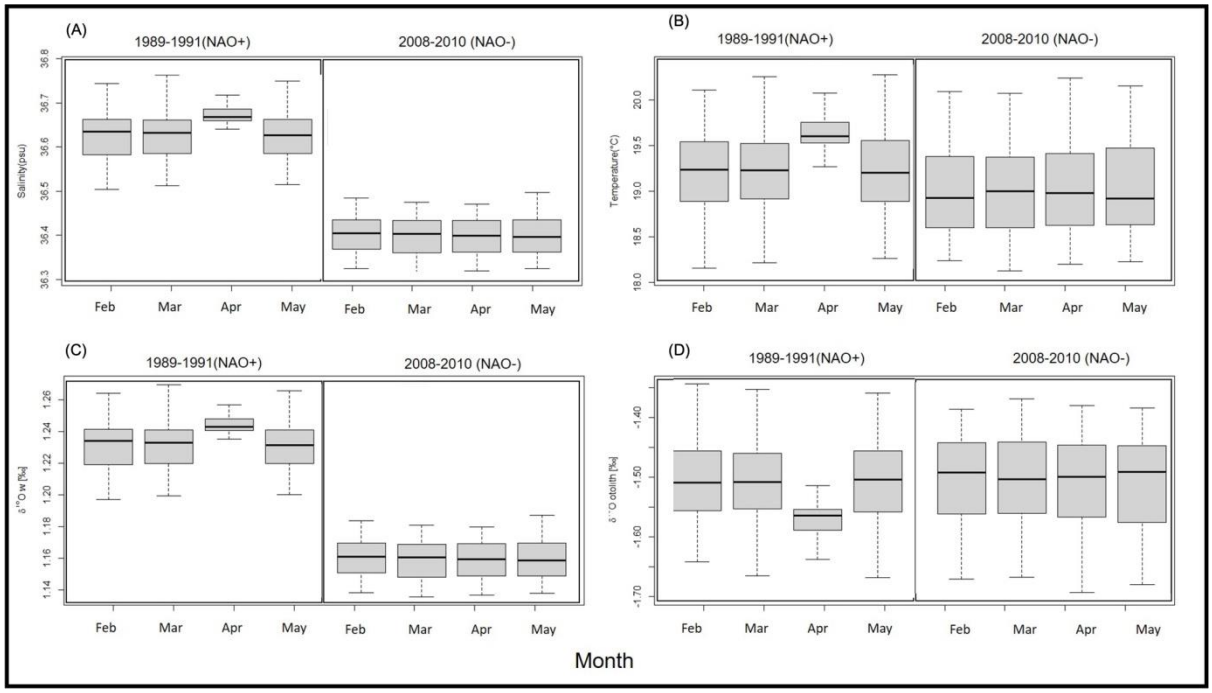


Figure 3-7. The hydrographic features of spawning areas 200m from February to May: (A) salinity (psu), (B) temperature (°C), (C) $\delta^{18}O$ w, and (D) $\delta^{18}O$ otolith.

### 3.3.3 Hydrography and inferred isotopic ratios along drift pathways

I chose May spawning area 1, which was fixed at 200 m depth for further analysis because this combination of factors in the simulation resulted in the highest probability of successfully reaching 20°W without considering swimming behaviour. The ambient salinity and temperature along particle trajectories was recorded, from which I infer estimates for $\delta^{18}O_w$ and $\delta^{18}O_{otolith}$. For particles released on May spawning 1 area 1989 (NAO+) and 2008 (NAO-), the properties of particles that succeeded in crossing 20°W with geolocation are shown in Figure 3-98 and Figure 3-9.

In Figure 3-98, time series of properties for the successfully arrived particles are shown. The particles that successfully cross 20°W follow similar trajectories in both years. The trajectories show that the particles flow through the Straits of Florida, continue along the east coast to Cape Hatteras, and then flow away from the US Eastern seaboard. However, the drift time before drift to the Gulf Stream was also shorter (300 days) for particles released in the NAO- period compared to the NAO+ period (400 days). This phenomenon was observed during the drift equatorward of

50°N. The time series of salinity and temperature (Figure 4-9) shows along-trajectory data for particles that reached 20ºW, released in May at 200m from sub-area 1 in 1989 (NAO+) and 2008 (NAO-).The decreasing trend of temperature and salinity imparts an increasing temporal trend in $\delta^{18}O_{otolith}$ values. For the NAO- periods, the particles drift to high latitude earlier than NAO-, with a shorter period of drifting. The temperature and salinity, followed by the particle drifting to a higher latitude, decreased from 300 days and remained steady after 500 days. The signal is correspondingly reflected in the estimated $\delta^{18}O_{otolith.}$

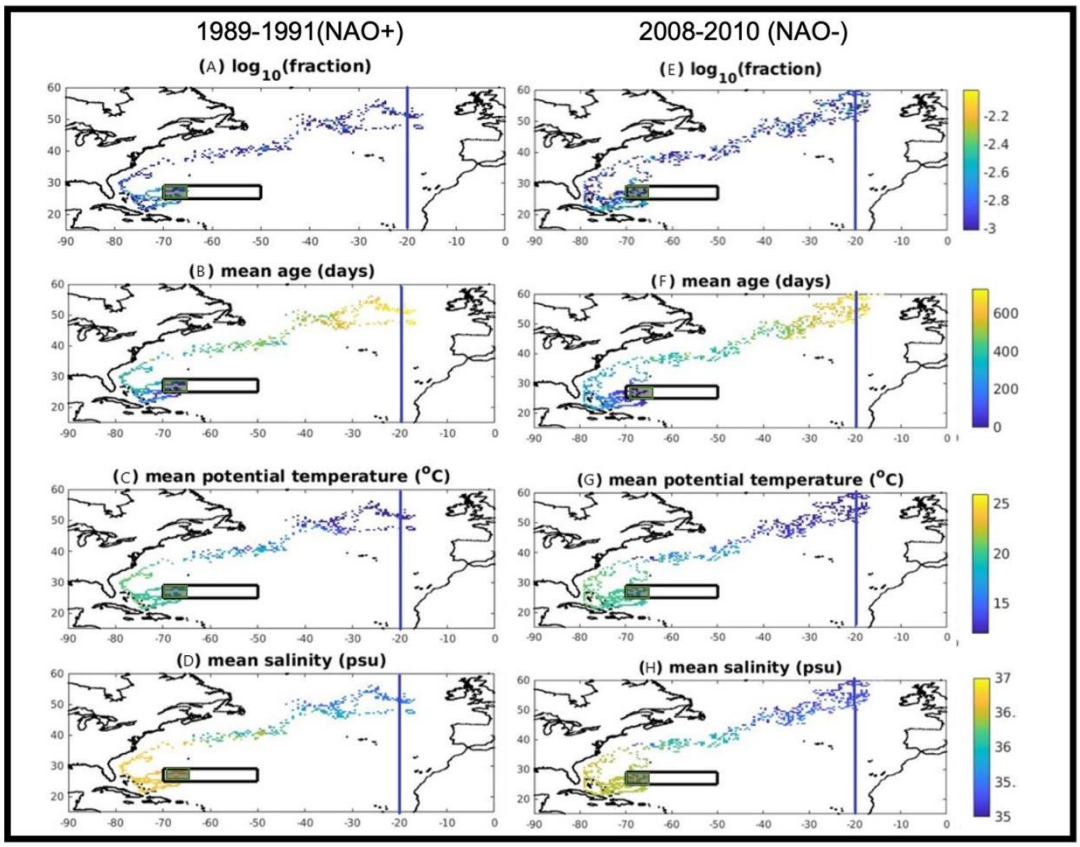


Figure 3-8. Particles selected for reaching 20ºW, released in May at 200m and spawning in subarea 1, in 1989 (NAO+) and 2008 (NAO-): (A), (E) particle density; (B),(F) mean age; (C),(G) mean potential temperature(ºC); (D),(H) mean salinity (psu). The initial positions of these particles are represented by black rectangles, and the subareas are depicted in grey on the map.

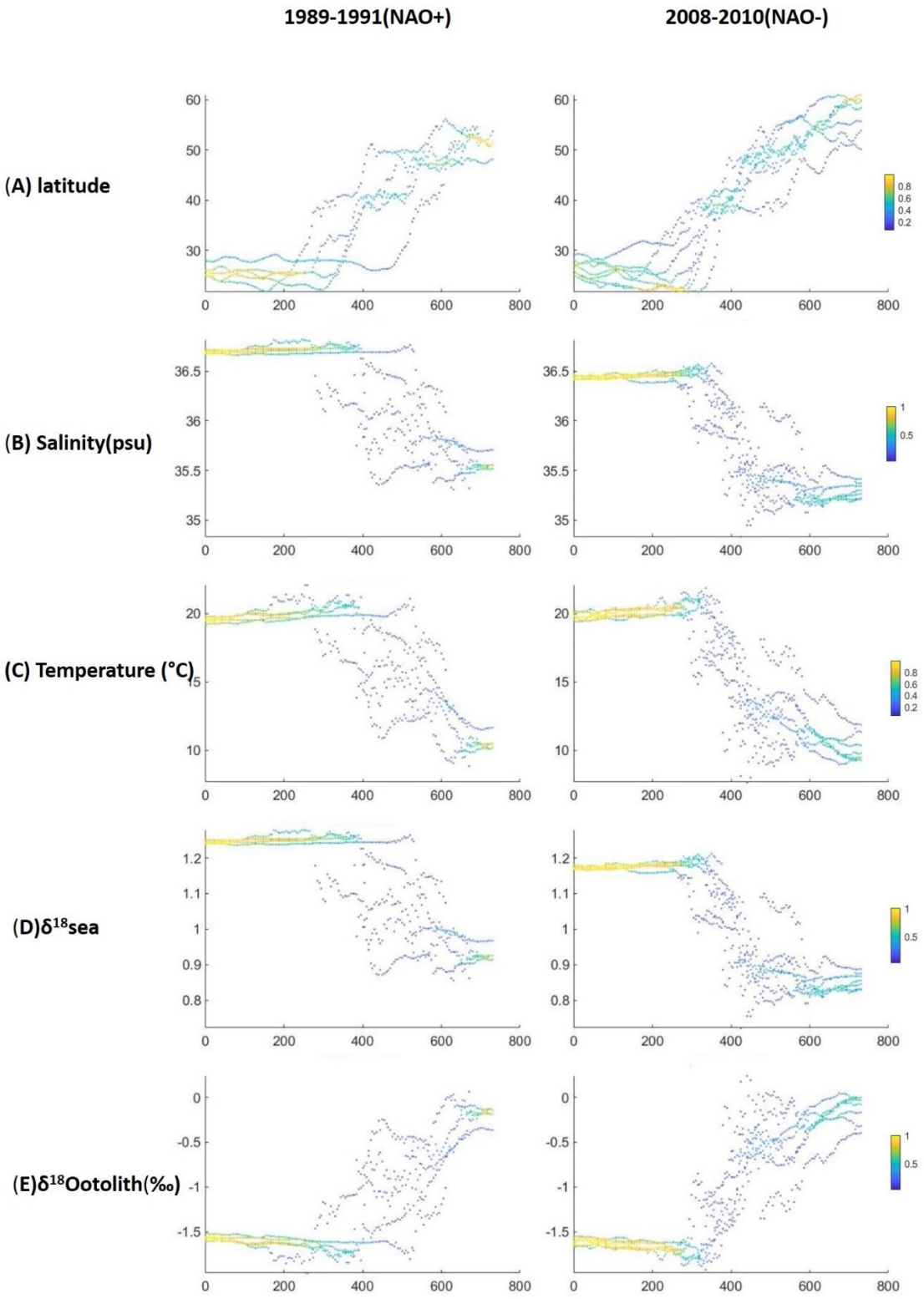


Figure 3-9. Along-trajectory data for particles successfully reaching 20ºW, released in May at 200m, spawning in sub-area 1, in 1989 (NAO+) and 2008 (NAO-): (A)latitude; (B) salinity; (C)temperature (ºC); (D)$\delta^{18}O_w$; (E) $\delta^{18}O_{otolith}$. The density of particles relative to the total is represented by a color scale bar.

For particles failing to cross 20°W, in the 1989-1991 experiment, the highest percentage of particles flowed with the Gulf Stream to 50°W, then turned south-eastwards to drift with the Azores Current and finally returned to circulate in the subtropical gyre

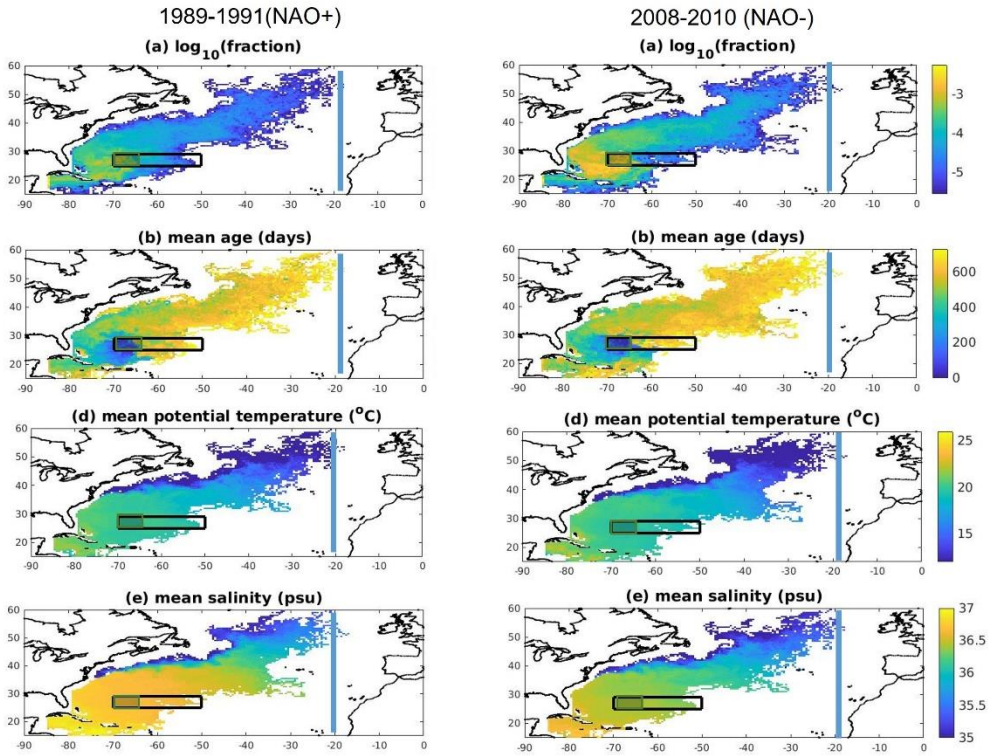


(

Figure 3-10A). However, in 2008-2010, a higher percentage of particle trajectories followed a primary flow to the south with the North Equatorial Counter Current and crossed 20°W between 19°N and the equator

(

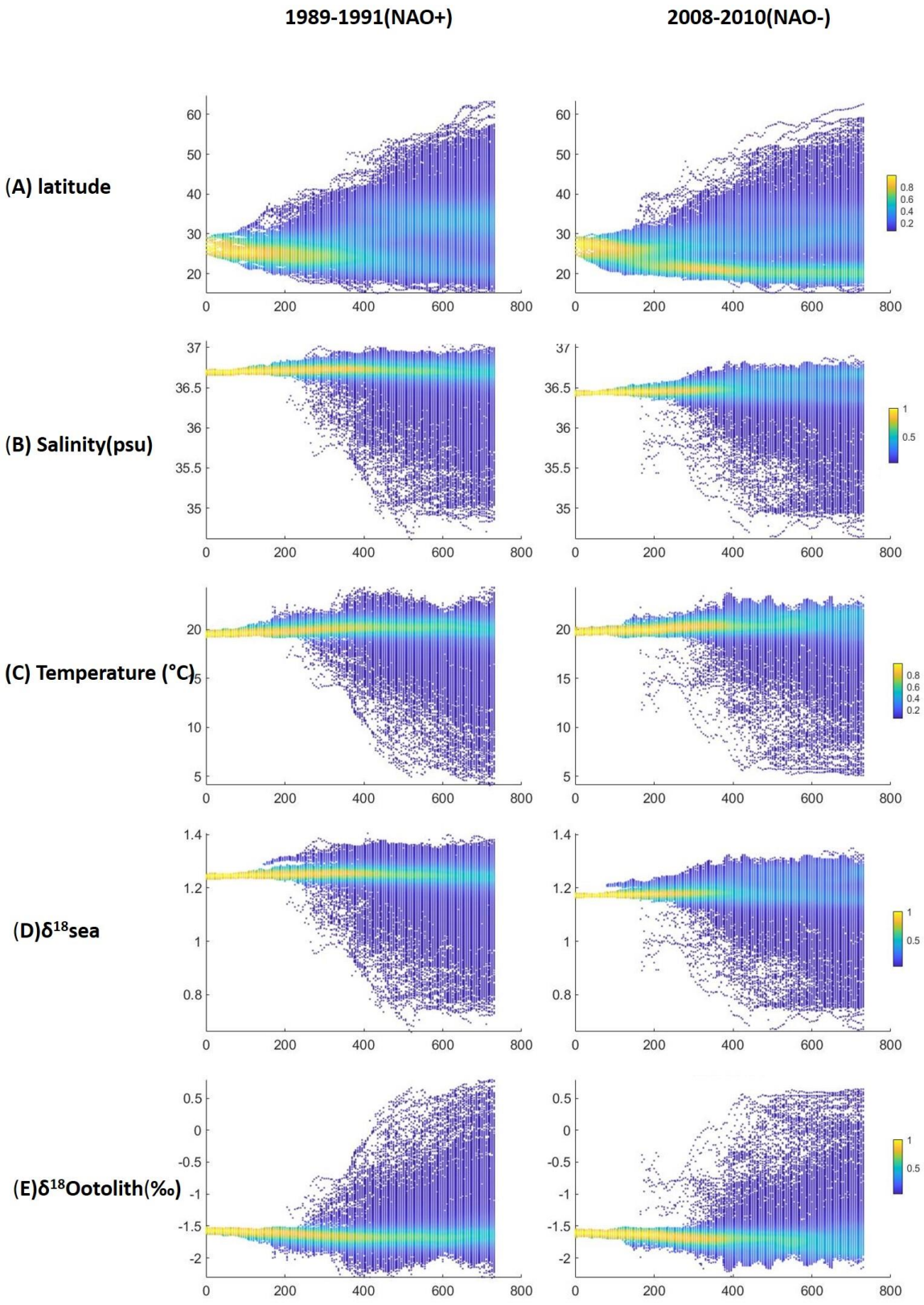


Figure 3-11(E)). The density of particles relative to the total is represented by a color scale bar.

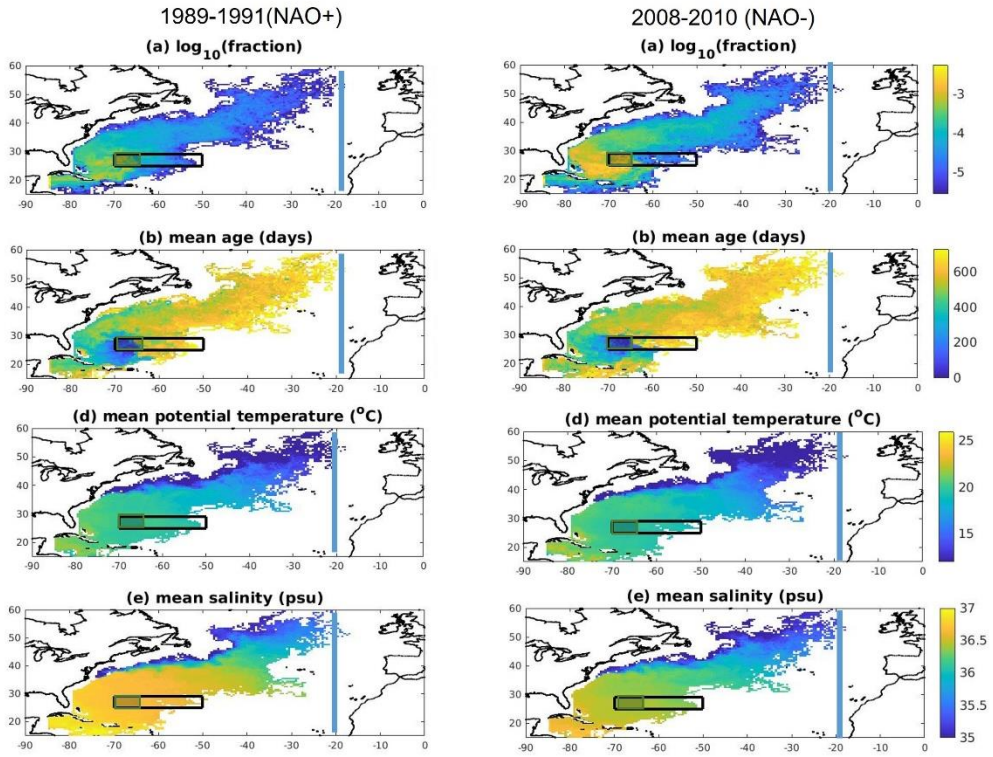


Figure 3-10. Particles failing to reach 20°W released in May at 200m and spawning in sub-area 1, in 1989 (NAO+) and 2008 (NAO-): (A),(E) particle density; (B),(F) mean age; (C),(G) mean potential

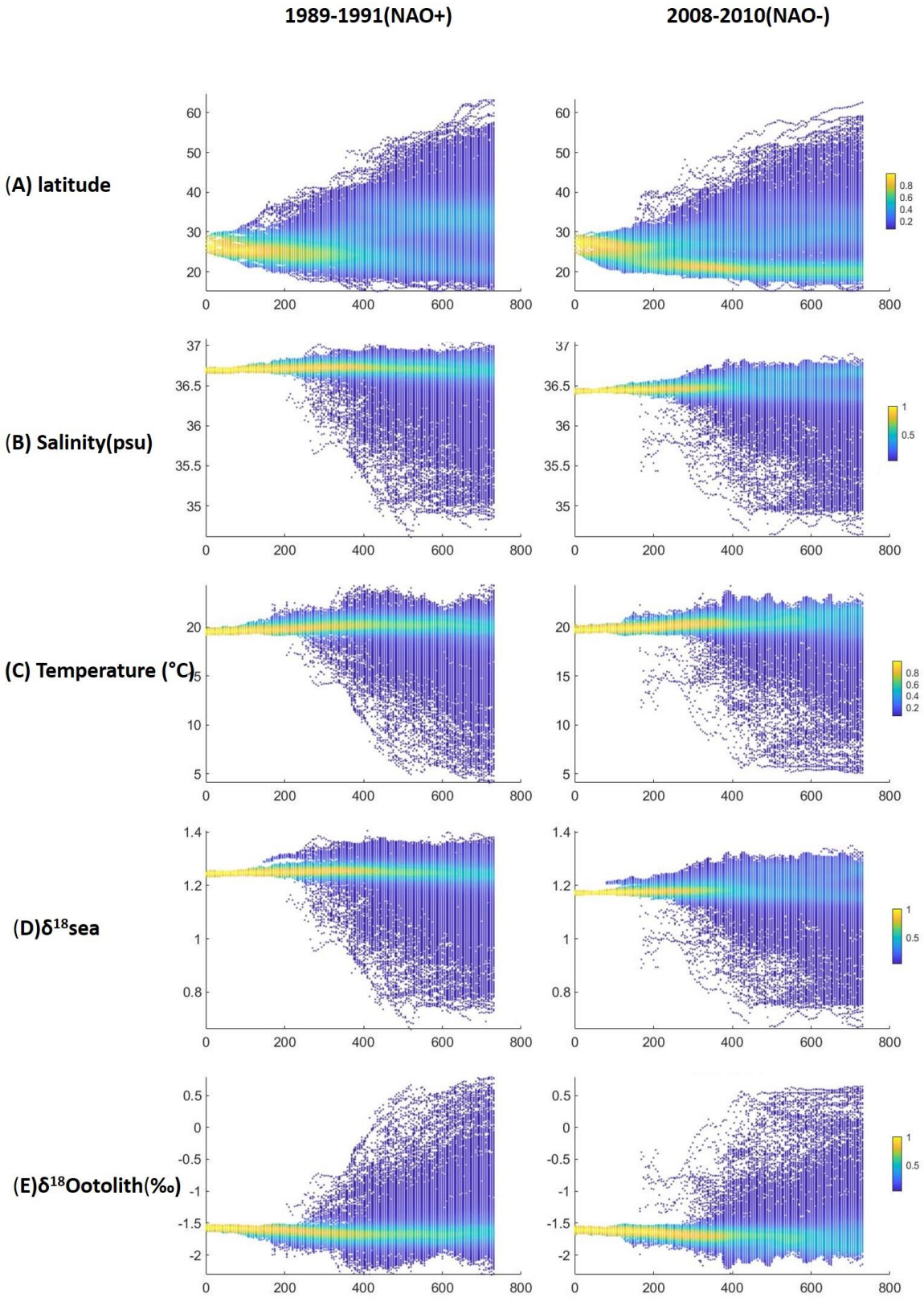


Figure 3-11. Along-trajectory data for particles failing to reach 20ºW released in May at 200m and spawning in sub-area 1, in 1989 (NAO+) and 2008 (NAO-): (A)latitude; (B) salinity; (C)temperature (ºC); (D)$\delta^{18}O_w$; (E) $\delta^{18}O_{otolith}$. The density of particles relative to the total is represented by a color scale bar.

From the temperature and oxygen isotope time series in Figure 3-12, it is clear that when the swimming direction is fixed at 45°, we observe an increase in $\delta^{18}O$ values after 300 days due to the decrease in temperature caused by northward movement. However, there is no significant change when the fixed angle is 30°. When the angle is fixed at 15°, we can see a sharp decrease in temperature after 300 days, from an average of 18 to 15°C. This phenomenon can also be observed in the isotope time series plot, where the average oxygen isotope value increases from -1.6‰ to -1.2‰. Since the migration area is located near the equator when swimming is fixed at 15°, the temperature is higher on average than for the other two angles, leading to a lower oxygen isotope value.

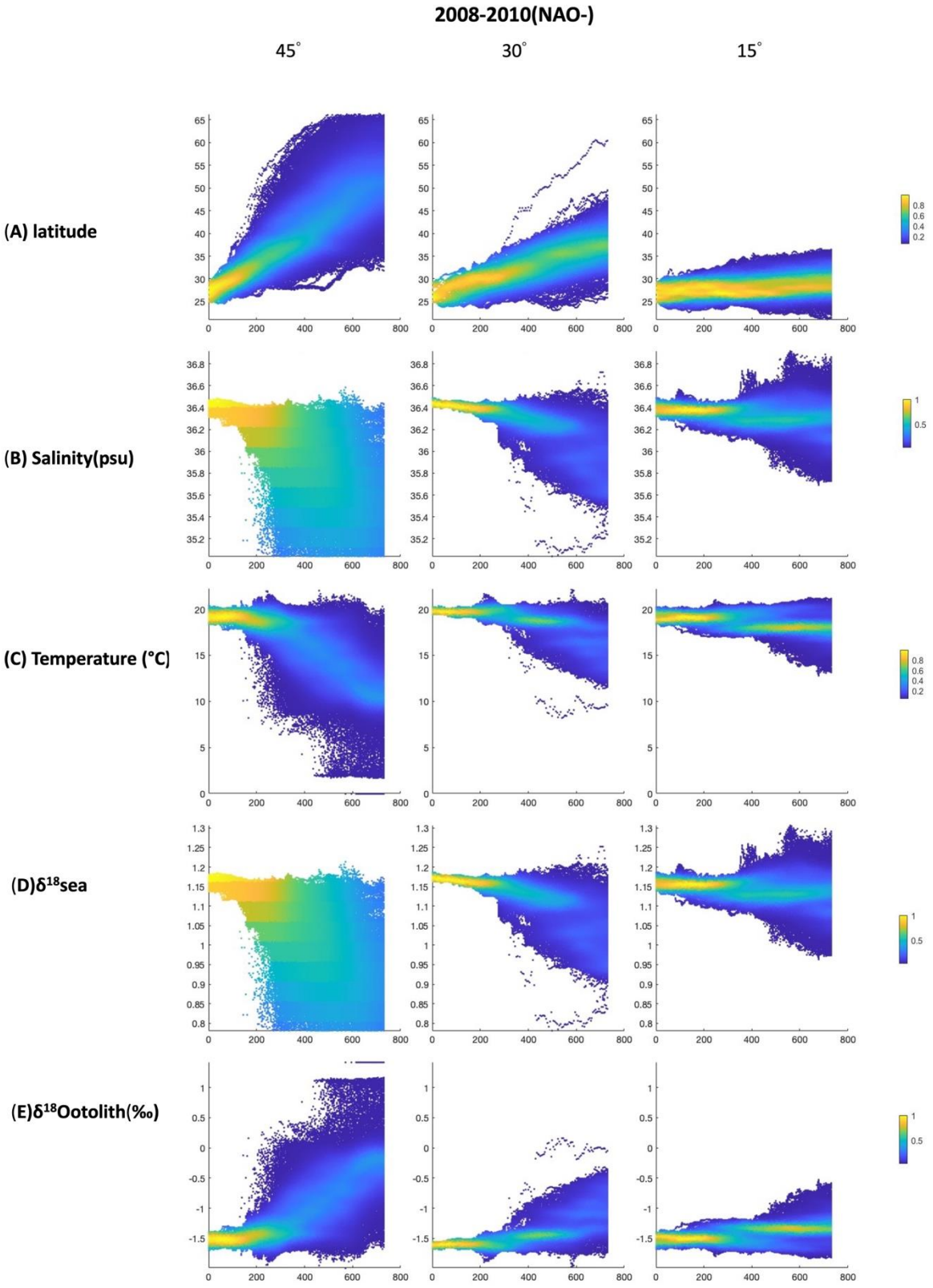


Figure 3-12. Along-trajectory data for particles in May 2008 (NAO-) at 200m with fixed swimming direction at 45, 30 and 15°: (A)latitude; (B) salinity; (C)temperature (ºC); (D)$\delta^{18}O_w$; (E) $\delta^{18}O_{otolith}$. The density of particles relative to the total is represented by a color scale bar.

### 3.3.4 Ocean currents during positive and negative phases of the NAO

As shown in Figure 3-13, the surface ocean currents are more likely to form anti-cyclonic eddies in the equatorial region due to wind stress. Over the NAO+ years 1989-91, stronger meridional pressure gradients across the northern subtropics and mid-latitudes supported stronger westerly winds, compared to the NAO- period of 2008-10. It is also worth noting that the Azores Current was stronger during the NAO+ period.

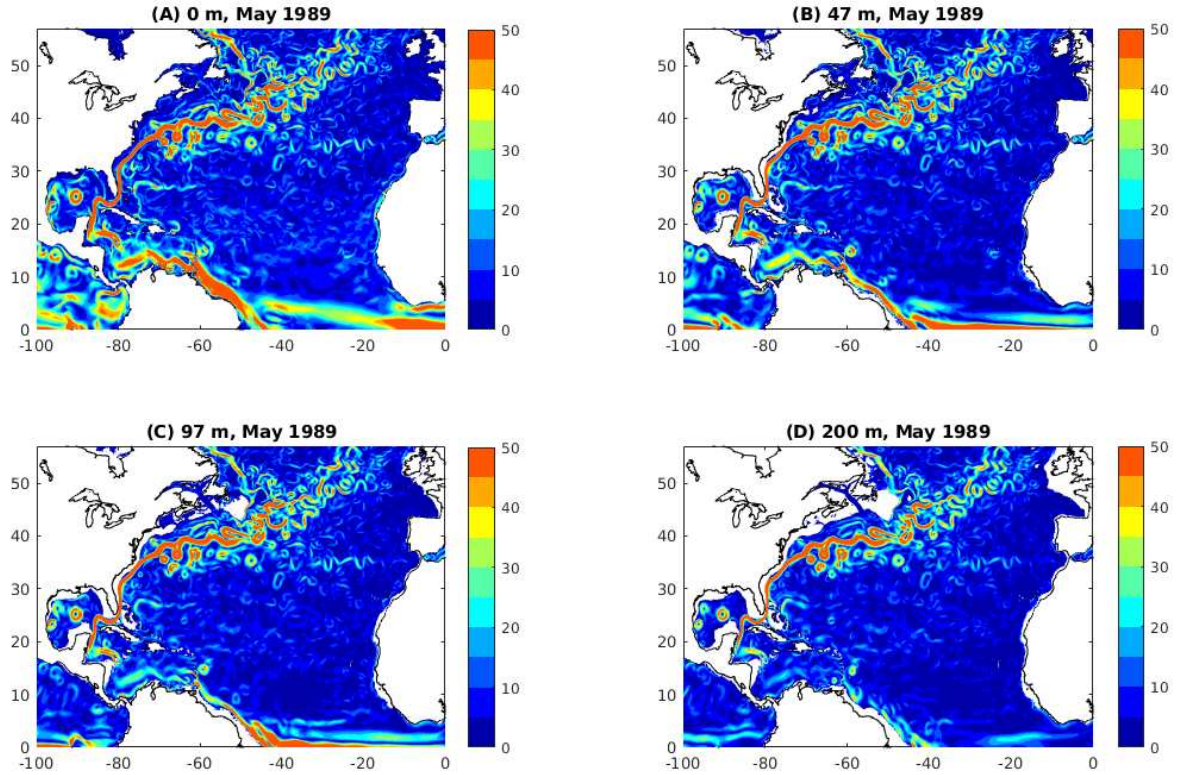


Figure 3-13.Ocean current speed at different depths during the NAO+ period: (A) 0m, (B) 47m, (C) 97m, (D) 200m. Colours indicate current speeds in meters per second ($ms^{-1}$).

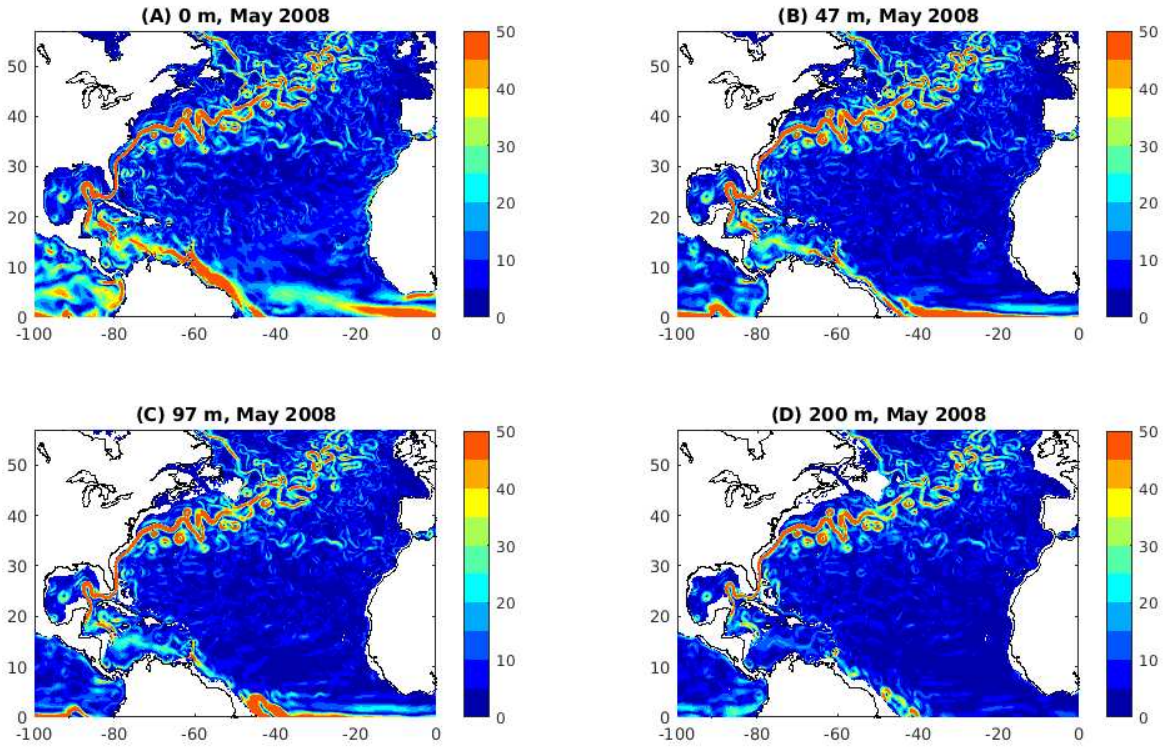


Figure 3-14. Ocean current speed at different depths during the NAO- Period: (A) 0m, (B) 47m, (C) 97m, (D) 200m. Colours indicate current speeds in meters per second ($ms^{-1}$).

To examine the differences in high current speed between the two time periods, I record the number of model grid points where speed exceeds 50 cm $s^{-1}$ north of 30°N and west of 20°W (Figure 3-15), at 200 m (Fig. 3-14(A)) and at the surface (Fig. 3-14(B)) for 1989-91 and 2008-10. During NAO+ years (1989-91) compared to NAO- years (2008-10), the higher number of 'fast grid points' indicates strengthened flows, consistent with stronger winds. Note 20-30% more places with fast flows under NAO+ compared with NAO-.

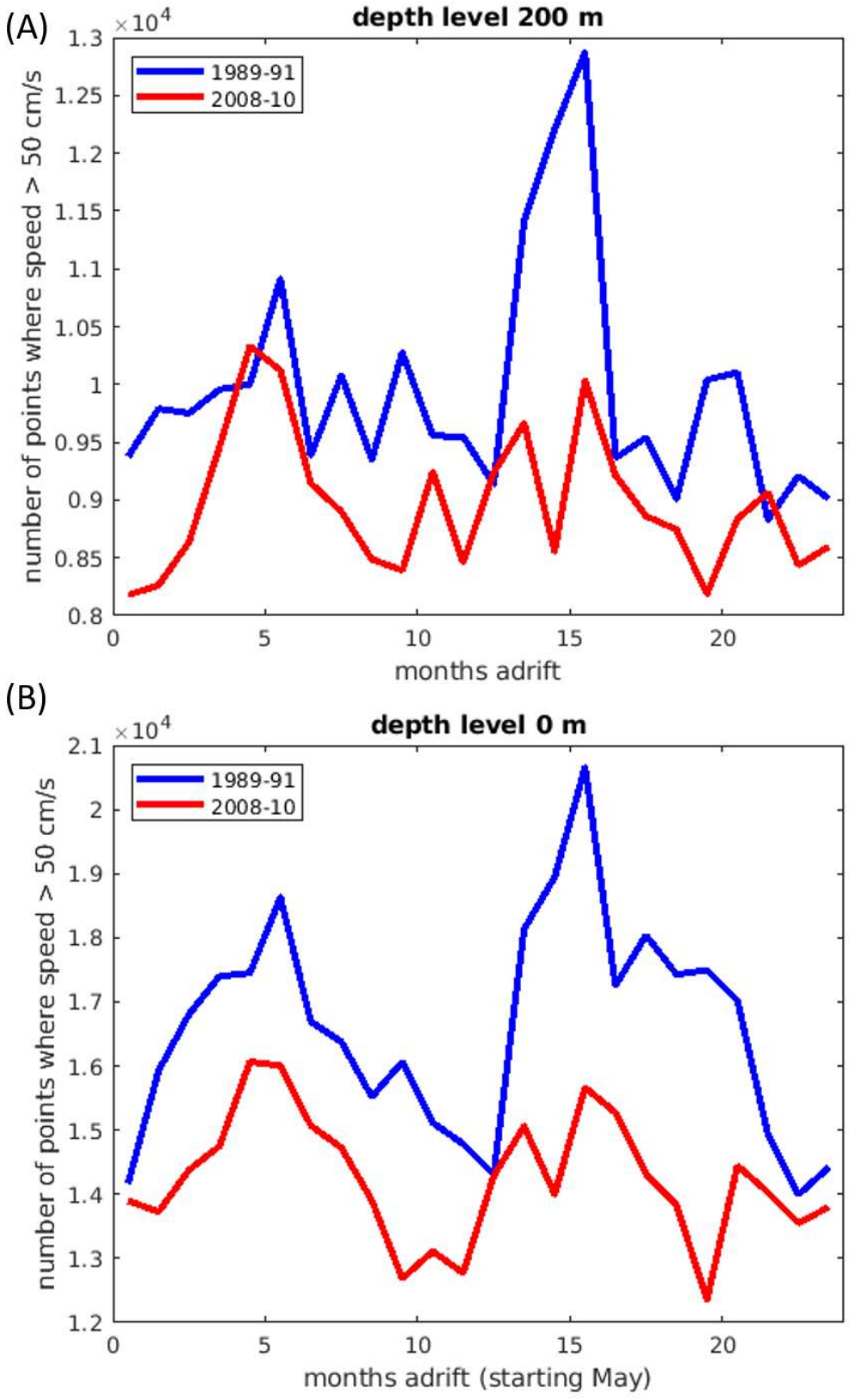


Figure 3-15. Number of model grid points where current speed exceeds 50 cm $s^{-1}$ everywhere north of 30°N and west of 20°W, at depths of (A) 200 m and (B) 0 m, over May 1989 to April 1991 (NAO+, blue) and May 2008 to April 2010 (NAO-, red).

## 3.4 Discussion

By calculating the trajectories of virtual particles embedded in near-surface ocean currents of an ocean model, I have predicted the drift of European eels that started from initial positions in 4 sub-areas of spawning locations in the subtropical North Atlantic between February and May. I also tested the successful arrival probabilities at four different depths, namely 0 m, 47 m, 97 m, and 200 m, and selected the highest probability at a certain depth and month to perform simulations for two different release years representing NAO+ (1989-91) and NAO- (2008-10), respectively.

Given the model temperature and salinity along particle trajectories, I further quantified the potential of $\delta^{18}O_{otolith}$ values to distinguish between success and failure to drift east of 20ºW, in NAO- and NAO+ year, and to characterize spawning areas. In addition, I also tested the swimming speed of European eels and compared the possible migratory routes with different bearings of directional swimming. I used the model temperature and salinity along particle trajectories to compare the differences between the routes.

The main findings are as follows:

### 3.4.1 Predicting the probability of successful larval drift

I tested the importance of factors such as starting location and the spawning period between February and May, depth, and NAO+ and NAO- years, for successful larval migration (defined east of 20ºW). Depth and year have a significant impact on success in reaching 20°W. Success rates were lowest for drift with currents at water depths of 0 m and 47 m; this was since a significant fraction of particles entered the equatorial counter current to the south, crossing 20°W between 19°N and the Equator (Figure 3-3). Among the four depths from 1989 to 1991 (NAO+) and 2008 to 2010 (NAO-), the percentage of particles that successfully crossed 20°W was highest for drift with currents at 200 m. Simulation results from Blanke et al., (2012) also show that the movement depth of larvae and juveniles during the drifting stage has a significant influence on the success rate because the near-surface layer of the southern branch of the Gulf Stream is most affected by the wind, hence eels drifting in deeper water are more likely to reach a destination than eels drifting on the surface.

I also found that the NAO significantly impacts the success rate of eel migration. The success rate in the NAO- period (0.0012%) was significantly higher than in the NAO+ period (0.00069%). Paradoxically, the success rate is lower when currents are on average stronger during NAO+ years, associated with stronger winds. This may be a consequence of stronger recirculation and

southward Ekman drift in the subtropics, reducing the fraction of particles that can navigate the inter-gyre zone to reach 20ºW. Simulating drift with currents at 200 m, the arrival rate was significantly higher from April to May, regardless of whether it was subject to NAO+ conditions from 1989 to 1991 or NAO- conditions from 2008 to 2010. The simulation results thus indicate a link between the migration pattern of the European freshwater eel and the NAO. In addition, the starting position has a great influence on the arrival rate. The results of the simulation started in 1989 showed that only particles from spawning area 1 in the west of the spawning area migrated successfully(Figure 3-5.A), with a success rate of 0.002 %, and in the simulation process from 2008 to 2010 (NAO-), the success rate of spawning area 1 was the highest at 0.0027% (Figure 3-5.E). Individuals successfully crossed 20° from spawning area 3 only sporadically.

### 3.4.2 Passive drift and swimming trajectories

From the results of simulating passive drift, I found that the probability of eels reaching their destination through passive drift alone was very low. Therefore, I incorporated active swimming behaviour into the model and tested three speeds and angles. I found that an eel swimming speed between 0.05 and 0.01 m $s^{-1}$ was more consistent with current observations of sample collection. I also simulated the effect of increased swimming ability on migration time and found that even with increased swimming ability, only a tiny proportion of eels could reach their destination within one year. Therefore, the model suggests that a two-year migration time is more likely consistent with current ecology, physiology, and physical oceanography knowledge.

### 3.4.3 Hydrological characteristics of spawning ground

Changes in oceanographic conditions caused by the NAO have been hypothesized as a possible contributing factor to the decline in European eel populations. While many studies have found correlations between glass eel recruitment and the NAO and eel recruitment (Knights, 2003), the mechanism controlling successful recruitment has not been directly determined. One hypothesis is that temperature and salinity changes in the spawning area directly affect eel recruitment. This study also attempted to narrow down the spawning area of the eels and found that only the larvae from the Westernmost spawning area could successfully reach their destination in our simulation. This may be related to the proximity of this region to the axis of the Gulf. Although younger eel larvae have not yet been collected along the axis of the Gulf Stream, this could be attributed to the vast expanse of the presumed anguillid eel spawning area within the subtropical convergence zone of the Sargasso Sea. The quest for specific spawning sites in both space and time through traditional fisheries or larval surveys is challenging, laborious, and costly, akin to

searching for a needle in a haystack. Modelling exercises prove to be extremely useful, serving to critically evaluate purportedly established scientific hypotheses.

My simulation results showed that during the NAO+ period, the salinity of the spawning ground is lower than that of NAO-, while the temperature is not significantly different between these two periods. This resulted in no significant difference in the oxygen isotope in the otolith core, making it impossible to use oxygen isotopes to distinguish eel spawning dates and years based on salinity differences alone. However, it is worth noting that in April of the NAO+ period, the temperature and salinity of the eel spawning ground showed significant differences, resulting in a clear difference in oxygen isotopes compared to other months. Therefore, it is possible to distinguish the period when the eels were born (NAO+ or NAO-) through otolith isotopes. If otoliths collected during the NAO+ period can be obtained, it may be possible to determine the timing of eel migration more accurately.

### 3.4.4 Hydrogeography and inferred isotope ratios along drift paths

The migration of European eel is believed to be the longest among all anguillid species, which makes its recruitment highly susceptible to changes in the oceanic environment. However, due to a lack of tracking and environmental information, the mechanism by which the North Atlantic Oscillation (NAO) index affects the migration of eel larvae is not clear. Based on the assumptions, I simulated the migration of eel larvae under positive and negative NAO indices. My study revealed that the NAO index significantly impacts the probability of eels reaching their destination. I present a time series of environmental factors for particles reaching their destination successfully and potential factors that may impact the failure of eel migration.

My study also recorded the ambient salinity and temperature along the trajectories of particles, which allowed us to estimate $\delta^{18}$Ow and $\delta^{18}$Ootolith. Furthermore, I provide experimental suggestions and methods for using otolith isotopes to verify model assumptions, demonstrating the potential of otolith isotopes for validating migration models.

As with many studies, the current simulations found that the distribution of leptocephalus most likely use the Gulf Stream/North Atlantic Drift system after moving west through the southern Sargasso Sea (Kettle & Haines, 2006; Kleckner & McCleave, 1988). However, some studies suggest that a direct eastward or north eastward movement of some leptocephali may also be possible, due to flows associated with the frontal jets that form in the subtropical convergence zone each year. Although this route was also observed in my simulations, it was not successfully reached within the two-year simulation period, suggesting that this route may require a more extended period of passive drift to be successfully reached. It is noteworthy that during the NAO+ period,

the probability of using the second route increases due to the strengthening of the Azores Current.

The current model simulation found that during NAO+ periods, larvae had lower success rates, while during NAO- periods, they had higher success rates and approached the European coast more quickly. Before entering the Gulf Stream, larvae during NAO+ periods required nearly 400 days, while during NAO- periods, they only needed 300 days. This may be due to the strong wind enhancing anticyclonic gyre currents, recirculation towards the centre, and local weakening of westerly winds and wind-stress curl effects, reducing transport rates and hence prolonging migrations. Additionally, the simulation showed that NAO- years with high dispersal rates were characterized by predominantly westward currents in the variable flow regime east of the Bahamas, providing a "shortcut" to the Gulf Stream through the Caribbean Sea. In theory, by sampling successfully migrated eel specimens and analysing otolith samples between 300 to 700 days, we observed the slope of otolith oxygen isotopes and the beginning and end times of sharp increases, providing insights into the impact of ocean currents on eel migration routes and return times. However, according to Fukuda et al. (2009), during the larval migration phase, the increment formation speed and otolith growth rates could decrease if they experienced low ambient temperature. Otolith growth and daily increment deposition of *Anguilla japonica* glass eels and elvers decreased at temperatures below 15°C and ceased at temperatures below 10°C. Assuming that European eels undergo a similar situation as Japanese eels, it is recommended to collect otoliths within the 300 to 600-day range during sample collection, as temperatures below 15°C may be encountered during the 600-day period of migration, potentially introducing errors.

During NAO+ periods, eel larvae required more time to reach the European coast by following the Gulf Stream, as the Gulf of Mexico was further away from the coast and they only joined the North Atlantic Current at 45°W. Despite having a stronger current during NAO+ periods that overlapped with the eel migration time, it took longer for them to reach the coast compared to NAO- periods. Different migration times produce distinct signals in otolith oxygen isotope records. By sampling the time series of otolith oxygen isotopes between days 300 and 700, we have excellent potential to verify the effect of the NAO index on eel migration time and its impact.

During the NAO+ period of 1989-1991, my model simulation found that the inability of eels to migrate to 20°W within two years was mainly due to the backflow of the Gulf of Mexico Current. However, in the 2008-2010 period, a larger percentage of particles drifted southward with the equatorial counter current and then flowed with the Gulf Stream/NAC towards 50°W. They subsequently turned southeast with the Azores Current and recirculated back to the subtropics. These two pathways did not involve significant northward drift, resulting in no significant

differences in $\delta^{18}O_{otolith}$ values. Therefore, it was challenging to confirm the effect of NAO on eel recruitment failure through the collection of otolith oxygen isotope samples.

Many studies have suggested that late-stage leptocephali may be able to swim (Miller & Tsukamoto, 2017; Yamada et al., 2009), but it is unknown whether they actively use swimming for migration. However, related studies have shown that directed swimming may be crucial for successful recruitment, as demonstrated by model simulations (Rypina et al., 2014). Given the complexity of age and growth models and transmission studies, the current study focuses on whether the hypothesis of different strengths and orientations of swimming can be distinguished through the record of otolith oxygen isotopes. Therefore, I ran simulations with three different average swimming speeds and directions and found that incorporating swimming behaviour not only significantly increased the probability of successfully reaching the European coast, but also resulted in paths that were more consistent with field sampling results(Figure 3-1). I also observed significant differences in temperature and oxygen isotope responses among the three different swimming directions, at an optimal swimming speed of $0.5ms^{-1}$, even after 300 days. This suggests that if sampling is conducted within this period, it may confirm the hypothesis of directional swimming behaviour in eels and demonstrate the potential of using otolith isotopes to distinguish a possible second migration route.

Shirai's otolith temperature equation, which we used in this simulation, presents a novel approach compared to traditional fish oxygen isotope thermometry models. The smaller slope of 0.15, as opposed to the typical 0.25, results in reduced sensitivity of $\delta^{18}O_{otolith}$ values to temperature variation. It is important to note that this reduced sensitivity also implies that our simulation using the Shirai equation likely represents a conservative estimate of potential isotope differentiation. Therefore, while the Shirai equation offers a robust baseline for estimating migration and isotope differentiation, further refinement and empirical validation through otolith analysis would strengthen our understanding of these complex processes.

### 3.4.5 Comparing simulation results with catch data

The Den Oever glass eel recruitment index (DOI) has utilized standardized glass eel sampling methods at Den Oever in the Netherlands at the barrage between the IJsselmeer and the North Sea since 1938 (ICES, 2001). My results align with Friedland et al. (2007), which found that the NAO shows the same negative correlation with the Den Oever glass eel index. High NAO years were associated with lower eel abundance in the Skagerrak. However, this is different from the findings of Caroline et al. (2010), who suggested that faster transport within the Gulf Stream (high NAO index) results in a shorter migration and stronger currents towards southern Europe. They

argued that a shorter migration time would cause the larvae to arrive too early at the upper limit of their distribution area, impacting their ability to metamorphose and colonize northern coastal and inland waters. Despite these differences, both studies support the notion that eel abundance may decrease in high NAO years. Caroline et al. also hypothesized that this might lead to an increase in resources in the south. My results indicate that in high NAO years, eel migration success rates are lower in both northern and southern regions, which is consistent with Kettle et al. (2007). Kettle found both negative and positive correlations between NAO and fishery-dependent data on Food and Agricultural Organization (FAO) landings from clusters of European countries, with no obvious latitudinal pattern. However, FAO landings from Norway showed positive correlations with NAO, which contradicts my results

However, the application of the NEMO model in shelf and coastal settings may have some limitations, particularly regarding its accuracy. A key limitation is that NEMO does not account for tidal forces, which are essential in many coastal and shelf environments. Tidal currents play a significant role in influencing larval dispersal, water circulation, and the overall dynamics of marine ecosystems in these areas. By excluding tidal effects, NEMO may fail to accurately capture the movement patterns and behaviours of larvae, potentially leading to misrepresentations of migration success and recruitment in regions where tides are a dominant factor. This omission could reduce the model's precision in environments where tidal influences are critical to understanding ecological processes.

## 3.5 Conclusions

Despite significant efforts, our understanding of the spawning grounds, larval migration behaviour, and pathways of European eels is limited due to sampling difficulties. However, understanding the behavior and pathways of eel larvae is crucial for effective management and conservation strategies, especially as long migrations may make eels more vulnerable to the effects of climate change. In this study, I used virtual particle trajectories embedded in ocean currents to predict the drift of European eels. The eels were initially positioned in four sub-areas of spawning locations between February and May at four different depths. I found that the highest success rate for eel migration occurred in May at a depth of 200 meters. Using this setup to compare the effects of different North Atlantic Oscillation (NAO) periods on eel behaviour, I found that during NAO+ periods, eels required a longer time for migration and had a lower migration success rate, likely due to stronger recirculation in the subtropics. I also demonstrated the swimming necessary for successful return and discovered two potential migration pathways for eels, with more eels moving towards pathways requiring longer migration times during NAO+ periods.

The temperature and salinity data obtained from the particle trajectories were used to infer the otolith $\delta^{18}O$ values. Through the model's predicted stable isotopes and migration paths, I found that otolith oxygen isotope ratios can distinguish the characteristics of spawning locations in April during NAO+ periods and can distinguish between successful and failed drifts. By sampling successfully migrated eel specimens and analysing otolith samples between 300 to 600 days, I observed the slope of otolith oxygen isotopes and the beginning and end times of sharp increases, providing insights into the impact of ocean currents on eel migration routes and return times.

My study indicates that using otoliths to analyse stable isotopes can provide valuable information on the environmental conditions experienced by the larvae during their journey, which can help understand the factors affecting their survival and recruitment success. This study demonstrates the potential of using a combined model and otolith analysis to validate findings. The study's findings can also be applied to other species with similar pelagic larvae stages and oceanic migration patterns, providing a valuable tool for assessing recruitment dynamics and developing effective conservation measures. Overall, this study highlights the importance of understanding the ecological and environmental factors that affect the recruitment success of migratory species and the potential of using stable isotopes to address these questions.

# Chapter 4 First in-situ measurements of field metabolic rate in wild Atlantic mackerel

**Abstract**

The effect of temperature on animal phenotypic and life history traits plays a crucial role in population dynamics, community structure, and evolutionary ecology. Metabolic rate (and therefore food and oxygen requirement) also dictates habitat suitability and growth rate and informs bioenergetic models. While laboratory-based respirometry has provided insights into metabolic level, thermal performance curves and aerobic scope in many marine fishes, our current understanding of fish ecophysiology primarily relies on extremes of metabolic rates under laboratory conditions.

In natural settings, energy-demanding processes such as movement, feeding and growth, coupled with individual variability likely dampens population-level effects of temperature on realised field metabolic rates. However, direct measurements of field metabolic rates (FMR) in marine ecosystems pose challenges, motivating the novel use of otoliths for FMR estimation. Here I outline a four-step approach to assessing realized thermal sensitivity of FMR in juvenile mackerel (*Scomber scombrus*) from UK waters. I draw on otolith stable isotope compositions to infer experienced temperatures and FMR, and therefore quantify mass and temperature scaling of field metabolism in these pelagic fish within UK waters. I find that FMR is strongly related to body mass with an allometric scaling exponent of -0.1 (whole organism scaling of 0.89). Thermal effects on realised FMR were negligible, suggesting that factors beyond temperature contribute substantially to individual variations in FMR. The wide-ranging individual FMR variation suggests a robust aerobic capacity under current conditions, potentially affording resilience against temperature fluctuations. However, the adaptability of aerobic scope to future changes in temperature or food availability remains a crucial consideration. The innovative utilization of otoliths as a proxy for FMR offers a promising monitoring tool to assess the ecological and physiological vulnerability of wild fish populations. This study provides valuable insights into the intricate interplay between temperature, metabolism, and individual variability, with implications for understanding and managing the impacts of environmental change on marine ecosystems.

**Key words:** $\delta^{13}C$, otolith, metabolic rate, Atlantic mackerel

## 4.1 Introduction

Temperature is a key factor affecting the phenotypic and biological features of marine ectotherms, and it can have significant impacts on population dynamics, community structure, and evolutionary responses to climate change. Ambient water temperature directly influences metabolic rate in marine ectotherms both through the thermal effect on reaction rates and the availability of dissolved oxygen (Chung, et al., 2021; Ohlberger, 2013; Seebacher et al., 2015). The effects of temperature on fish performance are well-established, and it is the primary driver in most physiologically-informed models of fish distribution and performance, (The Fisheries and Marine Ecosystem Model Intercomparison Project (Fish-MIP) , Tittensor et al., 2010; van Denderen et al., 2020). However, the effects of warming on enzyme activity can be amplified or offset by acclimation and metabolic plasticity, which can affect the distribution of energy budgets among individuals (Norin & Metcalfe, 2019). Therefore, a thorough understanding of the mechanisms linking performance and temperature is essential to make accurate predictions of animal responses to climate change.

The potential effects of temperature on fish metabolism can be inferred from laboratory measurements of the normal (SMR) and maximal metabolic rate (MMR), and which are used to calculate the aerobic scope (Clark et al., 2013). However, pelagic fishes can be difficult to maintain in small tank respirometry systems, which has led to a relative lack of knowledge on the ecophysiology of these commercially important taxa. Furthermore, physiological limits measured in the laboratory do not necessarily predict metabolism in the field. Therefore, it has been suggested that time-integrated field metabolic rate (FMR) is a more ecologically relevant measure of energy use in wild organisms (Payne et al., 2011; Treberg et al., 2016). However, measuring FMR in situ can be challenging due to the inaccessibility of marine ecosystems (Chung, Jørgensen, et al., 2021a; Sarah Rose Alewijnse, 2022; Treberg et al., 2016; William & Msci, 2022).

The retrospective estimation of field metabolic rate (FMR) for teleost fishes from otolith aragonite carbon isotopes is a recent development in the field of fish ecophysiology (Chung et al., 2019; Martino et al., 2020; Trueman et al., 2019). Otolith biomineral contains carbon from two sources: dissolved inorganic carbon (DIC) from the water and respired dietary carbon. The isotopic difference between these two sources allows the proportion of carbon in the otolith derived from metabolic sources ($C_{resp}$) to be estimated using a two-component mixing model. As the proportion of metabolic carbon entrained in the otolith is directly proportional to rate of respiration of carbon, this method provides insight into individual-level variations in FMR under natural environmental conditions, which was previously difficult to measure in situ. Several studies have demonstrated the potential of this method, showing that FMR can be estimated retrospectively

from stable carbon isotopes in otoliths (Chung et al 2019, Smolinski et al 2022, Alewijnse et al 2021, Priester et al 2024, Trueman et al 2023).

Atlantic mackerel (*Scomber scombrus*) is a fast-swimming, pelagic species within the Scombridae, widespread in the North East Atlantic (NEA), from Morocco to Norway, the Mediterranean Sea, Skagerrak, Kattegat, and Westernmost Baltic Sea and North Sea (Trenkel et al., 2014). The Northeast Atlantic mackerel (NEAM) spawning season starts from the southern stock, along the coast of Spanish and Portuguese waters, in late January, reaching a peak in April. This is followed by the Western stocks from March to June (Berge et al., 2015; Cunningham et al., 2007), and the north stocks in the North Sea in June (Cunningham et al., 2007; Jansen, 2016; Jansen et al., 2012a). After the spawning season, during spring or early summer, the mackerel migrates northward to feed in the Norwegian Sea, along the Norwegian coast, and partly in the North Sea before returning south along the continental shelf edge from mid-November to early March. This migration path coincides with a relatively warm shelf edge current (Berge et al., 2015; Jansen, 2016; Jansen, Campbell, et al., 2012; Uriarte & Lucio, 2001). Mackerel juveniles (0–2 years old) generally remain closer to the coastal nursery areas, and they join the general adult migratory pattern when they are three years old (Cotano et al., 2003).

In the late 1960s-70s, there was a collapse in NEAM's spawning activity, since then, a shift in the spawning location towards the north, a trend that has continued until now. In warmer years, mackerel in the North Sea spawn earlier than in colder years (Jansen & Gislason, 2011). The southern and western spawning components also show interannual variation, but there is no clear relationship with water temperature (Punzón & Villamor, 2009). The optimum range of sea surface temperatures for spawning is 13-15.5°C. The latitudinal propagation of spawning appears to follow the increase of sea surface temperatures in the spring, coupled with the spring spawning migration of adults (Borja et al., 2002).

In recent years, mackerel have been observed in coastal areas around Iceland during warm periods in the North Atlantic Ocean, indicating the species' northward and westward expansion. This expansion of mackerel distribution might to be related to increasing sea surface temperatures in the NEA during summer, which has implications for management of this population across nations (Berge et al., 2015; Trenkel et al., 2014). However, most of the above analyses were based on correlations or lab experiences due to the difficulty of directly exploring the temperature history experienced by mackerel in early life stages, leaving significant knowledge gaps regarding the effects of climate change on fish species' habitat patterns, including their growth, migration, and environmental history.

Here, I provide the first estimates of the experienced temperature and FMR (and therefore thermal performance curve of field metabolism) in a wild juvenile pelagic fish (*Scomber scombrus*) based on the otolith FMR proxy approach. The results provide physiologists and fish ecologists with a powerful tool for exploring some of the current challenges in fish and fisheries ecology.

## 4.2 Methods

I first describe field collection of juvenile fish followed by otolith sample preparation and analysis (Sect. 2.2) and data processing to reconstruct experienced temperature (Sect. 2.3) FMR and equivalent oxygen consumption rates. (Sect. 2.4).

***4.2.1***

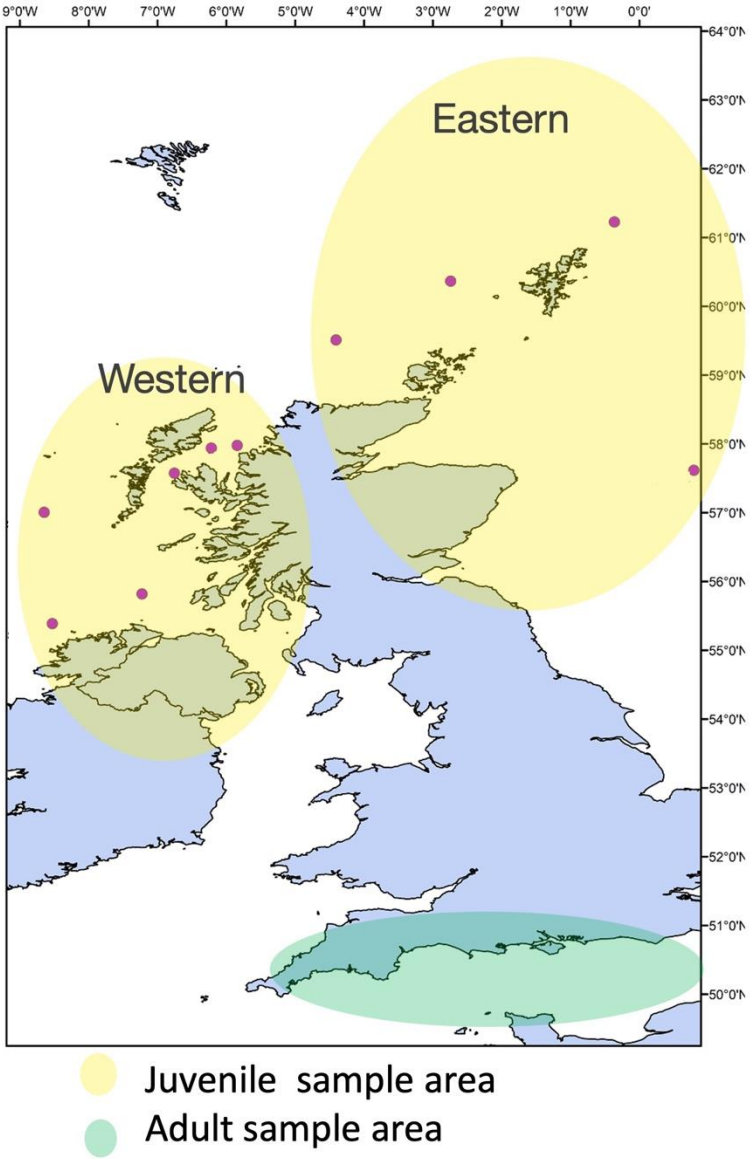


Figure 4-1. The samples of juvenile mackerel (age 0+) were collected from surveys conducted by Marine Scotland from the research vessel Scotia between 2020 and 2021. The sampling locations are indicated in yellow and divided into two zones (east and west) at 50 degrees. The samples of adult mackerel (age 3) were caught by commercial trawlers in the English Channel in August 2020, and the sampling location is shown in green.

### 4.2.2 Otolith preparation and isotope analysis

Sagittal otoliths were removed from defrosted fish and cleaned. Otoliths were mounted to microscope slides using Loctite precision superglue, with the sulcus acoustics facing upwards. Diamond-encrusted drill bits attached to a Dremel hand-held engraving tool were used to recover aragonite powder form the outermost growing surfaces of otoliths. Milling targeted the fastest

growing portion of the otolith, with depth adjusted to recover sufficient sample for analyses (target of 20-40µg). Stable isotope compositions of otolith aragonite were analysed using a Kiel carbonate auto sampling device coupled to a Thermo Finnegan MAT 252 isotope ratio mass spectrometer. Aragonite powder was reacted with 102% phosphoric acid at 60ºC. Water vapor and other gases were cryogenically removed before the resulting $CO_2$ was measured against a reference gas multiple time. Precision and accuracy were monitored through repeat analyses of international carbonate standards (NBS18, NBS19) and reported relative to Vienna-Pee Dee Belemnite (VPDB) standard. The mass effect and instrumental drift were corrected using a certified in-house reference material (GS-1). Overall precision was ± 0.04‰ (SD) for $\delta^{13}C$ and ± 0.08‰ (SD) for $\delta^{18}O_{otolith}$.

### 4.2.3 Otolith $\delta^{18}O$ based reconstructions of experienced temperature

The temperature experienced by each individual fish averaged across the period represented by the sampled otolith outer section was estimated from $\delta^{18}O_{otolith}$ values according to the otolith thermometry regression (Morissette et al.,2023.)

$$\delta^{18}O_{carbonate,VPDB} - \delta^{18}O_{water,VSMOW} = -0.209 * T(°C) + 3.465 \quad (1)$$

As the location of the fish during otolith growth is unknown, the median salinity across regions known to be occupied by juvenile mackerel, salinity was estimated at 35.2 psu.

$\delta^{18}O_{seawater}$ values (relative to VSMOW) are related to salinity based on (Benetti et al., 2017; Darnaude et al., 2014; Harwood et al., 2008a)

Northeast Atlantic: $\delta^{18}O_{seawater}\ \mathrm{VSMOW} = (-16.06 + 0.47 \times Salinity)$
(2)

Eastern Region: $\delta^{18}O_{seawater}\ \mathrm{VSMOW} = (-9.3 + 0.274 \times Salinity)$
(3)

### 4.2.4 Otolith $\delta^{18}C$ based field metabolic rate calculation

The relative proportion of respiratory carbon in otolith carbonate ($C_{resp}$) was estimated from a two-component mixing model (Chung et al., 2021):

$$Cresp = (\delta^{13}Coto - \delta^{13}CDIC.W)/(\delta^{13}Cdiet - \delta^{13}CDIC.W) + \varepsilon \quad (3)$$

Where $\delta^{13}C_{oto}$ is the carbon isotope value recorded in otoliths, $\delta^{13}C_{diet}$ is the average $\delta^{13}C$ value of the diet, and $\delta^{13}C_{DIC.W}$ is the average $\delta^{13}C$ value of dissolved inorganic carbon (DIC) in seawater.

$\delta^{13}C_{diet}$ was estimated as a value of -20.4‰ based on the measurements of $\delta^{13}C$ values *S. scombrus* muscle tissue (Jennings & Cogan,2015). $\delta^{13}C_{DIC.W}$ values were estimated as 0.40‰ based on measurements made in the southern Eastern region (Burt et al., 2016).

The total net isotopic fractionation during carbon exchange between DIC and the blood and between the blood and endolymph (ε) was set as 0. (Chung et al., 2021)

#### 4.2.5 Conversion to oxygen consumption rates ($mgO_2kg^{-1}hr^{-1}$)

An exponential decay model developed for juvenile Atlantic cod relates $C_{resp}$ values to oxygen consumption rates ($mgO_2kg^{-1}hr^{-1}$). The Chung et al., 2019 calibration model is subject to uncertainty at high metabolic rates due to additional metabolic components (such as SDA) contributing to estimates of standard metabolic rate. Consequently, the linear form of this equation may provide more accurate FMR estimates less subject to error (Chung et al., 2019)

$$FMR\ (mgO_2kg^{-1}hr^{-1}) = (Cresp - 0.041)/0.000971 \quad (4)$$

#### 4.2.6 Estimation of mass-specific standard metabolic rate (SMR)

The expected scaling relationship between metabolic rate, body size, and temperature can be mathematically expressed as:

$$metabolic\ rate \propto e^{-E/kT} \quad (5)$$

Where E is the activation energy (in eV), T represents the temperature in Kelvin, and k is Boltzmann's constant ($8.62 \times 10{-}5\ eVK^{-1}$), $i_0$ is a normalisation constant (set as $1.64x10^{13}$, based on statistical regression(Chung et al., 2021).

According to metabolic theory of ecology (MTE) proposed by Brown and Sibly, metabolic rate (SMR) is predicted to scale with body mass with an allometric exponent of 0.75 (or -0.25 for mass-specific metabolic rate) (Brown et al., 2004):

$$SM(mgO2kg{-}1hr{-}1) = i0M^{-0.25}e^{-E/kT} \quad (6)$$

Further, the universal temperature dependence hypothesis (UTD) proposes that thermal sensitivity of metabolic rate (E ) approximates a constant value of 0.65eV. These canonical scaling

terms are commonly used in biometric models to predict energetic consequences of temperature, oxygen limitation on species distributions or body sizes (e.g. Cheung et al2011, Deutsch et al 2020, 2022). However the existence of mechanistically-based universal mass and temperature scaling exponents is hotly debated (White et al 2023), and very little data are available to test realised population-level mass or temperature scaling of field metabolic rates.

### 4.2.7 Statistical analyses

Initially, to compare otolith $C_{resp}$ values, FMR, and experienced temperature across life stage, locations, and years, a three-way ANOVA was executed.

Fulton's condition factor was applied to represent body condition (Fulton, 1904):

$$K=100\times W/L^3 \quad (7)$$

The best fitting model was chosen based on comparison of Akaike Information Criterion (AIC) values. All statistical analyses were performed in R (<www.r-project.org>) using the glm function and figures were generated using the ggplot2 package(Gómez-Rubio, 2017).

Finally, the thermal sensitivity of FMR was expressed as an equivalent activation energy (E) and as $Q_{10}$ values:

$$Q_{10} = (R2/R1)^{(10/T2-T1)} \quad (8)$$

T1 and T2 are the minima and maximum experienced temperatures, and R1 and R2 are the respective rates measured at T1 and T2 (Kent, 2006).

To compare data with other species' laboratory-derived metabolic rate estimates contained in the FishBase database, I use recovered thermal sensitivity terms to rescale inferred oxygen consumption rates to 20°C. The FishBase OXYGEN database contains close to 7,000 records for about 300 species, obtained from over 400 references including (Congleton, 1974; Marais, 1978; Neumann et al., 1981; Subrahmanyam, 1980; Winberg, 1956). Of these records, 6,400 come from the OXYREF database compiled by Thurston and Gehrke (1990),while the rest have been added by FishBase staff.

## 4.3 Results

I first describe the in-situ field metabolic rate in wild juvenile Atlantic mackerel. I then focus on the relationship between field metabolic rate, the body mass, and experienced temperatures.

### 4.3.1 Sampled fish and raw isotope data

165 sagittal otolith samples were sampled from fish caught in UK waters between 2020 and 2021. Of these samples, 79 came from the Eastern region, and the remaining 88 came from the Western region. The body length range for the Eastern samples was 12.60-20.60cm, while the body length range for the Western samples was 15.40-20.80cm, estimated age for all fish was under one years old.

The mean $C_{resp}$ value for the Eastern samples was 0.28±0.03, while the Western samples had a mean $C_{resp}$ value of 0.27±0.03. The $C_{resp}$ values correspond to estimated oxygen consumption rates of 244±26 (mg $O_2$ $kg^{-1}$ $h^{-1}$), and 236±34 (mg $O_2$ $kg^{-1}$ $h^{-1}$) for Eastern and Western fish respectively. There were no significant differences in the $C_{resp}$ and FMR values between the Eastern and Western populations based on ANOVA.

The K value, which is a measure of growth rate, was also estimated, and the results showed that the Eastern samples had a K value of 0.79±0.11, which was higher than the Western samples with a K value of 0.70±0.12.In August 2020, 25 mackerel caught by commercial trawlers in the English Channel were collected and otoliths removed. The mean fork length was 29.7cm, estimated at age 3+ and reaching sexual maturity (Villamor et al., 2004). Otolith $\delta^{13}C$ values ranged from −3.02 to −5.23 ‰. The summarized information is shown in (Table 4-1,Figure 4-2).

Table 4-1.Summary of results recorded in the present study. The reported number represents mean ± SD

| Year | Life stage | Location | Number | Length(cm) | $\delta^{18}O$oto ( ‰) | Experienced temperature (°C) | $\delta^{13}C$oto (‰) | $C_{resp}$ | FMR ($mgO_2kg^{-1}hr^{-1}$) | SMR($mgO_2kg^{-1}hr^{-1}$) | K | |
|---|---|---|---|---|---|---|---|---|---|---|---|---|
| 2021 | Adult | Channel | 26 | 20.00~34.50 | 1.24±0.76 | 12.95±3.64 | -3.81±0.50 | 0.22±0.03 | 187.07±26.33 | 83.99±36.91 | 1.25±0.38 | Brock, 2021) |
| 2020 - 2021 | Juvenile | Eastern | 79 | 12.60~20.60 | 1.28±0.46 | 12.10±2.19 | -5.44±0.58 | 0.28±0.03 | 244.63±26.46 | 131.21±39.40 | 0.79±0.11 | In this study |
| | | Western | 88 | 15.40~20.80 | 1.36±0.30 | 12.41±1.42 | -5.24±0.75 | 0.27±0.03 | 235.65±34.26 | 129.54±18.59 | 0.70±0.12 | In this study |

### 4.3.2 Temperature reconstruction

$\delta^{18}O_{otolith}$ values of juvenile mackerel otolith edges ranged between -0.4 and 2.2‰ corresponding to a range of experienced temperature estimates from 7.7 to 20.1°C, with a median temperature of approximately 15°C. For adult mackerel, $\delta^{18}O_{otolith}$ values ranged between -0.4 and 2.18‰, corresponding to experienced temperature estimates from 8.46 to 24.15°C, with a median temperature of approximately 12°C (Table 4-1,Figure4-2).

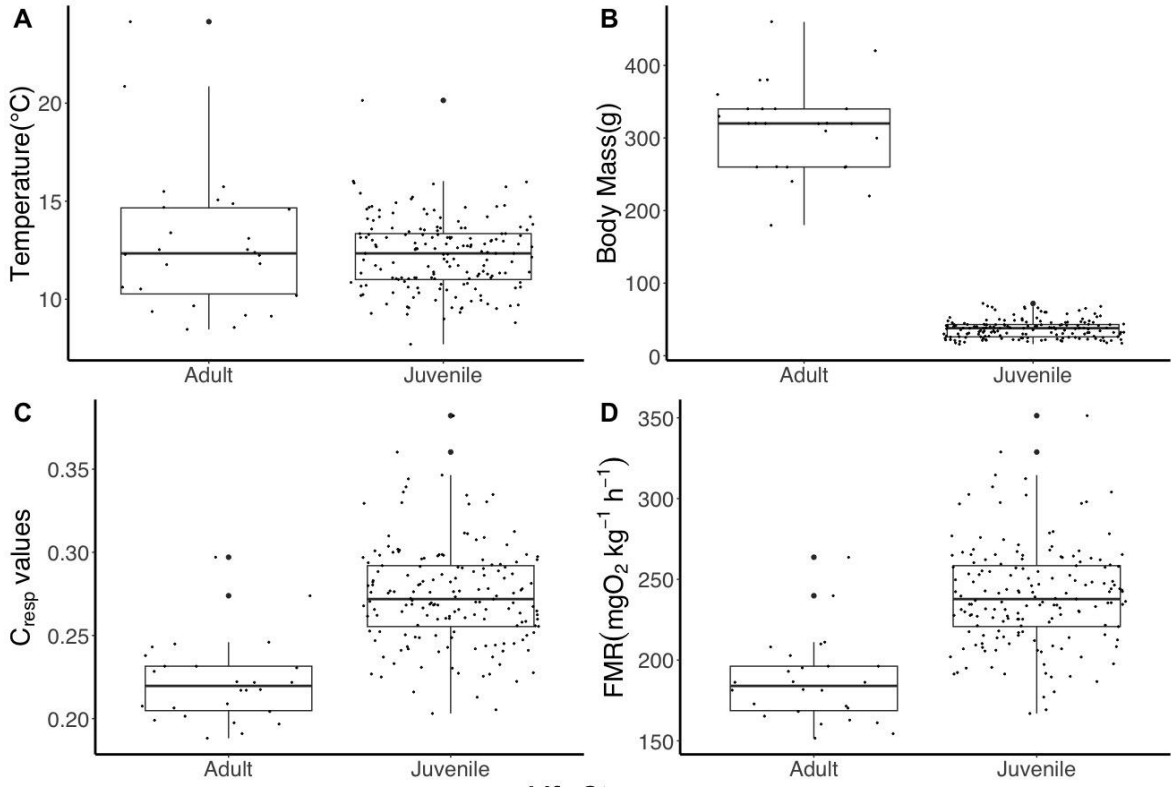


Figure 4-2. (A) Experienced temperature (°C), (B) body mass (grams), (C) $C_{resp}$ value, and (D) field metabolic rate (FMR) ($mgO_2kg^{-1}h^{-1}$) recorded amongst all *Scomber scombrus* individuals between juveniles (which were sampled in the present study in North Atlantic during 2020 to 2021) and adults (which were caught off the coasts of Sussex and Devon in August 2020). Boxes represent the 25–75 percentiles, horizontal lines within represent medians, and vertical lines represent the box ± 1.5 times the interquartile range.

### 4.3.3 Relationship between Scaling of metabolic rate ($C_{resp}$) and otolith FMR values with body mass

Across all individuals, $C_{resp}$ values (reflecting mass-specific metabolic rate) generally decreased with increasing log body mass, with a slope of -0.05 (Figure4-3). (A)) (Simple regression analysis,

p-value <0.05). The residual variation of $C_{resp}$ among juveniles was higher than that among adults (F-test,p-value <0.05). Estimated mass-specific field oxygen consumption had a negative scaling relationship (Simple regression analysis, p-value <0.05) with logged body mass, the body mass scaling exponents were -0.165 for mass-specific oxygen consumption, while whole-organism field oxygen consumption had a positive relationship with body mass (Simple regression analysis ,p-value <0.05) (Figure4-3(B)). The metabolic scaling exponent (b) = 0.89 for whole-organism oxygen consumption.

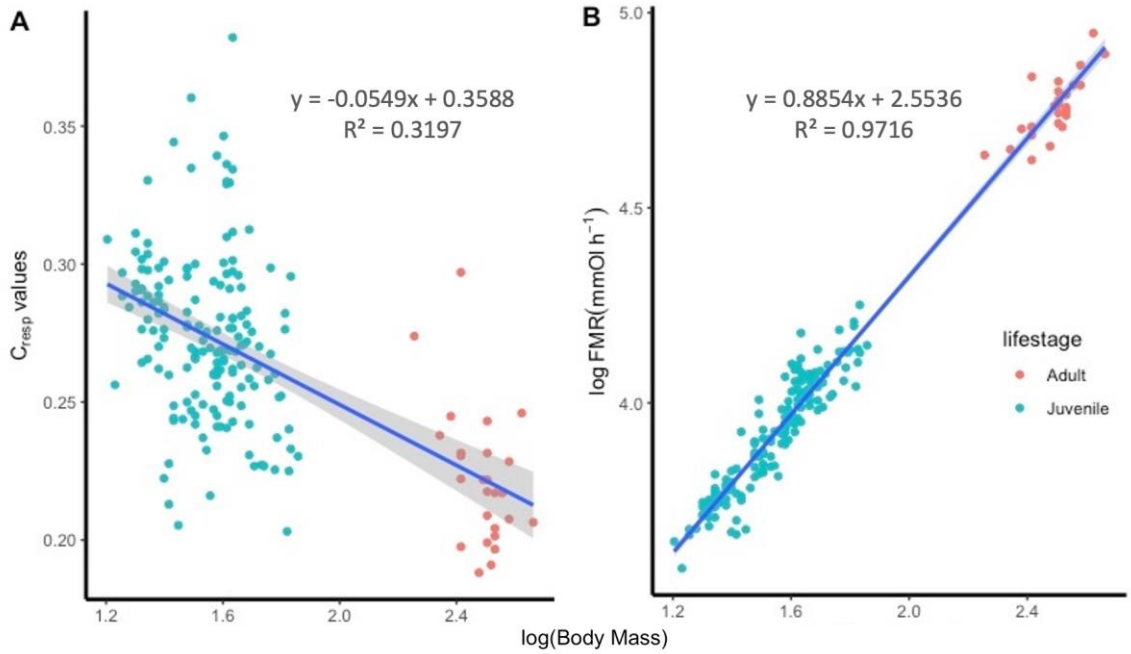


`

Figure4-3. Individual (A) $C_{resp}$ and (B) whole-organism field oxygen consumption (oxygen consumption mmol $h^{-1}$) plotted by log body mass. On plots the black line shows the best fit, with 95% confidence intervals shaded in grey, with points coloured by life stage.

### 4.3.4 Relationship between Scaling of metabolic rate ($C_{resp}$) and otolith FMR values with experienced temperature estimated based on $\delta^{18}O_{otolith}$

The $C_{resp}$ values did not show a significant relationship with experienced temperature in the full dataset or in adults alone (based on a simple regression analysis with p-values of 0.1 and 0.07, respectively) as shown (Figure4-4 (A)). However, when focusing on the juvenile data from the Eastern region, there was an increase in $C_{resp}$ values with experienced temperature (based on a simple regression analysis with a p-value < 0.05) as shown in Figure 4-5(A). If the data from the eastern region is further separated into fall and winter based on the sampling time, it can be

observed that the $C_{resp}$ values increase with temperature at both sampling time Figure 4-6(A), and that after accounting for mass and temperature, fall-sampled fish show higher inferred oxygen consumption rates than winter sampled fish. On the other hand, the $C_{resp}$ values of juvenile data from the Western region did not show a significant relationship with temperature, similar to the adults (based on a simple regression analysis with a p-value of 0.2449), as shown in Figure 4-5(A).

After accounting for FMR according to Arrhenius model and the body mass scaling exponents (-0.165) mentioned above, FMR showed no significant relationship with inverse experienced temperature across the Adults and juvenile data from the Western region (Simple regression analysis, p value = 0.94 and 0.51(Figure4-4 (B)), respectively. The inferred oxygen consumption rate's Q10 value for adults was 0.96, while it was 0.78 for juveniles from the Eastern. When using the Arrhenius model, the activation energy (E) derived from all the data was 0.44, which is lower than the predicted value of 0.65 eV proposed by UTD.

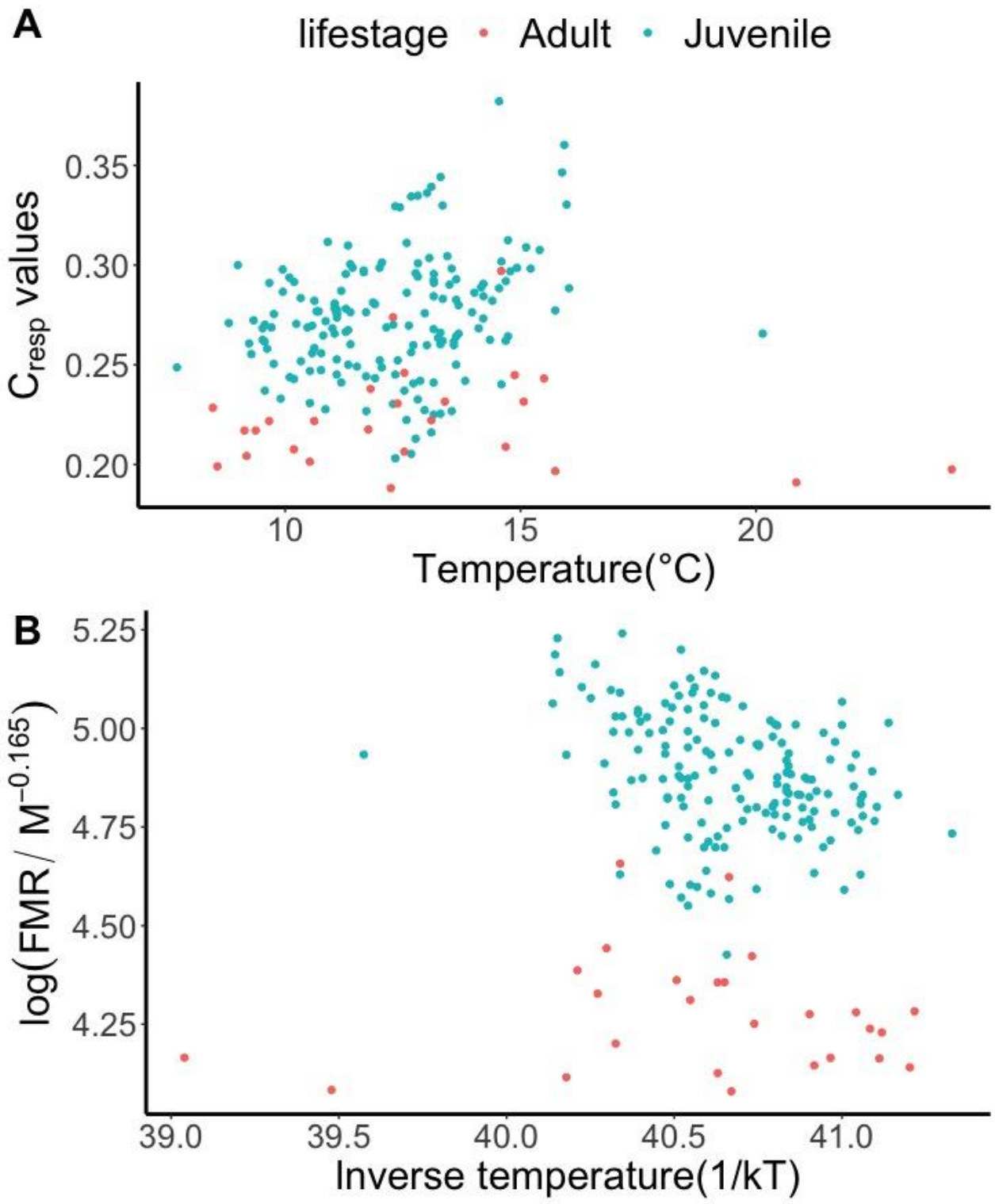


Figure4-4. The relationship of $C_{resp}$ values with temperature of full data set. The field metabolic rate (FMR) and inverse temperature following the Arrhenius modelof (A)full data set (C) Adult(E) Juvenile. k is Boltzmann's constant ($8.62 \times 10^{-5}$ $eVK^{-1}$), T is the absolute temperature in K, and M is body mass in grams.

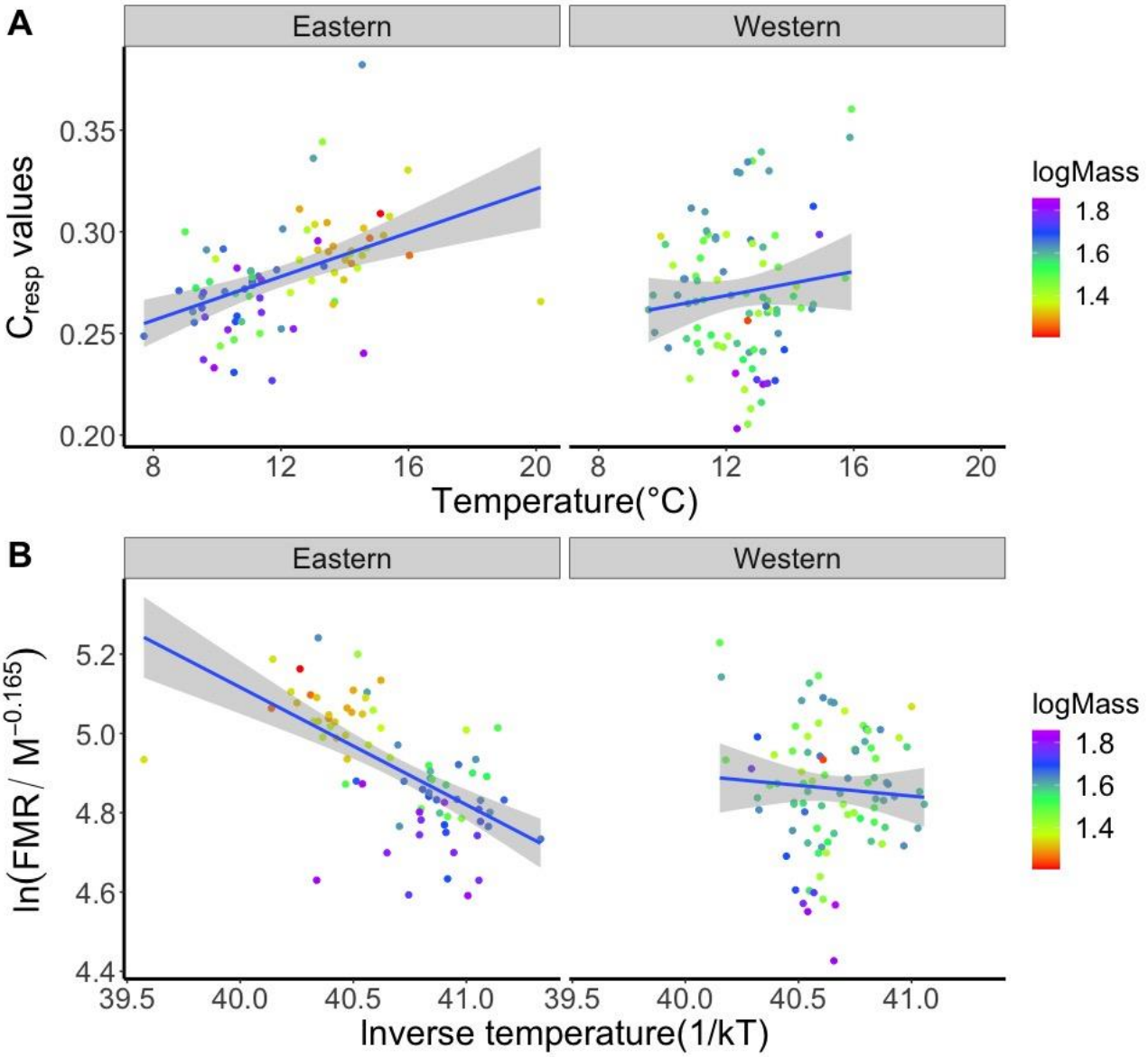


Figure 4-5. The relationship of $C_{resp}$ values with temperature of Eastern and Western area. The field metabolic rate (FMR) and inverse temperature following the Arrhenius model of k is Boltzmann's constant ($8.62 \times 10^{-5}$ $eVK^{-1}$), T is the absolute temperature in K, and M is body mass in grams.

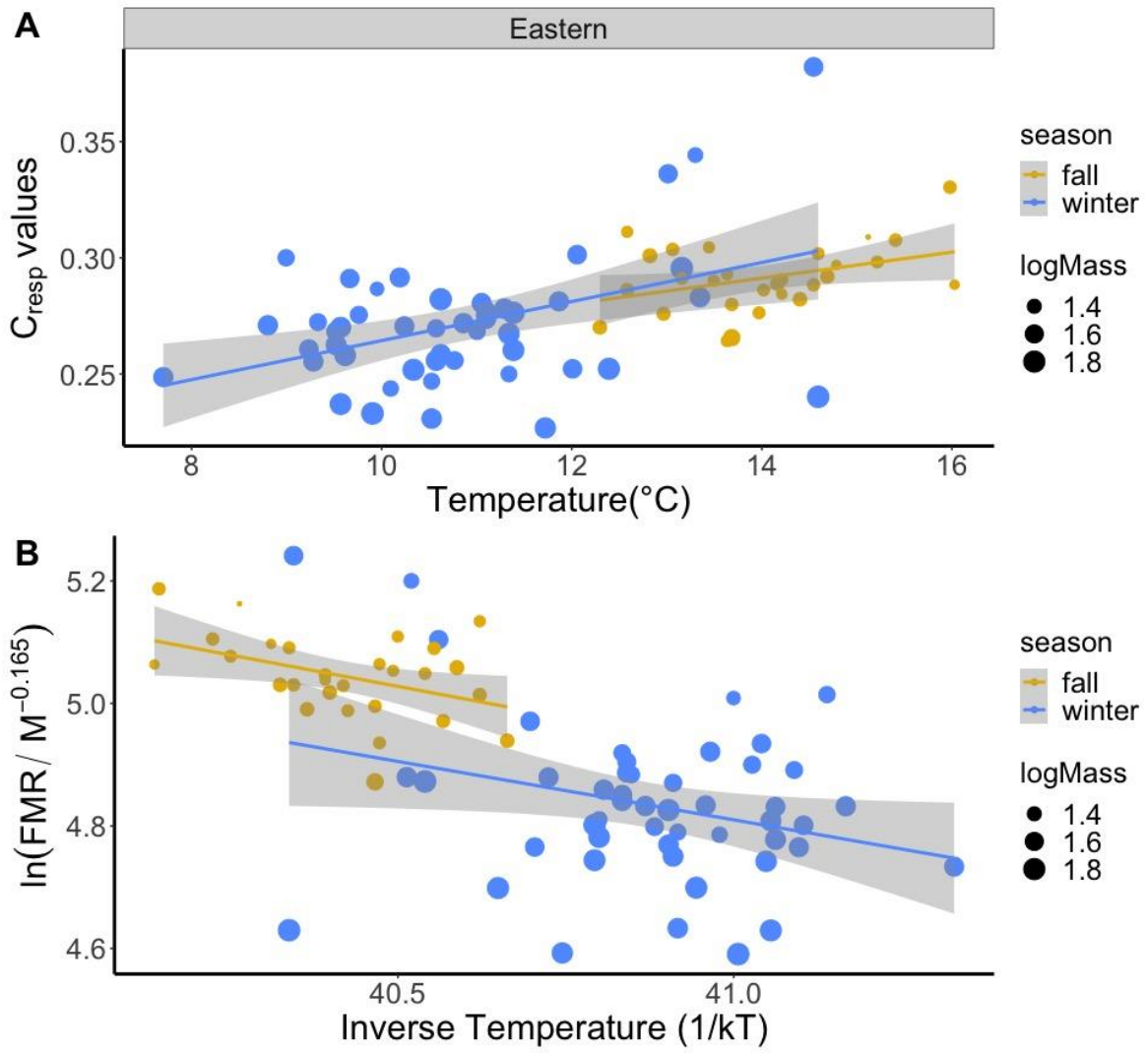


Figure 4-6. The relationship of $C_{resp}$ values with temperature of juveniles from Eastern of fall and winter. The field metabolic rate (FMR) and inverse temperature following the Arrhenius model of k is Boltzmann's constant ($8.62 \times 10^{-5}$ $eVK^{-1}$), T is the absolute temperature in K, and M is body mass in grams.

## 4.4 Discussion

In this study, I estimated the field metabolic level and thermal performance curve of field metabolism in Atlantic mackerel (*Scomber scombrus*) using otolith FMR proxy approach.

I make several key observational findings：

### 4.4.1 Relative metabolic level of Atlantic mackerel

The estimated oxygen consumption rates of 244±26 (mg $O_2$ $kg^{-1}$ $h^{-1}$), and 236±34 (mg $O_2$ $kg^{-1}$ h−1) for Eastern and Western fish respectively. Jonstone et al 1993 estimated oxygen consumption

rates via respirometry, reporting values of of 118 (mg $O_2$ $kg^{-1}$ $h^{-1}$) for mackerel between 290-380g at 11 degrees, which is very similar to our estimate of 187±26 (mg $O_2$ $kg^{-1}$ $h^{-1}$) for adult mackerel of 350g at 13 degrees.

There are no recorded metabolic rate values for *S. scombrus* in the FishBase data repository, reflecting the difficulty of maintaining these pelagic fishes in respirometry chambers. However, based on our comparison of experimental results with FishBase data (Figure 4-7), we found that the inferred oxygen consumption rate of *S. scombrus* was relatively lower than the estimated MR for other species in the Scombridae family, which includes Mackerel tuna, Skipjack tuna, Pacific bonito, and Albacore. These species have more red muscle tissue and require more energy to support their movement and activity. Nevertheless, when compared to other non-scombroid teleost fish species of the same body weight, *S. scombrus* still has a relatively higher metabolism according to our study.

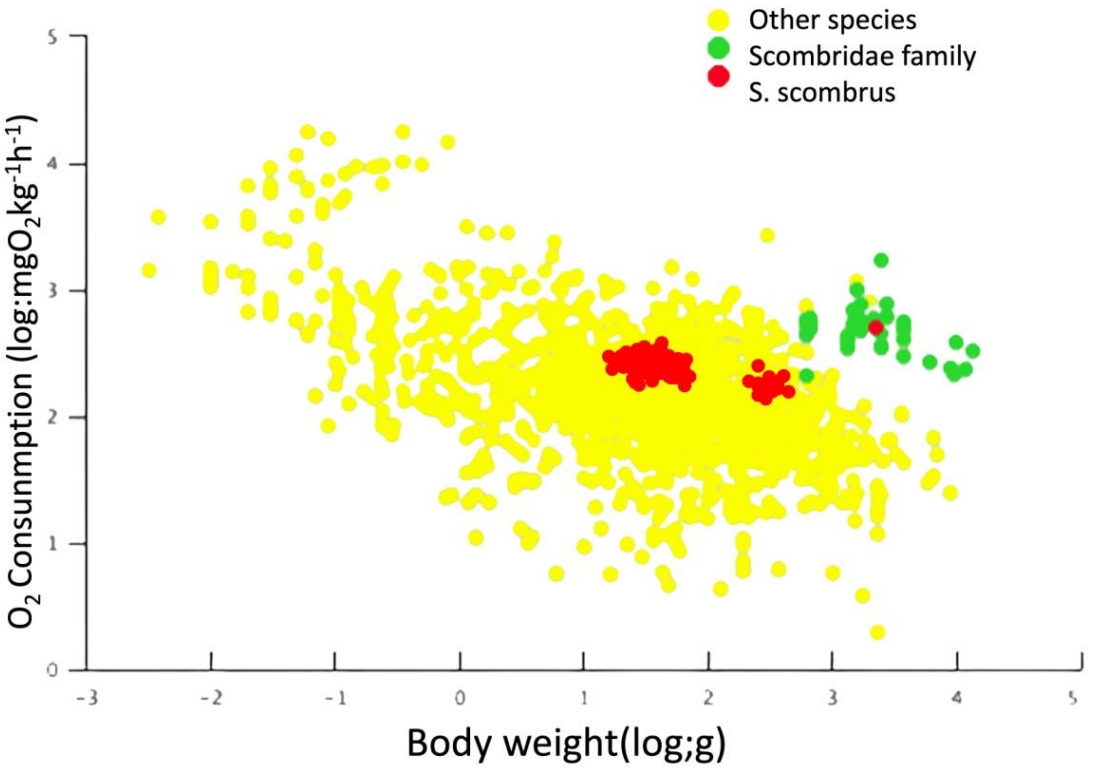


Figure 4-8. Relative oxygen consumption based on our comparison of experimental results with FishBase. The oxygen consumption of our study on mackerel are shown in red, while those of other species in the Scombridae family are shown in green. The oxygen consumption of other species are shown in yellow.

We further compared the FMR estimates for *S. scombrus* using the otolith isotope method with otolith-derived FMR estimates for a range of other marine teleosts. These data, primarily from unpublished sources within the same laboratory at the University of Southampton, were analyzed

using a consistent methodology (Figure 4.8). We found that *S. scombrus* exhibited relatively high metabolic rates compared to temperate demersal fishes including Atlantic cod (Gadus morhua, Haddock (Melanogrammus aglefinnus) and also herring (Clupea harengus), but lower than small tuna species (*Sarda sarda, Euthynnus alletteratus*) and the dolphinfish *Coryphaena hipparus*.

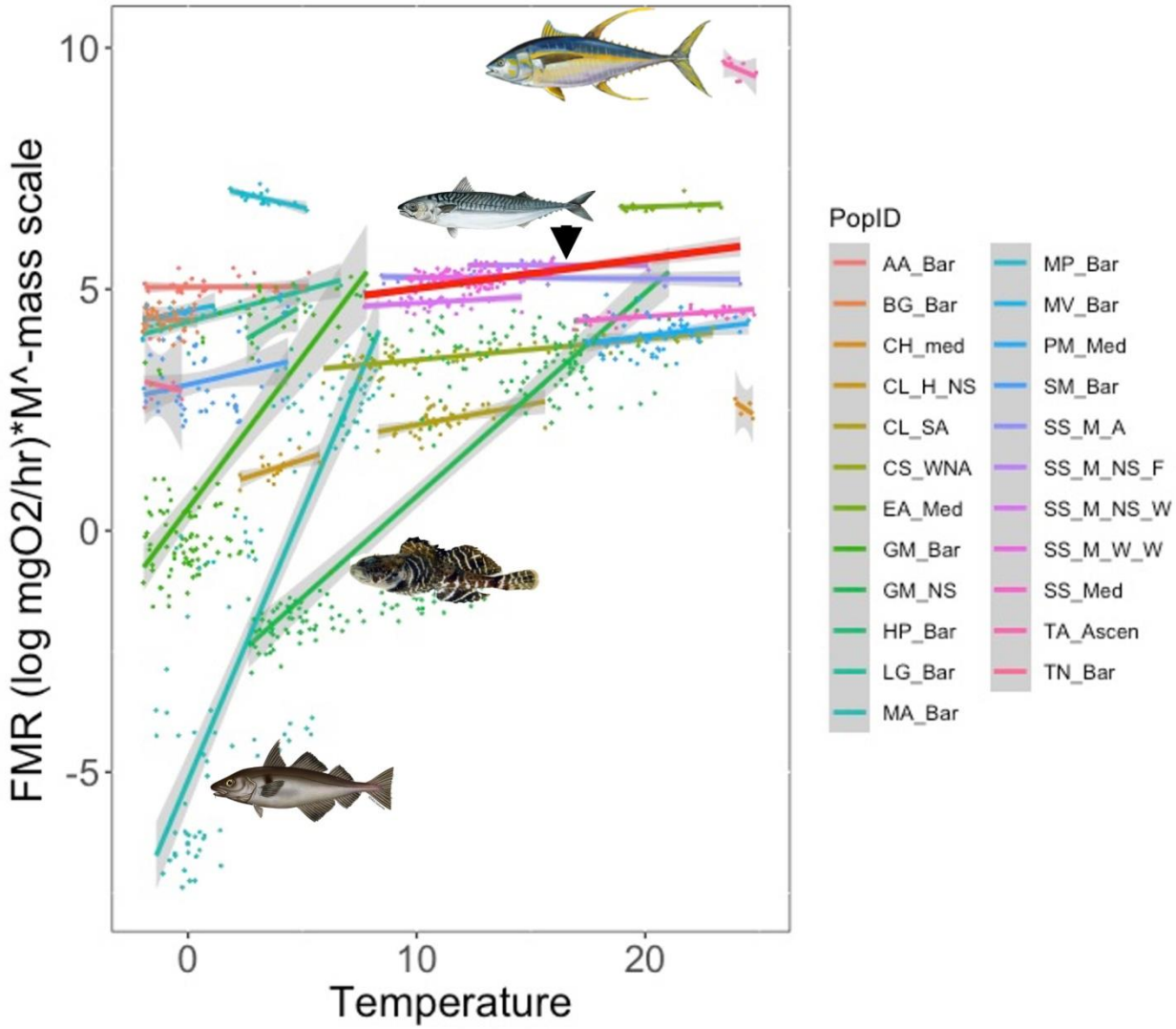


Figure 4-9. Relative oxygen consumption data

### 4.4.2 Body mass scaling

The allometric mass scaling exponent for whole organism oxygen consumption in Atlantic mackerel was 0.88 in this study, which is greater than the 0.75 value proposed by MTE, but lying within the range of 0.67- 1.0 expected based on the Metabolic Level Boundary Hypothesis (Glazier) and observed in 89 teleost species(Killen et al., 2010). A growing number of studies record mass scaling exponents for teleost metabolic rate closer to 1 than 0.75 (Brown et al., 2004; Norin & Clark, 2016; Alewijnse, 2021; West et al., 1997). Most marine ecosystem models, however, currently rely on values of b that are based on or close to the 0.75 value proposed by

MTE. Unrealistically low values of mass scaling exponents in physiologically informed ecosystem models could lead to an overestimation of the impact of body mass on fish metabolic or growth performance or distribution (Alewijnse, 2021).

Recently studies found that the metabolic scaling exponent varied with different developmental stages in fish, with the highest oxygen consumption demand occurring before the onset of piscivory. This is likely related to the development of the digestive system and external characteristics that improve once the fish begin to consume fish prey, as reported in other studies such as (Kaji et al., 2003; Yúfera et al., 2014). The MLBH theory also suggests that individuals (or life stages or species) with very high levels of activity (i.e. metabolic rates close to the maximum metabolic rate or MMR) have higher mass scaling exponents than those with lower energy demands or in resting conditions. This is because the energy expended by the muscles during swimming is linked to the resource demand of the body mass. The mackerel sampled here show relatively high overall mass and temperature scaled metabolic level compared to other marine teleost, so a relatively high scaling exponent might be expected, particularly in juvenile stages with high energy requirements to support fast growth. Giguère et al. (1988) also reported an isometric exponent with increasing body mass during the larval stage.

### 4.4.3 Temperature scaling

The $Q_{10}$ value expressing the relationship between FMR and temperature in the Eastern population of juvenile mackerel was 1.3, lower than expected based on the UTD and enzyme thermodynamics. Relatively low thermal sensitivities for FMR have been recovered across many marine teleost species and inferred from fish growth rate (van Denderen et al., 2020). The data from mackerel and other teleosts imply that temperature-dependent thermodynamic or physiological processes setting the limits for SMR, and MMR do not necessarily predict among-individual variations in expressed field metabolic rates, at least for fishes operating within their aerobic scope.

It has been argued that theories invoking oxygen limitation as a mechanism explaining reductions in performance at high temperatures have limited application in the natural environment, as where possible, individuals will avoid conditions that significantly limit performance (Jutfelt et al., 2018). Sampled mackerel show no decline in absolute $C_{resp}$ values at the maximum experienced temperatures suggesting that no individuals experienced temperatures that limited metabolic performance.

It should be noted that the Eastern sampled population, which exhibits increased thermal sensitivity of FMR, also shows a clear seasonal effect on FMR. The maximum and minimum

metabolic rate observed during winter in the Eastern population was 351 and 191mg$O_2$ $Kg^{-1}$ $Hr^{-1}$, whereas the maximum and minimum metabolic rates observed in the Western region were 328 and 161 mg$O_2$ $Kg^{-1}$ $Hr^{-1}$, respectively. Additionally, the variation in metabolic rate is higher in fish from the western region. The thermal performance curve for FMR of the Eastern population suggests that individual variations in field metabolism are primarily influenced by ambient water temperature additional cold adaptation might influence the thermal sensitivity of field metabolism in Eastern region to a greater extent than the Western. It is worth noting that there is a high individual variation in FMR despite the lack of covariance with temperature in fish from the western region. This implies that variables independent of temperature dominate among individual variance in FMR. When individuals are operating within a large aerobic scope there is more opportunity for phenotypic variability, energy budgeting and food availability to influence FMR as there is less constraint by the max or min MR which are likely strongly dependent on temperature. Thus, the finding of low thermal sensitivity combined with high among-individual variance in FMR implies a large effective aerobic scope in the water conditions experienced, and consequently relatively low vulnerability to changes in temperature.

The current study is not without limitations, particularly in the assessment of the metabolic rate of mackerel. One notable constraint arises from the small influence of food on the carbon isotope, accounting for no more than 1% (DeNiro and Epstein, 1978; 1981). This minimal impact allows for the use of an average value in the calculation. However, it is important to acknowledge that this simplification might introduce a slight degree of uncertainty into our results. The reliance on an average value may not fully capture the potential variability in metabolic rates associated with different dietary compositions. Future research could explore more nuanced approaches to incorporate dietary variations and enhance the precision of metabolic rate estimations in mackerel.

## 4.5 Conclusions

Otolith-based metabolic rate estimates are consistent with limited available respirometry based data and suggest that Atlantic mackerel has relatively low field metabolic rates compared to other members of the Scombridae family, and that the thermal effects on FMR are relatively small, compared to predictions of the Universal Thermal Dependence model. I found that the waters of the Northeast Atlantic north of Scotland currently offer a wide aerobic scope for juvenile Atlantic mackerel, which allows temperature-independent effects such as food availability and individual metabolic phenotype to have a stronger impact on inter-individual variation in FMR than temperature. I also identify differences in expressed metabolic level between fall and winter which may reflect either direct thermal effects or related effects of increased activity during fall.

The majority of previous bioenergetics modelling studies have assumed a fixed metabolic rate that applies to individuals across their entire life history. However, the current study on mackerel found that the FMR is highly correlated with fish size. This suggests that incorporating size dependence into a function to replace the fixed metabolic rate may need to be considered when applying individual-based models IBMs to mackerel and other species. My finding also suggests that while temperature can have an impact on metabolic rate, the effects of temperature on ecological factors such as food availability or competition for resources may be more important in determining an organism's overall fitness and FMR. This has implications for ecological models that attempt to predict the impacts of climate change on marine ecosystems, as it may be more difficult to accurately predict how changes in temperature will affect these ecological factors and ultimately impact FMR. Further research is needed to better understand the complex interactions between temperature, ecology, and metabolism in marine organisms.

# Chapter 5 Conclusions

## 5.1 Thesis summary

The primary aim of this thesis is to establish a connection between the theoretical movement predicted by an ocean model and the empirical data obtained from the otolith isotope-based method. Specifically, the goal is to explore how these two methods can be used together to gain a better understanding of early life history spatial and physiological ecology in marine fishes. The thesis examines the potential of combining IBM models and otolith isotope-based methods to reconstruct larval dispersal through three main approaches:

1. A case study of North East Atlantic mackerel, where individual-based drift models were applied to simulate high-resolution salinity and temperature experienced by drifting fish larvae and their corresponding predicted otolith isotopic histories. Subsequently, model predictions were explored to assess whether high-resolution otolith analyses of larval otoliths would be likely to have the potential to discriminate among different larval drift scenarios.

2. The application of the model-otolith isotope combination analysis method to a broader range of open-sea eel larvae, specifying a range of hypothetical swimming, to explore the wider potential of using otoliths to investigate the impact of swimming behaviour and NAO-related ocean variability on the migration time and path of eel larvae and juvenile fish.

3. Analysis of stable isotopes of otoliths to infer the realized thermal sensitivity of Field Metabolic Rate (FMR) in juvenile mackerel. Juvenile *S. scombrus* were collected from the North Atlantic for the study. Experienced temperature was estimated from otolith $\delta^{18}O$ values and metabolic rate was inferred from otolith $\delta^{13}C$ analyses.

The main findings are summarised as follows:

1. In the case of Northeast Atlantic mackerel, otolith $\delta^{18}O$ profiles can potentially provide highly accurate, low-cost "natural tags" for stock discrimination and broad-scale geolocation of fish, however any high-resolution isotope analyses should be carefully targeted both in terms of the drift pathways potentially to be discriminated and the portion of otolith most likely to provide discrete signals. Isotope-enabled IBM models can help to target such analyses. In the case of NE

Atlantic mackerel around the British Isles, targeting otolith growth between 30-90 days of life provided the maximum signal potential to discriminate among different simulated drift pathways,

2. In the case of open sea eel larvae, IBM demonstrated swimming necessary for successful return. Most returning eels needed >2 year to cross, and NAO state and starting location affected the potential successful migration rate. The study demonstrated the potential of using otolith analysis to understand the environmental conditions experienced by the larvae during their journey and found that otolith oxygen isotope ratios can distinguish between successful and failed drifts. The analysis of otolith samples are potential to provide insights into the impact of ocean currents on eel migration routes and return times. Through the collection of larger larvae transported by ocean currents back to spawning areas, I aim to understand how these conditions may influence their recruitment success.

3. Individual juvenile Atlantic mackerel sampled in the first year of life experienced a range of ambient temperatures and expressed metabolic rates, but these variables did not covary. Consequently, it is inferred that factors largely independent of temperature such as individual phenotype and access to food explain the majority of the individual-level variation in field metabolic rate. Seasonal differences in temperature-corrected metabolic rate were apparent, with higher temperature- and mass-corrected FMR expressed in autumn compared to winter, presumably reflecting increased feeding rates.

## 5.2 Implications of thesis findings

### 5.2.1 The application of otolith isotopes in individual-based models (IBMs):

1. Due to the difficulties in tracking fish, required parameters such as spawning areas, time, and fish movement behaviour in individual-based models (IBMs) can only be inferred from sampling data. However, sampling data may be biased due to sampling methods, effort, and returns, and there is also a lack of long-term fish tracking data. Otolith oxygen isotopes show great potential for further validating hypotheses and establishing models that better reflect wild fish behaviour.
2. In the case of mackerel: Comparing our passive simulation results with actual sampling, I found that juvenile nursery areas tend to be observed further inshore, in contrast to our simulated distributions. Therefore, it is suggested that late-stage larvae may have active swimming behaviour and tend to stay closer to the shore. Through otolith isotopic sampling analysis, signals of oxygen isotope changes caused by drastic salinity changes may show the

time from nearshore to offshore, providing further optimization of model assumptions to better reflect the results of wild fish migration.

3. In the case of eel: I found that otolith $\delta^{18}O$ has the potential to distinguish between successful and failed drifts, and to verify the hypothesis that the North Atlantic Oscillation (NAO) affects eel migration, with higher successful arrivals in the northeast Atlantic during a negative phase of the NAO.
4. Most previous bioenergetics modelling studies have assumed a fixed metabolic rate that applies to individuals across their entire life history. However, our study on mackerel found that the FMR is highly correlated with fish size through ontogeny. In juvenile mackerel of similar body size, large among-individual variation in FMR was observed, which was relatively unrelated to temperature and varied seasonally presumably related to feeding rate. This suggests that incorporating size and seasonal dynamic dependence into a function to replace the fixed metabolic rate may need to be considered when applying individual-based models (IBMs) to mackerel and other species.

### 5.2.2 Wider implications for co-use of otolith isotope-based methods and individual-based models IBMs:

1. Through high-resolution modelling, this study identifies the potential and limitations of using an otolith isotope-based method on tracking larval fish and provides suggestions for future experimental design such as sampling area, timing, and analysis resolution for different growth stages of larvae and juvenile fish. Furthermore, this research methodology can be adjusted based on existing analytical capabilities, allowing for the prediction of the overall results of otolith analysis This will facilitate obtaining better analytical results while reducing the need for manpower and resources in experiments.
2. At the same time, I demonstrate that $\delta^{18}O$ signatures can allow broad-scale geolocation on a finer spatial-temporal scale than currently applied in most offshore fisheries management. In the Northeast Atlantic, this enables mapping of population dynamics through recruitment identification for fish mixed across spawning grounds.
3. In addition, I also demonstrate the extension of this predictive method to open ocean areas and the study of more complex long-term migration behaviour tracking and understand the potential application otolith isotope-based method under climate change.
4. As ion probes and other spatial sampling techniques improve, the otolith would be suited to studying migrations in larval and juvenile fishes and become a viable option for tracking movements of fully marine fishes.

#### 5.2.2.1 Application in fishery management:

1.By combining IBM and high-precision micro-milling systems and microvolume isotope analysis, it would be helpful to reveal population structure and early life transport. Additionally, this method has a unique and robust advantage of examining the environmental history of successfully recruited individuals, providing crucial information for understanding the environmental conditions necessary for fish survival. This method can also provide insights into how environmental variability drives fish population fluctuations, making it a valuable tool for fishery management.

2. The study provides new insights into the potential effects of the North Atlantic Oscillation (NAO) index on the behaviour and migration routes of European eel larvae, and sheds light on the possible factors that influence the survival and recruitment success of these larvae during their lengthy journeys. Additionally, the study provides recommendations on how to verify these hypotheses, which are essential for developing effective management and conservation strategies.

3. My study observed significant individual variation in FMR among juvenile mackerel, suggesting that they have a broad aerobic scope in their current environmental conditions, potentially allowing them to withstand temperature fluctuations. However, I found that mackerel in the Eastern region were more susceptible to temperature changes than those in the Western region and had less flexibility in responding to such changes. Additionally, changes in temperature or food availability could alter the aerobic scope potential, making otolith FMR a useful monitoring tool for assessing eco-physiological vulnerability in wild populations. This can provide valuable insights for fisheries conservation and management.

## 5.3 Original contribution of the thesis

So far, relatively few studies have combined IBM and otolith isotope analyses, despite the prospects for a wealth of complementary information. The work here represents the first attempt to use an ocean model to predict the potential of high-resolution otolith analyses and applying to improve the experiment design.

In Chapter 3, I test the potential of otolith isotope records to verify the validity of the eel migration model's hypotheses. I discuss various hypotheses related to the impact of environmental variability on eel migration behaviour, particularly the influence of the Nao index on migration routes and the resulting impact on migration success rates.

In Chapter 4 of this thesis,I introduced a newly developed proxy to measure in-situ field metabolic rate (FMR) in wild juvenile fishes. Our findings indicate that juvenile *Scomber scombrus* in Northwest Atlantic exhibit a low thermal sensitivity. Additionally, as the temperature or food availability changes in the future, the potential aerobic scope could be altered. The otolith FMR provides a monitoring tool to determine the eco-physiological vulnerability in wild populations. I also found that the effects of temperature and body weight on the metabolic rate of wild mackerel differ from theoretical values. Therefore, when analysing model data using theoretical values, some errors may occur, and caution should be exercised in their use.

## 5.4 Limitations of the current study

In Chapter 2,I did not consider vertical migration and active movement, as the mackerel's early life stage was passively drifting. In Chapter 3, the assumption of active swimming behaviour was included in the eel model due to the eel's longer migration time, but the change in swimming behaviour according to its body growth was not considered. In a more nuanced simulation, swimming speed could increase with time, and directional swimming could likewise be variable in response to regional stimuli. I also did not include likely diurnal movements vertically in the water column, through surface currents that are strongly sheared, which would alter drift pathways. Overall, in Chapters 2 and 3 variable currents and hydrography could be more widely sampled, as factors that determine isotopic variability. Regarding the metabolic rate of mackerel in Chapter 4, since the food has a small influence on the carbon isotope, the average value may be used for calculation, which may have a slight impact on our results.

This study demonstrates the potential and limitations of using high-resolution otolith isotope-based methods to track larval fish, offering specific recommendations for experimental design—such as optimal sampling areas, timing, and analysis resolution for different growth stages—to enhance resource efficiency. Additionally, I show that $\delta^{18}O$ signatures provide fine-scale geolocation capabilities, which can support recruitment tracking and population mapping in mixed spawning grounds, particularly in the Northeast Atlantic. The method's applicability extends to open ocean studies and complex, long-term migration tracking, making it a valuable tool for understanding fish migration patterns in the context of climate change. With advancements in ion probes and spatial sampling techniques, otolith analysis is becoming an increasingly viable option for studying the movements of both larval and juvenile marine fishes.

However, it is important to note that the primary design of this IBM was for predicting otolith isotope compositions. For this purpose, I implemented certain simplifications to streamline the model, focusing on factors that directly impact otolith formation rather than a comprehensive

suite of ecological variables. While these simplifications are suitable and justifiable for otolith isotope prediction, they may limit the model's applicability for broader ecological questions. Consequently, adaptations would be necessary for the model to accurately address more complex aspects of juvenile mackerel and eel ecology, particularly those requiring a finer resolution of behavioral or habitat-specific interactions.

## 5.5 Future work

High-resolution otolith isotope analysis is a powerful tool for studying the migration of larval fish, but its application is currently limited to studies that involve large-scale movements across water masses due to sampling difficulties and technological limitations. However, in this thesis ,the potential of using this method for a wider range of regions and fish species has been identified, and the use of individual-based models to simulate and predict experimental results has been demonstrated to be beneficial. Therefore, it is recommended to use individual-based models before conducting high-resolution otolith isotope analysis to simulate possible outcomes and save time and effort.

Conducting high-resolution otolith isotope analysis can provide valuable information about the movements, habitat use, and feeding ecology of fish. By analysing the stable isotopes of oxygen and carbon in the otoliths, we can determine the location and temperature of the water where the fish lived at different life stages, as well as their trophic level and diet. This information can help us understand the migratory patterns of fish, their interaction with their environment, and the potential impact of environmental changes on their survival and reproduction.

To improve our understanding of ecosystem metabolic thermal interaction, it is crucial to measure multiple species from separate habitats to understand the variability in metabolic thermal dependence and functionality between species. This can be achieved by combining multiple approaches such as FMR, otolith oxygen isotopes, and individual-based models. This approach can help us understand the impact of climate change on larval fish migration and ecological adaptation, and measuring the vulnerability of subpopulations can contribute to policy formation and fishing quota calculations.

In conclusion, combining different approaches and techniques (such as FMR, otolith oxygen isotopes, and individual-based models) can help us gain a comprehensive understanding of the complex interactions and dynamics of aquatic ecosystems, and improve our ability to make informed decisions regarding fisheries management and conservation.

# List of References

Albaina, A., Iriondo, M., Velado, I., Laconcha, U., Zarraonaindia, I., Arrizabalaga, H., Pardo, M. A., Lutcavage, M., Grant, W. S., & Estonba, A. (2013). Single nucleotide polymorphism discovery in albacore and Atlantic bluefin tuna provides insights into worldwide population structure. *Animal Genetics*, *44*(6), 678–692. https://doi.org/10.1111/age.12051

Arnold, G., & Dewar, H. (2001). *Electronic Tags in Marine Fisheries Research: A 30-Year Perspective* (pp. 7–64). Springer, Dordrecht. https://doi.org/10.1007/978-94-017-1402-0_2

Azetsu-Scott, K., & Tan, F. C. (1997). Oxygen isotope studies from Iceland to an East Greenland Fjord: Behaviour of glacial meltwater plume. *Marine Chemistry*, *56*(3–4), 239–251.

Baltazar-Soares, M., Biastoch, A., Harrod, C., Hanel, R., Marohn, L., Prigge, E., Evans, D., Bodles, K., Behrens, E., Böning, C. W., & Eizaguirre, C. (2014). Recruitment collapse and population structure of the european eel shaped by local ocean current dynamics. *Current Biology*, *24*(1), 104–108. https://doi.org/10.1016/j.cub.2013.11.031

Bartsch, J. (2005). The influence of spatio-temporal egg production variability on the modelled survival of the early life history stages of mackerel (*Scomber scombrus*) in the Eestern North Atlantic. *ICES Journal of Marine Science*, *62*(6), 1049–1060. https://doi.org/10.1016/j.icesjms.2005.04.012

Bartsch, J., Reid, D., & Coombs, S. H. (2004). Simulation of mackerel (*Scomber scombrus*) recruitment with an individual-based model and comparison with field data. *Fisheries Oceanography*, *13*(6), 380–391. https://doi.org/10.1111/j.1365-2419.2004.00306.x

Begg, G., & Weidman, C. (2001). Stable $d^{13}C$ and $d^{18}O$ isotopes in otoliths of haddock Melanogrammus aeglefinus from the northwest Atlantic Ocean. *Marine Ecology Progress Series*, *216*, 223–233. https://doi.org/10.3354/meps216223

Benetti, M., Reverdin, G., Aloisi, G., & Sveinbjörnsdóttir, Á. (2017). Stable isotopes in surface waters of the Atlantic Ocean: Indicators of ocean-atmosphere water fluxes and oceanic mixing processes. *Journal of Geophysical Research: Oceans*, *122*(6), 4723–4742. https://doi.org/10.1002/2017JC012712

Berge, J., Heggland, K., Lønne, O. J., Cottier, F., Hop, H., Gabrielsen, G. W., Nøttestad, L., & Misund, O. A. (2015). First records of Atlantic mackerel (*Scomber scombrus*) from the Svalbard

archipelago, Norway, with possible explanations for the extension of its distribution. *Arctic*, *68*(1), 54–61. https://doi.org/10.14430/arctic4455

Blaker, A. T., Hirschi, J. J. M., McCarthy, G., Sinha, B., Taws, S., Marsh, R., Coward, A., & de Cuevas, B. (2015). Historical analogues of the recent extreme minima observed in the Atlantic meridional overturning circulation at 26°N. *Climate Dynamics*, *44*(1–2), 457–473. https://doi.org/10.1007/s00382-014-2274-6

Blanke, B., Bonhommeau, S., Grima, N., & Drillet, Y. (2012). Sensitivity of advective transfer times across the North Atlantic Ocean to the temporal and spatial resolution of model velocity data: Implication for European eel larval transport. *Dynamics of Atmospheres and Oceans*, *55–56*, 22–44. https://doi.org/10.1016/j.dynatmoce.2012.04.003

Blanke, B., & Raynaud, S. (1997). Kinematics of the Pacific Equatorial Undercurrent: An Eulerian and Lagrangian Approach from GCM Results. *Journal of Physical Oceanography*, *27*(6), 1038–1053. https://doi.org/10.1175/1520-0485(1997)027<1038:KOTPEU>2.0.CO;2

Block, B. A., Teo, S. L. H., Walli, A., Boustany, A., Stokesbury, M. J. W., Farwell, C. J., Weng, K. C., Dewar, H., & Williams, T. D. (2005). Electronic tagging and population structure of Atlantic bluefin tuna. *Nature*, *434*(7037), 1121–1127. https://doi.org/10.1038/nature03463

Bolle, L. J., Hunter, E., Rijnsdorp, A. D., Pastoors, M. A., Metcalfe, J. D., & Reynolds, J. D. (2005). Do tagging experiments tell the truth? Using electronic tags to evaluate conventional tagging data. *ICES Journal of Marine Science*, *62*(2), 236–246. https://doi.org/10.1016/j.icesjms.2004.11.010

Bonhommeau, S., Castonguay, M., Rivot, E., Sabatié, R., & Le Pape, O. (2010). The duration of migration of Atlantic Anguilla larvae. *Fish and Fisheries*, *11*(3), 289–306. https://doi.org/10.1111/j.1467-2979.2010.00362.x

Bonhommeau, S., Chassot, E., & Rivot, E. (2008). Fluctuations in European eel (Anguilla anguilla) recruitment resulting from environmental changes in the Sargasso Sea. *Fisheries Oceanography*, *17*(1), 32–44. https://doi.org/10.1111/j.1365-2419.2007.00453.x

Borja, A., Uriarte, A., & Egana, J. (2002). Environmental factors and recruitment of mackerel, *Scomber scombrus* L. 1758, along the north-east Atlantic coasts of Europe. *Fisheries Oceanography*, *11*(2), 116–127. https://doi.org/10.1046/j.1365-2419.2002.00190.x

Brett, J. R., & Groves, T. D. D. (1979). Physiological energetics. *Fish Physiology*, *8*(6), 280–352.

Brock, E. C. (2021). Applying the otolith δ13C metabolic proxy to provide the first in-situ measurements of field metabolic rate in a pelagic fish species (*Scomber scombrus*) with reference to the influence of temperature and body size(Master's thesis). *UNIVERSITY OF SOUTHAMPTON*, 1–58. https://doi.org/10.1016/0041-2678(70)90288-5

Brown, J. H., Gillooly, J. F., Allen, A. P., Savage, V. M., & West, G. B. (2004). Toward a metabolic theory of ecology. *Ecology*, *85*(7), 1771–1789.

Burt, W. J., Thomas, H., Hagens, M., Pätsch, J., Clargo, N. M., Salt, L. A., Winde, V., & Böttcher, M. E. (2016). Carbon sources in the North Sea evaluated by means of radium and stable carbon isotope tracers. *Limnology and Oceanography*, *61*(2), 666–683. https://doi.org/10.1002/lno.10243

Campana, S. (1999). Chemistry and composition of fish otoliths:pathways, mechanisms and applications. *Marine Ecology Progress Series*, *188*, 263–297. https://doi.org/10.3354/meps188263

Chang, N. N., Liu, E. Y., Liao, Y. C., & Shiao, J. C. (2015). Vertical habitat shift of viviparous and oviparous deep-sea cusk eels revealed by otolith microstructure and stable-isotope composition. *Journal of Fish Biology*, *86*(2), 845–853. https://doi.org/10.1111/jfb.12605

Chang, Y. L. K., Feunteun, E., Miyazawa, Y., & Tsukamoto, K. (2020). New clues on the Atlantic eels spawning behavior and area: the Mid-Atlantic Ridge hypothesis. *Scientific Reports*, *10*(1). https://doi.org/10.1038/s41598-020-72916-5

Chiang, C. I., Chung, M. T., Shiao, J. C., Wang, P. L., Chan, T. Y., Yamaguchi, A., & Wang, C. H. (2020). Seasonal Movement Patterns of the Bigfin Reef Squid Sepioteuthis lessoniana Predicted Using Statolith δ18O Values. *Frontiers in Marine Science*, *7*(April), 1–14. https://doi.org/10.3389/fmars.2020.00249

Christensen, A., Jensen, H., Mosegaard, H., st. John, M., & Schrum, C. (2008). Sandeel (Ammodytes marinus) larval transport patterns in the North Sea from an individual-based hydrodynamic egg and larval model. *Canadian Journal of Fisheries and Aquatic Sciences*, *65*(7), 1498–1511. https://doi.org/10.1139/F08-073

Chung, M. T., Chen, C. Y., Shiao, J. C., Shirai, K., & Wang, C. H. (2021). Metabolic proxy for cephalopods: Stable carbon isotope values recorded in different biogenic carbonates. *Methods in Ecology and Evolution*, *12*(9), 1648–1657. https://doi.org/10.1111/2041-210X.13630

Chung, M. T., Jørgensen, K. E. M., Trueman, C. N., Knutsen, H., Jorde, P. E., & Grønkjær, P. (2021). First measurements of field metabolic rate in wild juvenile fishes show strong thermal sensitivity but variations between sympatric ecotypes. *Oikos*, *130*(2), 287–299. https://doi.org/10.1111/oik.07647

Chung, M. T., Trueman, C. N., Godiksen, J. A., & Grønkjær, P. (2019). Otolith δ13C values as a metabolic proxy: Approaches and mechanical underpinnings. *Marine and Freshwater Research*, *70*(12), 1747–1756. https://doi.org/10.1071/MF18317

Clark, T. D., Sandblom, E., & Jutfelt, F. (2013). Aerobic scope measurements of fishes in an era of climate change: Respirometry, relevance and recommendations. *Journal of Experimental Biology*, *216*(15), 2771–2782. https://doi.org/10.1242/jeb.084251

Clarke, L. M., Munch, S. B., Thorrold, S. R., & Conover, D. O. (2010). High connectivity among locally adapted populations of a marine fish (Menidia menidia). *Ecology*, *91*(12), 3526–3537. https://doi.org/10.1890/09-0548.1

Congleton, J. L. (1974). The respiratory response to asphyxia of Typhlogobius californiensis (Teleostei: Gobiidae) and some related gobies. *The Biological Bulletin*, *146*(2), 186–205.

Cotano, U., Álvarez, P., Alvarez, P., & Álvarez, P. (2003). Growth of young-of-the-year mackerel in the Bay of Biscay. *Journal of Fish Biology*, *62*(5), 1010–1020. https://doi.org/10.1046/j.1095-8649.2003.00093.x

Cunningham, C., Reid, D., McAllister, M., Kirkwood, G., & Darby, C. (2007). African Journal of Marine Science A Bayesian state-space model for mixed-stock migrations, with application to Northeast Atlantic mackerel *Scomber scombrus* A Bayesian state-space model for mixed-stock migrations, with application to Northeast Atlantic mac. *African Journal of Marine Science*, *29*(3), 1814–2338. https://doi.org/10.2989/AJMS.2007.29.3.4.334

Cushing, D. H. (1975). Marine ecology and fisheries Cambridge University Press. *Cambridge.[Google Scholar]*.

Cushing, D. H. (1981). *Fisheries biology: a study in population dynamics*.

D'amours, D., Landry, J. G., & Lambert, T. C. (1990). Growth of juvenile (0-group) Atlantic mackerel (*Scombrus*) in the Gulf of St. Lawrence. *Canadian Journal of Fisheries and Aquatic Sciences*, *47*(11), 2212–2218.

Darnaude, A. M., & Hunter, E. (2018). Validation of otolith d18O values as effective natural tags for shelf-scale geolocation of migrating fish. *Marine Ecology Progress Series*, *598*(December), 167–185. https://doi.org/10.3354/meps12302

Darnaude, A. M., Sturrock, A., Trueman, C. N., Mouillot, D., EIMF, Campana, S. E., & Hunter, E. (2014). Listening in on the past: what can otolith δ18O values really tell us about the environmental history of fishes? *PloS One*, *9*(10), e108539. https://doi.org/10.1371/journal.pone.0108539

DeCelles, G., & Zemeckis, D. (2014). Acoustic and Radio Telemetry. *Stock Identification Methods*, 397–428. https://doi.org/10.1016/B978-0-12-397003-9.00017-5

Del Raye, G., & Weng, K. C. (2015). An aerobic scope-based habitat suitability index for predicting the effects of multi-dimensional climate change stressors on marine teleosts. *Deep-Sea Research Part II: Topical Studies in Oceanography*, *113*, 280–290. https://doi.org/10.1016/j.dsr2.2015.01.014

Di Franco, A., Calò, A., Pennetta, A., De Benedetto, G., Planes, S., & Guidetti, P. (2015). Dispersal of larval and juvenile seabream: Implications for Mediterranean marine protected areas. *Biological Conservation*, *192*, 361–368. https://doi.org/10.1016/j.biocon.2015.10.015

Dorf, B. A., & Powell, J. C. (1997). Distribution, abundance, and habitat characteristics of juvenile tautog (Tautoga onitis, Family Labridae) in Narragansett Bay, Rhode Island, 1988–1992. *Estuaries*, *20*(3), 589–600.

Duchez, A., Frajka-Williams, E., Josey, S. A., Evans, D. G., Grist, J. P., Marsh, R., McCarthy, G. D., Sinha, B., Berry, D. I., & Hirschi, J. J. M. (2016). Drivers of exceptionally cold North Atlantic Ocean temperatures and their link to the 2015 European heat wave. *Environmental Research Letters*, *11*(7). https://doi.org/10.1088/1748-9326/11/7/074004

Elsdon, T. S., & Gillanders, B. M. (2003). Reconstructing migratory patterns of fish based on environmental influences on otolith chemistry Travis. *Reviews in Fish Biology and Fisheries*, *13*(3), 217–235. https://doi.org/10.1023/B:RFBF.0000033071.73952.40

Fisher, M., & Hunter, E. (2018). Digital imaging techniques in otolith data capture, analysis and interpretation. *Marine Ecology Progress Series*, *598*(July), 213–231. https://doi.org/10.3354/meps12531

Fowler, A. J., Hamer, P. A., & Kemp, J. (2017). Age-related otolith chemistry profiles help resolve demographics and meta-population structure of a widely-dispersed, coastal fishery species. *Fisheries Research*, *189*, 77–94. https://doi.org/10.1016/J.FISHRES.2017.01.010

Fraile, I., Arrizabalaga, H., & Rooker, J. R. (2015). Origin of Atlantic bluefin tuna (Thunnus thynnus) in the Bay of Biscay. *ICES Journal of Marine Science*, *72*(2), 625–634. https://doi.org/10.1093/icesjms/fsu156

Friedland, K. D., Miller, M. J., & Knights, B. (2007). Oceanic changes in the Sargasso Sea and declines in recruitment of the European eel. ICES Journal of Marine Science, 64(3), 5Fulton, T. W. (1904). The rate of growth of fishes. *Twenty-Second Annual Report*, 141–241.

Gallagher, C. A., Grimm, V., Kyhn, L. A., Kinze, C. C., & Nabe-Nielsen, J. (n.d.). *Movement and Seasonal Energetics Mediate Vulnerability to Disturbance in Marine Mammal Populations*. https://doi.org/10.5061/dryad.80gb5mkpn

Gangopadhyay, A., Cornillon, P., & Watts, D. R. (1992). A test of the Parsons–Veronis hypothesis on the separation of the Gulf Stream. *Journal of Physical Oceanography*, *22*(11), 1286–1301.

Garrido, S., Ben-Hamadou, R., Santos, A. M. P., Ferreira, S., Teodósio, M. A., Cotano, U., Irigoien, X., Peck, M. A., Saiz, E., & Ré, P. (2015). Born small, die young: Intrinsic, size-selective mortality in marine larval fish. *Scientific Reports*, *5*(1), 17065. https://doi.org/10.1038/srep17065

Gaspar, P., Benson, S. R., Dutton, P. H., Réveillère, A., Jacob, G., Meetoo, C., Dehecq, A., & Fossette, S. (2012). Oceanic dispersal of juvenile leatherback turtles: Going beyond passive drift modellingmodelling. *Marine Ecology Progress Series*, *457*(May 2020), 265–284. https://doi.org/10.3354/meps09689

Gaspar, P., & Lalire, M. (2017). A model for simulating the active dispersal of juvenile sea turtles with a case study on Western Pacific leatherback turtles. *PLoS ONE*, *12*(7). https://doi.org/10.1371/JOURNAL.PONE.0181595

Geffen, A. J., Nash, R. D. M., & Dickey-Collas, M. (2011). Characterization of herring populations west of the British Isles: an investigation of mixing based on otolith chemistry. *ICES Journal of Marine Science*, *68*(7), 1447–1458. https://doi.org/10.1093/icesjms/fsr051

Gerard, T., & Muhling, B. (2010). Variation in the isotopic signatures of juvenile gray snapper (Lutjanus griseus) from five southern Florida region.

Giguère, V., Yang, N. A., Segui, P., & Evans, R. M. (1988). Identification of a new class of steroid hormone receptors. *Nature*, *331*(6151), 91–94.

Gómez-Rubio, V. (2017). ggplot2 - Elegant Graphics for Data Analysis (2nd Edition) . *Journal of Statistical Software*, *77*(Book Review 2). https://doi.org/10.18637/jss.v077.b02

Grammer, G. L., Morrongiello, J. R., Izzo, C., Hawthorne, P. J., Middleton, J. F., & Gillanders, B. M. (2017). Coupling biogeochemical tracers with fish growth reveals physiological and environmental controls on otolith chemistry. *Ecological Monographs*, *87*(3), 487–507. https://doi.org/10.1002/ecm.1264

Hane, Y., Ushikubo, T., Yokoyama, Y., Miyairi, Y., & Kimura, S. (2022). Natal origin of Pacific bluefin tuna Thunnus orientalis determined by SIMS oxygen isotope analysis of otoliths. *PLoS ONE*, *17*(8 August), 1–21. https://doi.org/10.1371/journal.pone.0272850

Hansen, L., & Jacobsen, J. A. (2003). Origin and migration of wild and escaped farmed Atlantic salmon, Salmo salar L., in oceanic areas north of the Faroe Islands. *ICES Journal of Marine Science*, *60*(1), 110–119. https://doi.org/10.1006/jmsc.2002.1324

Harden Jones, F. R. (1968). *Fish migration*. Edward Arnold.

Hartog, J. R., Patterson, T. A., Hartmann, K., Jumppanen, P., Cooper, S., & Bradford, R. (2009). Developing integrated database systems for the management of electronic tagging data. In *Tagging and tracking of marine animals with electronic devices* (pp. 367–380). Springer.

Harwood, A. J. P., Dennis, P. F., Marca, A. D., Pilling, G. M., & Millner, R. S. (2008). The oxygen isotope composition of water masses within the North Sea. *Estuarine, Coastal and Shelf Science*, *78*(2), 353–359. https://doi.org/10.1016/j.ecss.2007.12.010

Helser, T. E., Kastelle, C. R., McKay, J. L., Orland, I. J., Kozdon, R., & Valley, J. W. (2018). Evaluation of micromilling/conventional isotope ratio mass spectrometry and secondary ion mass spectrometry of δ18O values in fish otoliths for sclerochronology. *Rapid Communications in Mass Spectrometry*, *32*(20), 1781–1790. https://doi.org/10.1002/rcm.8231

Higuchi, T., Ito, S. ichi, Ishimura, T., Kamimura, Y., Shirai, K., Shindo, H., Nishida, K., & Komatsu, K. (2019). Otolith oxygen isotope analysis and temperature history in early life stages of the chub mackerel Scomber japonicus in the Kuroshio–Oyashio transition region. *Deep-Sea Research Part II: Topical Studies in Oceanography*, *169–170*(October). https://doi.org/10.1016/j.dsr2.2019.104660

Hining, K. J., West, J. L., Kulp, M. A., & Neubauer, A. D. (2000). Validation of Scales and Otoliths for Estimating Age of Rainbow Trout from Southern Appalachian Streams. *North American Journal of Fisheries Management*, *20*(4), 978–985. https://doi.org/10.1577/1548-8675(2000)020<0978:VOSAOF>2.0.CO;2

Hinrichsen  Dickey-Collas, M., Huret, M., Peck, M. A., Vikebø, F.B., H.-H. (2011). *Evaluating the suitability of coupled biophysical models for fishery management. ICES J. Mar. Sci. 67: –. DOI: 10.1093/icesjms/fsq115*. *68*, 1478–1487.

Hixon, M. A., Pacala, S. W., & Sandin, S. A. (2008). Population Regulation : Historical Context and Contemporary Challenges of Open vs . Closed Systems Published by : Ecological Society of America Stable URL : http://www.jstor.org/stable/3071969. *America*, *83*(6), 1490–1508.

Hobson, K. A., & Wassenaar, L. I. (Eds.). (2018). *Tracking animal migration with stable isotopes*. Academic Press. Jansen, T. (2016). First-year survival of North East Atlantic mackerel (*Scomber scombrus*) from 1998 to 2012 appears to be driven by availability of Calanus, a preferred copepod prey. *Fisheries Oceanography*, *25*(4), 457–469. https://doi.org/10.1111/fog.12165

Jansen, T., Campbell, A., Kelly, C., Hátún, H., & Payne, M. R. (2012). Migration and Fisheries of North East Atlantic Mackerel (*Scomber scombrus*) in Autumn and Winter. *PLoS ONE*, *7*(12), e51541. https://doi.org/10.1371/journal.pone.0051541

Jansen, T., & Gislason, H. (2011). Temperature affects the timing of spawning and migration of North Sea mackerel. *Continental Shelf Research*, *31*(1), 64–72. https://doi.org/10.1016/j.csr.2010.11.003

Jansen, T., Kristensen, K., Kooij, J. Van Der, Post, S., Campbell, A., Utne, K. R., Carrera, P., Jacobsen, J. A., Gudmundssdottir, A., Roel, B. A., & Hatfield, E. M. C. (2015). *Nursery areas and recruitment variation of Northeast Atlantic mackerel (Scomber scombrus)*. *72*, 1779–1789.

Jansen, T., Kristensen, K., Payne, M., Edwards, M., Schrum, C., & Pitois, S. (2012). Long-term retrospective analysis of mackerel spawning in the North Sea: A new time series and modellingmodelling approach to CPR data. *PLoS ONE*, *7*(6). https://doi.org/10.1371/journal.pone.0038758

Jennings, S., & Cogan, S. M. (n.d.). *Nitrogen and carbon stable isotope variation in northeast Atlantic fishes and squids Ecological Archives E096-226*.

Jobling, M., Meloy, O. H., Santos, J. Dos, & Christiansen, B. (1994). The compensatory growth response of the Atlantic cod: effects of nutritional history. In *Aquaculture International* (Vol. 2).

Jutfelt, F., Norin, T., Ern, R., Overgaard, J., Wang, T., McKenzie, D. J., Lefevre, S., Nilsson, G. E., Metcalfe, N. B., Hickey, A. J. R., Brijs, J., Speers-Roesch, B., Roche, D. G., Gamperl, A. K., Raby, G. D., Morgan, R., Esbaugh, A. J., Gräns, A., Axelsson, M., … Clark, T. D. (2018). Oxygen- and capacity-limited thermal tolerance: Blurring ecology and physiology. In *Journal of Experimental Biology* (Vol. 221, Issue 1). Company of Biologists Ltd. https://doi.org/10.1242/jeb.169615

Kaji, H., Saito, H., Yamauchi, Y., Shinkawa, T., Taoka, M., Hirabayashi, J., Kasai, K., Takahashi, N., & Isobe, T. (2003). Lectin affinity capture, isotope-coded tagging and mass spectrometry to identify N-linked glycoproteins. *Nature Biotechnology*, *21*(6), 667–672.

Kent, M. (2006). *Oxford dictionary of sports science and medicine*. OUP Oxford.

Kettle, A. J., & Haines, K. (2006). How does the European eel (Anguilla anguilla) retain its population structure during its larval migration across the North Atlantic Ocean? *Canadian Journal of Fisheries and Aquatic Sciences*, *63*(1), 90–106.

Kettle, A. J., Bakker, D. C. E. & Haines, K. 2008 Impact of the North Atlantic Oscillation on the trans-Atlantic migrations of the European eel (Anguilla anguilla). J. Geophys. Res. Biogeosci. 113, 26. (doi:10.1029/ 2007jg000589)

Killen, S. S., Atkinson, D., & Glazier, D. S. (2010). The intraspecific scaling of metabolic rate with body mass in fishes depends on lifestyle and temperature. *Ecology Letters*, *13*(2), 184–193. https://doi.org/10.1111/j.1461-0248.2009.01415.x

Kim, S.-T., & O'Neil, J. R. (2005). Comment on "An experimental study of oxygen isotope fractionation between inorganically precipitated aragonite and water at low temperatures" by G.-T. Zhou and Y.-F. Zheng. *Geochimica et Cosmochimica Acta*, *69*(12), 3195–3197. https://doi.org/10.1016/j.gca.2004.05.052

Kimirei, I. A., Nagelkerken, I., Trommelen, M., Blankers, P., van Hoytema, N., Hoeijmakers, D., Huijbers, C. M., Mgaya, Y. D., & Rypel, A. L. (2013). What Drives Ontogenetic Niche Shifts of Fishes in Coral Reef Ecosystems? *Ecosystems*, *16*(5), 783–796. https://doi.org/10.1007/s10021-013-9645-4

Knights, B. (2003). A review of the possible impacts of long-term oceanic and climate changes and fishing mortality on recruitment of anguillid eels of the Northern Hemisphere. *Science of the total Environment*, *310*(1-3), 237-244.

Klapper, R., Kochmann, J., O'Hara, R. B., Karl, H., & Kuhn, T. (2016). Parasites as Biological Tags for Stock Discrimination of Beaked Redfish (Sebastes mentella): Parasite Infra-Communities vs. Limited Resolution of Cytochrome Markers. *PLOS ONE*, *11*(4), e0153964. https://doi.org/10.1371/journal.pone.0153964

Kleckner, R. C., & McCleave, J. D. (1988). The northern limit of spawning by Atlantic eels (<I>Anguilla</I> spp.) in the Sargasso Sea in relation to thermal fronts and surface water masses. *Journal of Marine Research*, *46*(3), 647–667. https://doi.org/10.1357/002224088785113469

Kooijman, B., & Kooijman, S. (2010). *Dynamic energy budget theory for metabolic organisation*. Cambridge university press.

Lin, H. Y., Shiao, J. C., Chen, Y. G., Iizuka, Y., Higuchi, T., Ito, S. ichi, Ishimura, T., Kamimura, Y., Shirai, K., Shindo, H., Nishida, K., & Komatsu, K. (2012). Ontogenetic vertical migration of grenadiers revealed by otolith microstructures and stable isotopic composition. *Deep-Sea Research Part II: Topical Studies in Oceanography*, *169–170*(January), 104660. https://doi.org/10.1016/j.dsr2.2019.104660

Longmore, C., Fogarty, K., Neat, F., Brophy, D., Trueman, C., Milton, A., & Mariani, S. (2010). A comparison of otolith chemistry and otolith shape analysis for the study of spatial variation in a deep-sea teleost, Coryphaenoides rupestris. *Environmental Biology of Fishes*, *89*(3), 591–605. https://doi.org/10.1007/s10641-010-9674-1

Longmore, C., Trueman, C. N., Neat, F., Gorman, E. J. O., Milton, J. A., & Mariani, S. (2014). *Otolith geochemistry indicates life-long spatial population structuring in a deep-sea fish , Coryphaenoides rupestris*. *August 2011*. https://doi.org/10.3354/meps09197

Madec, G. (2008). *NEMO ocean engine. Note du pôle de môdellisation de Institute Pierre Simon*. *27*, 1–332. http://www.nemo-ocean.eu/About-NEMO/Reference-manuals$%5C$npapers2://publication/uuid/73E7FF17-99BE-4B10-A823-0037C823EF6E

Malishev, M., & Kramer-Schadt, S. (2021). Movement, models, and metabolism: Individual-based energy budget models as next-generation extensions for predicting animal movement outcomes across scales. *Ecological Modelling*, *441*. https://doi.org/10.1016/j.ecolmodel.2020.109413

Marais, J. F. K. (1978). Routine oxygen consumption of Mugil cephalus, Liza dumerili and L. richardsoni at different temperatures and salinities. *Marine Biology*, *50*, 9–16.

Martino, J. C., Doubleday, Z. A., Chung, M. T., & Gillanders, B. M. (2020). Experimental support towards a metabolic proxy in fish using otolith carbon isotopes. *Journal of Experimental Biology*, *223*(6). https://doi.org/10.1242/jeb.217091

Marzocchi, A., Hirschi, J. J. M., Holliday, N. P., Cunningham, S. A., Blaker, A. T., & Coward, A. C. (2015). The North Atlantic subpolar circulation in an eddy-resolving global ocean model. *Journal of Marine Systems*, *142*, 126–143. https://doi.org/10.1016/j.jmarsys.2014.10.007

Mikalsen, G., & Sejrup, H. P. (2000). Oxygen Isotope Composition of Fjord and River Water in the Sognefjorden Drainage Area, Western Norway. Implications for Paleoclimate Studies. *Estuarine, Coastal and Shelf Science*, *50*(4), 441–448. https://doi.org/10.1006/ECSS.1999.0581

Miller, J. A., & Hurst, T. P. (2020). Growth rate, ration, and temperature effects on otolith elemental incorporation. *Frontiers in Marine Science*, *7*, 320.

Miller MJ, Marohn L, Wysujack K, Bonhommeau S, Kuroki M, Freese M, Pohlmann J-D, Watanabe S, Blancke T, Weist P, Castonguay M, Westerberg H, Tsukamoto K, Hanel R (2019) Larval size-distributions of Ariosoma balearicum cryptic species during the March–April season in the Sargasso Sea Subtropical convergence zone. Environ Biol Fish 102:1231–1252

Miller, M. J., & Tsukamoto, K. (2017). The ecology of oceanic dispersal and survival of anguillid leptocephali. *Canadian Journal of Fisheries and Aquatic Sciences*, *74*(6), 958–971. https://doi.org/10.1139/cjfas-2016-0281

Morissette, O., Trueman, C., Sturrock, A., Geffen, A., & Shirai, K. (n.d.). Limited evidence for species-specific influence on temperature-dependent sensitivity of oxygen stable isotope fractionation in biominerals: a meta-analysis.

Muto, D., Ishimura, T., Takahashi, M., & Nishida, K. (2022). Extracting daily isotopic records on fish otolith ( *Trachurus japonicus* ) by combining micro-milling and micro-scale isotopic analysis (MICAL-CF-IRMS). *Rapid Communications in Mass Spectrometry*, *36*(20). https://doi.org/10.1002/rcm.9366

Nakamura, M., Yoneda, M., Ishimura, T., Shirai, K., Tamamura, M., & Nishida, K. (2020). Temperature dependency equation for chub mackerel (*Scomber japonicus*) identified by a

laboratory rearing experiment and microscale analysis. *Marine and Freshwater Research*. https://doi.org/10.1071/MF19313

Neumann, D. A., O'Connor, J. M., & Sherk Jr, J. A. (1981). Oxygen consumption of white perch (*Morone americana*), striped bass (*M. saxatius*) and spot (*Leiostomus xanthurus*). *Comparative Biochemistry and Physiology Part A: Physiology*, *69*(3), 467–478.

Newman, S. J., Allsop, Q., Ballagh, A. C., Garrett, R. N., Gribble, N., Meeuwig, J. J., Mitsopoulos, G. E. A., Moore, B. R., Pember, M. B., Rome, B. M., Saunders, T., Skepper, C. L., Stapley, J. M., van Herwerden, L., & Welch, D. J. (2010). Variation in stable isotope ($\delta^{18}O$ and $\delta^{13}C$) signatures in the sagittal otolith carbonate of king threadfin, Polydactylus macrochir across northern Australia reveals multifaceted stock structure. *Journal of Experimental Marine Biology and Ecology*, *396*(1), 53–60. https://doi.org/10.1016/j.jembe.2010.09.011

Newman, S. J., Wright, I. W., Rome, B. M., Mackie, M. C., Lewis, P. D., Buckworth, R. C., Ballagh, A. C., Garrett, R. N., Stapley, J., Broderick, D., Ovenden, J. R., & Welch, D. J. (2010). Stock structure of Grey Mackerel, Scomberomorus semifasciatus (Pisces: Scombridae) across northern Australia, based on otolith stable isotope chemistry. *Environmental Biology of Fishes*, *89*(3), 357–367. https://doi.org/10.1007/s10641-010-9668-z

Nishida, K., Yasu, A., Nanjo, N., Takahashi, M., Kitajima, S., & Ishimura, T. (2020). 2-1Microscale stable carbon and oxygen isotope measurement of individual otoliths of larvae and juveniles of Japanese anchovy and sardine. *Estuarine, Coastal and Shelf Science*, *245*(January), 106946. https://doi.org/10.1016/j.ecss.2020.106946

Norin, T., & Clark, T. D. (2016). Measurement and relevance of maximum metabolic rate in fishes. *Journal of Fish Biology*, *88*(1), 122–151. https://doi.org/10.1111/jfb.12796

Norin, T., & Metcalfe, N. B. (2019). Ecological and evolutionary consequences of metabolic rate plasticity in response to environmental change. Philosophical Transactions of the Royal Society B, 374(1768), 20180180.

Ohlberger, J. (2013). Climate warming and ectotherm body size - from individual physiology to community ecology. In *Functional Ecology* (Vol. 27, Issue 4, pp. 991–1001). https://doi.org/10.1111/1365-2435.12098

Okunishi, T., Ito, S. I., Ambe, D., Takasuka, A., Kameda, T., Tadokoro, K., Setou, T., Komatsu, K., Kawabata, A., Kubota, H., Ichikawa, T., Sugisaki, H., Hashioka, T., Yamanaka, Y., Yoshie, N., & Watanabe, T. (2012). A modellingmodelling approach to evaluate growth and movement for

recruitment success of Japanese sardine (Sardinops melanostictus) in the Western Pacific. *Fisheries Oceanography*, *21*(1), 44–57. https://doi.org/10.1111/j.1365-2419.2011.00608.x

OKUNISHI, T., ITO, S.-I., AMBE, D., TAKASUKA, A., KAMEDA, T., TADOKORO, K., SETOU, T., KOMATSU, K., KAWABATA, A., KUBOTA, H., ICHIKAWA, T., SUGISAKI, H., HASHIOKA, T., YAMANAKA, Y., YOSHIE, N., & WATANABE, T. (2012). A modellingmodelling approach to evaluate growth and movement for recruitment success of Japanese sardine (Sardinops melanostictus) in the Western Pacific. *Fisheries Oceanography*, *21*(1), 44–57. https://doi.org/10.1111/j.1365-2419.2011.00608.x

Payne, N. L., Gillanders, B. M., Seymour, R. S., Webber, D. M., Snelling, E. P., & Semmens, J. M. (2011). Accelerometry estimates field metabolic rate in giant Australian cuttlefish Sepia apama during breeding. *Journal of Animal Ecology*, *80*(2), 422–430. https://doi.org/10.1111/j.1365-2656.2010.01758.x

Peck, M. A., Buckley, L. J., & Bengtson, D. A. (2005). Effects of temperature, body size and feeding on rates of metabolism in young-of-the-year haddock. *Journal of Fish Biology*, *66*(4), 911–923.

Peck, M. A., Buckley, L. J., & Bengtson, D. A. (2006). Effects of temperature and body size on the swimming speed of larval and juvenile Atlantic cod (Gadus morhua): Implications for individual-based modelling. *Environmental Biology of Fishes*, *75*(4), 419–429. https://doi.org/10.1007/s10641-006-0031-3

Peck, M. A., Buckley, L. J., Caldarone, E. M., & Bengtson, D. A. (2003). Effects of food consumption and temperature on growth rate and biochemical-based indicators of growth in early juvenile Atlantic cod Gadus morhua and haddock Melanogrammus aeglefinus. *Marine Ecology Progress Series*, *251*, 233–243.

Punzón, A., & Villamor, B. (2009). Does the timing of the spawning migration change for the southern component of the Northeast Atlantic Mackerel (*Scomber scombrus*, L. 1758)? An approximation using fishery analyses. *Continental Shelf Research*, *29*(8), 1195–1204. https://doi.org/10.1016/J.CSR.2008.12.024

Röckmann, C., Dickey-Collas, M., Payne, M. R., & van Hal, R. (2011). Realized habitats of early-stage North Sea herring: looking for signals of environmental change. *ICES Journal of Marine Science*, *68*(3), 537–546. https://doi.org/10.1093/icesjms/fsq171

Rooker, J. R., Secor, D. H., De Metrio, G., Schloesser, R., Block, B. A., & Neilson, J. D. (2008). Natal homing and connectivity in Atlantic bluefin tuna populations. *Science*, *322*(5902), 742–744. https://doi.org/10.1126/science.1161473

Rooker, J. R., Secor, D. H., DeMetrio, G., Kaufman, A. J., Ríos, A. B., & Tičina, V. (2008). Evidence of trans-Atlantic movement and natal homing of bluefin tuna from stable isotopes in otoliths. *Marine Ecology Progress Series*, *368*, 231–239. https://doi.org/10.3354/meps07602

Ross, M. J., & McCormick, J. H. (1981). Effects of external radio transmitters on fish. *The Progressive Fish-Culturist*, *43*(2), 67–72.

Priester, C. R., Afonso, P., Trueman, C. N., Menezes, G., Graça, G., & Fontes, J. (2024). Contrasting ontogenetic shifts in habitat and metabolism of three sympatric key deep-sea fishes. Marine Ecology Progress Series, 729, 185-199.

Rypina, I. I., Llopiz, J. K., Pratt, L. J., & Lozier, M. S. (2014). Dispersal pathways of American eel larvae from the Sargasso Sea. *Limnology and Oceanography*, *59*(5), 1704–1714. https://doi.org/10.4319/lo.2014.59.5.1704

Sakamoto, T., Komatsu, K., Shirai, K., Higuchi, T., Ishimura, T., Setou, T., Kamimura, Y., Watanabe, C., & Kawabata, A. (2019). 2-1Combining microvolume isotope analysis and numerical simulation to reproduce fish migration history. *Methods in Ecology and Evolution*, *10*(1), 59–69. https://doi.org/10.1111/2041-210X.13098

Sarah Rose Alewijnse. (2022). Macroecological study of otolith-derived field metabolic rates of marine fishes [Doctor]. In *(Doctoral dissertation)University of Southampton,Southampton.UK*. University of Southampton.

Schloesser, R. W., Neilson, J. D., Secor, D. H., & Rooker, J. R. (2010a). Natal origin of Atlantic bluefin tuna (Thunnus thynnus) from Canadian waters based on otolith $\delta^{13}$C and $\delta^{18}$O. *Canadian Journal of Fisheries and Aquatic Sciences*, *67*(3), 563–569. https://doi.org/10.1139/F10-005

Schmidt, J. (1923). IV.—The breeding places of the eel. *Philosophical Transactions of the Royal Society of London. Series B, Containing Papers of a Biological Character*, *211*(382–390), 179–208.

Scott, R., Marsh, R., & Hays, G. C. (2014). Ontogeny of long distance migration. *Ecology*, *95*(10), 2840–2850. https://doi.org/10.1890/13-2164.1

Secor, D. H., Henderson-Arzapalo, A., & Piccoli, P. M. (1995). Can otolith chemistry chart patterns of migration and habitat utilization in anadromous fishes? *Journal of Experimental Marine Biology and Ecology*, *192*(1), 15–33. https://doi.org/10.1016/0022-0981(95)00054-U

Secor, D. H., & Piccoli, P. M. (2007). Oceanic migration rates of Upper Chesapeake Bay striped bass (Morone saxatilis), determined by otolith microchemical analysis. *Fishery Bulletin*, *105*(1), 62–73.

Seebacher, F., White, C. R., & Franklin, C. E. (2015). Physiological plasticity increases resilience of ectothermic animals to climate change. *Nature Climate Change*, *5*(1), 61–66. https://doi.org/10.1038/nclimate2457

Shephard, S., Trueman, C., Rickaby, R., & Rogan, E. (2007). Juvenile life history of NE Atlantic orange roughy from otolith stable isotopes. *Deep-Sea Research Part I: Oceanographic Research Papers*, *54*(8), 1221–1230. https://doi.org/10.1016/j.dsr.2007.05.007

Shiao, J. C., Wang, S. W., Yokawa, K., Ichinokawa, M., Takeuchi, Y., Chen, Y. G., & Shen, C. C. (2010). Natal origin of Pacific bluefin tuna Thunnus orientalis inferred from otolith oxygen isotope composition. *Marine Ecology Progress Series*, *420*, 207–219. https://doi.org/10.3354/meps08867

Shiao, J. C., Yui, T. F., Høie, H., Ninnemann, U., & Chang, S. K. (2009). Otolith O and C stable isotope compositions of southern bluefin tuna Thunnus maccoyii (Pisces: Scombridae) as possible environmental and physiological indicators. *Zoological Studies*, *48*(1), 71–82.

Shiao, J.-C., Sui, T.-D., Chang, N.-N., & Chang, C.-W. (2017). Remarkable vertical shift in residence depth links pelagic larval and demersal adult jellynose fish. *Deep Sea Research Part I: Oceanographic Research Papers*, *121*, 160–168. https://doi.org/10.1016/J.DSR.2017.01.011

Shirai, K., Otake, T., Amano, Y., Kuroki, M., Ushikubo, T., Kita, N. T., Murayama, M., Tsukamoto, K., & Valley, J. W. (2018). Temperature and depth distribution of Japanese eel eggs estimated using otolith oxygen stable isotopes. *Geochimica et Cosmochimica Acta*, *236*, 373–383. https://doi.org/10.1016/j.gca.2018.03.006

Sigurthsson, S., Palsson, O. K., Barbaro, A., Einarsson, B., Valdimarsson, H., Sveinbjornsson, S., Sigurthsson, T., & Birnir, B. (2009). Modelling and simulations of the migration of pelagic fish. *ICES Journal of Marine Science*, 826–838. https://doi.org/10.1093/icesjms/fsp067

Smith, W., Miller, J., Márquez-Farías, J., & Heppell, S. (2016). Elemental signatures reveal the geographic origins of a highly migratory shark: prospects for measuring population

connectivity. *Marine Ecology Progress Series*, *556*, 173–193. https://doi.org/10.3354/meps11844

Solomon, C. T., Weber, P. K., Cech, J. J., Ingram, B. L., Conrad, M. E., Machavaram, M. V., Pogodina, A. R., & Franklin, R. L. (2011). Experimental determination of the sources of otolith carbon and associated isotopic fractionation. *Https://Doi.Org/10.1139/F05-200*, *63*(1), 79–89. https://doi.org/10.1139/F05-200

Steffan, S. A., Chikaraishi, Y., Horton, D. R., Ohkouchi, N., Singleton, M. E., Miliczky, E., Hogg, D. B., & Jones, V. P. (2013). Trophic Hierarchies Illuminated via Amino Acid Isotopic Analysis. *PLoS ONE*, *8*(9), e76152. https://doi.org/10.1371/journal.pone.0076152

Stendardo, I., Rhein, M., & Steinfeldt, R. (2020). The North Atlantic Current and its Volume and Freshwater Transports in the Subpolar North Atlantic, Time Period 1993–2016. *Journal of Geophysical Research: Oceans*, *125*(9). https://doi.org/10.1029/2020JC016065

Sturrock, A. (2012). *Environmental and physiological influences on otolith chemistry in a marine fish Anna*. *PhD*(May), 208 pp.

Sturrock, A. M., Trueman, C. N., Darnaude, A. M., & Hunter, E. (2012). Can otolith elemental chemistry retrospectively track migrations in fully marine fishes? *Journal of Fish Biology*, *81*(2), 766–795. https://doi.org/10.1111/j.1095-8649.2012.03372.x

Stutchbury, B. J. M., Tarof, S. A., Done, T., Gow, E., Kramer, P. M., Tautin, J., Fox, J. W., & Afanasyev, V. (2009). Tracking long-distance songbird migration by using geolocators. *Science*, *323*(5916), 896. https://doi.org/10.1126/science.1166664

Subrahmanyam, C. B. (1980). Oxygen consumption of estuarine fish in relation to external oxygen tension. *Comparative Biochemistry and Physiology Part A: Physiology*, *67*(1), 129–133.

Taillebois, L., Barton, D. P., Crook, D. A., Saunders, T., Taylor, J., Hearnden, M., Saunders, R. J., Newman, S. J., Travers, M. J., Welch, D. J., Greig, A., Dudgeon, C., Maher, S., & Ovenden, J. R. (2017). Strong population structure deduced from genetics, otolith chemistry and parasite abundances explains vulnerability to localized fishery collapse in a large Sciaenid fish, *Protonibea diacanthus*. *Evolutionary Applications*, *10*(10), 978–993. https://doi.org/10.1111/eva.12499

Tesch, F. (1989). Changes in swimrning depth and direction of silver eels ( Anguilla anguilla L .) from the continental shelf to the deep sea. *Aquatic Living Resources*, *2*, 9–20.

Thorrold, S. R., Secor, D. H., Metrio, G. De, Schloesser, R., Block, B. A., & Neilson, J. D. (2001). Natal Homing in a Marine Fish Metapopulation. *Science*, *291*(5502), 297–299. https://doi.org/10.1126/science.291.5502.297

Thorstad, E. B., Rikardsen, A. H., Alp, A., & Okland, F. (2013). The Use of Electronic Tags in Fish Research - An Overview of Fish Telemetry Methods. *Turkish Journal of Fisheries and Aquatic Sciences*, *13*(January), 881–896. https://doi.org/10.4194/1303-2712-v13

Thorsteinsson, V. (2002). Tagging methods for stock assessment and research in fisheries. *Report*, *Report of*(FAIR CT.96.1394 (CATAG)), 183. https://doi.org/PDF 15 & 132

Thurston, R. V, & Gehrke, P. C. (1990). Respiratory oxygen requirements of fishes: description of OXYREF, a data file based on test results reported in the published literature. *Proceedings of the Second International Symposium on Fish Physiology, Fish Toxicology, and Water Quality Management. Sacramento, CA*, 95–108.

Tittensor, D. P., Mora, C., Jetz, W., Lotze, H. K., Ricard, D., Berghe, E. Vanden, & Worm, B. (2010). Global patterns and predictors of marine biodiversity across taxa. *Nature*, *466*(7310), 1098–1101. https://doi.org/10.1038/nature09329

Tomczak, M., & Godfrey, J. S. (2003). *Regional oceanography: an introduction*. Daya books.

Treberg, J. R., Killen, S. S., MacCormack, T. J., Lamarre, S. G., & Enders, E. C. (2016). Estimates of metabolic rate and major constituents of metabolic demand in fishes under field conditions: Methods, proxies, and new perspectives. *Comparative Biochemistry and Physiology -Part A : Molecular and Integrative Physiology*, *202*(January), 10–22. https://doi.org/10.1016/j.cbpa.2016.04.022

Trenkel, V. M. M., Huse, G., MacKenzie, B. R. R., Alvarez, P., Arrizabalaga, H., Castonguay, M., Goñi, N., Grégoire, F., Hátún, H., Jansen, T., Jacobsen, J. A. A., Lehodey, P., Lutcavage, M., Mariani, P., Melvin, G. D. D., Neilson, J. D. D., Nøttestad, L., Óskarsson, G. J. J., Payne, M. R. R., … Speirs, D. C. C. (2014). Comparative ecology of widely distributed pelagic fish species in the North Atlantic: Implications for modelling climate and fisheries impacts. *Progress in Oceanography*, *129*(PB), 219–243. https://doi.org/10.1016/J.POCEAN.2014.04.030

Tripp, A., Murphy, H. M., & Davoren, G. K. (2020). Otolith Chemistry Reveals Natal Region of Larval Capelin in Coastal Newfoundland, Canada. *Frontiers in Marine Science*, *7*, 258. https://doi.org/10.3389/fmars.2020.00258

Trueman, C. N., Grønkjær, P., Chung, M.-T., Holmstrup, M. E., & Godiksen, J. A. (2019). Field metabolic rates of teleost fishes are recorded in otolith carbonate. *Communications Biology*, *2*(1), 1–10. https://doi.org/10.1038/s42003-018-0266-5

Trueman, C. N., MacKenzie, K. M., & Palmer, M. R. (2012). Identifying migrations in marine fishes through stable-isotope analysis. *Journal of Fish Biology*, *81*(2), 826–847. https://doi.org/10.1111/j.1095-8649.2012.03361.x

Trueman, C. N., Artetxe-Arrate, I., Kerr, L. A., Meijers, A. J., Rooker, J. R., Sivankutty, R., ... & Fraile, I. (2023). Thermal sensitivity of field metabolic rate predicts differential futures for bluefin tuna juveniles across the Atlantic Ocean. Nature communications, 14(1), 7379.

Turan, C. (2006). The use of otolith shape and chemistry to determine stock structure of Mediterranean horse mackerel *Trachurus mediterraneus* (Steindachner). *Journal of Fish Biology*, *69*(sc), 165–180. https://doi.org/10.1111/j.1095-8649.2006.01266.x

Uriarte, A., & Lucio, P. (2001). Migration of adult mackerel along the Atlantic European shelf edge from a tagging experiment in the south of the Bay of Biscay in 1994. *Fisheries Research*, *50*(1–2), 129–139. https://doi.org/10.1016/S0165-7836(00)00246-0

van Denderen, D., Gislason, H., van den Heuvel, J., & Andersen, K. H. (2020). Global analysis of fish growth rates shows weaker responses to temperature than metabolic predictions. *Global Ecology and Biogeography*, *29*(12), 2203–2213. https://doi.org/10.1111/geb.13189

*Variation in the isotopic signatures of juvenile gray snapper (Lutjanus griseus) from five southern Florida region - Aquatic Commons*. (n.d.). Retrieved September 10, 2020, from http://aquaticcommons.org/8771/

Vieira, R. P., Trueman, C. N., Readdy, L., Kenny, A., & Pinnegar, J. K. (2019). Deep-water fisheries along the British Isles continental slopes: status, ecosystem effects and future perspectives. *Journal of Fish Biology*, *94*(6), jfb.13927. https://doi.org/10.1111/jfb.13927

Villamor, B., Abaunza, P., & Celso Fariña, A. (2004). Growth variability of mackerel (*Scomber scombrus*) off north and northwest Spain and a comparative review of the growth patterns in the northeast Atlantic. *Fisheries Research*, *69*(1), 107–121. https://doi.org/10.1016/j.fishres.2004.02.005

Walther, B., & Thorrold, S. (2006). Water, not food, contributes the majority of strontium and barium deposited in the otoliths of a marine fish. *Marine Ecology Progress Series*, *311*, 125–130. https://doi.org/10.3354/meps311125

Wang, C. H., Walther, B. D., Gillanders, B. M., Bouchard, C., Thorrold, S. R., Fortier, L., Hixon, M. A., Fowler, A. J., Campana, S. E., Thorrold, S. R., Jones, C. M., Elsdon, T. S., Gillanders, B. M., Lin, H. Y., Shiao, J. C., Chen, Y. G., Iizuka, Y., Higuchi, T., Ito, S. ichi, … Gillanders, B. M. (2019). Reconstructing migratory patterns of fish based on environmental influences on otolith chemistry Travis. *Canadian Journal of Fisheries and Aquatic Sciences*, *13*(4), 217–235. https://doi.org/10.1023/B:RFBF.0000033071.73952.40

Wang, X., Wang, L., Lv, S., & Li, T. (2018). Stock discrimination and connectivity assessment of yellowfin seabream (Acanthopagrus latus) in northern South China Sea using otolith elemental fingerprints. *Saudi Journal of Biological Sciences*, *25*(6), 1163–1169. https://doi.org/10.1016/j.sjbs.2017.09.006

West, G. B., Brown, J. H., & Enquist, B. J. (1997). A general model for the origin of allometric scaling laws in biology. *Science*, *276*(5309), 122–126.

William, J., & Msci, J. (2022). *3-1Variation in the field metabolic rate of wild living plaice (Pleuronectes platessa) from the North Sea: constraining influences of body size, temperature, seasonal cycle, individual level growth rate and year of sampling*. University of Southampton.

Williams, J., Jenkins, G. P., Hindell, J. S., & Swearer, S. E. (2018). Fine-scale variability in elemental composition of estuarine water and otoliths: Developing environmental markers for determining larval fish dispersal histories within estuaries. *Limnology and Oceanography*, *63*(1), 262–277. https://doi.org/10.1002/lno.10627

Willis, J., Phillips, J., Muheim, R., Diego-Rasilla, F. J., & Hobday, A. J. (2009). Spike dives of juvenile southern bluefin tuna (Thunnus maccoyii): a navigational role? *Behavioral Ecology and Sociobiology*, *64*(1), 57–68.

Willmes, M., Lewis, L. S., Davis, B. E., Loiselle, L., James, H. F., Denny, C., Baxter, R., Conrad, J. L., Fangue, N. A., Hung, T., Armstrong, R. A., Williams, I. S., Holden, P., & Hobbs, J. A. (2019). Calibrating temperature reconstructions from fish otolith oxygen isotope analysis for California's critically-endangered Delta Smelt. *Rapid Communications in Mass Spectrometry*, *March*, 1207–1220. https://doi.org/10.1002/rcm.8464

Winberg, G. G. (1956). 3-1Rate of metabolism and food requirements of fishes. *Fish. Res. Bd. Canada Trans. Ser.*, *433*, 1–251.

Yamada, Y., Okamura, A., Mikawa, N., Utoh, T., Horie, N., Tanaka, S., Miller, M. J., & Tsukamoto, K. (2009). Ontogenetic changes in phototactic behavior during metamorphosis of artificially

reared Japanese eel Anguilla japonica larvae. *Marine Ecology Progress Series*, *379*, 241–251. https://doi.org/10.3354/meps07912

Yúfera, M., Ortiz-Delgado, J. B., Hoffman, T., Siguero, I., Urup, B., & Sarasquete, C. (2014). Organogenesis of digestive system, visual system and other structures in Atlantic bluefin tuna (Thunnus thynnus) larvae reared with copepods in mesocosm system. *Aquaculture*, *426–427*, 126–137. https://doi.org/10.1016/j.aquaculture.2014.01.031